

12

ACOUSTICALLY SCANNED OPTICAL IMAGING DEVICES

AD A 090839

Semiannual Report No. 10
1 January - 30 June, 1980

LEVEL III
A082 028

Principal Investigator:

G. S. Kino
(415) 497-0205

Sponsored by
Advanced Research Projects Agency
ARPA Order No. 2778

Contract N00014-76-C-0129
Program Code Number: 4D10
Contract Period: 1 July 1975 - 30 September 1980
Amount of Contract: \$504,302.00
Form Approved, Budget Bureau - No. 22R0293

Approved for public release; distribution unlimited

Reproduction, in whole or in part, is permitted for any purpose of the U.S. Government.

The views and conclusions contained in this document are those of the authors and should not be interpreted as necessarily representing the official policies, either expressed or implied, of the Defense Advanced Research Projects Agency or the U.S. Government.

DDG FILE COPY

G. L. Report No. 3165

August 1980

Edward L. Ginzton Laboratory
W. W. Hansen Laboratories of Physics
Stanford University
Stanford, California

DTIC
ELECTE
S OCT 28 1980 D
D

80 70 23 039

UNCLASSIFIED

⑨ Semiannual Rept. no. 10,
1 JAN - 30 JUN 80

SECURITY CLASSIFICATION OF THIS PAGE (When Data Entered)

REPORT DOCUMENTATION PAGE		READ INSTRUCTIONS BEFORE COMPLETING FORM
1. REPORT NUMBER 318-037-010	2. GOVT ACCESSION NO. ADA090839	3. RECIPIENT'S CATALOG NUMBER
4. TITLE (and Subtitle) Acoustically Scanned Optical Imaging Devices.		5. TYPE OF REPORT & PERIOD COVERED Technical Report 1 January - 30 June, 1980
		6. PERFORMING ORG. REPORT NUMBER GL-3163
7. AUTHOR(s) G. S./Kino, J./Bowers, B./Khuri-Yakub, R./Thornton		8. CONTRACT OR GRANT NUMBER(s) N00014-76-C-0129, ARPA Order 2778
9. PERFORMING ORGANIZATION NAME AND ADDRESS Edward L. Ginzton Laboratory W. W. Hansen Laboratories of Physics Stanford University, Stanford, CA 94305		10. PROGRAM ELEMENT, PROJECT, TASK AREA & WORK UNIT NUMBERS PE 61101E 8D10 Order No. 2778-5
11. CONTROLLING OFFICE NAME AND ADDRESS Defense Advanced Research Projects Agency 1400 Wilson Boulevard Arlington, VA 22209		12. REPORT DATE August 1980
14. MONITORING AGENCY NAME & ADDRESS (if different from Controlling Office) Office of Naval Research Code 427 Arlington, VA 22217		13. NUMBER OF PAGES 143
		15. SECURITY CLASS. (of this report) Unclassified
16. DISTRIBUTION STATEMENT (of this Report) Approved for public release; distribution unlimited		15a. DECLASSIFICATION/DOWNGRADING SCHEDULE
17. DISTRIBUTION STATEMENT (of the abstract entered in Block 20, if different from Report)		
18. SUPPLEMENTARY NOTES ONR Scientific Office (202) 696-4218		
19. KEY WORDS (Continue on reverse side if necessary and identify by block number) Sputtered ZnO; ZnO on Si; Sezawa mode; monolithic storage correlator; monolithic convolver; broadband matching; acoustic surface waves		
20. ABSTRACT (Continue on reverse side if necessary and identify by block number) We have carried out ZnO deposition at a rate of 18 μm per hour and obtained films comparable to single crystal. We have made a ZnO on Si Sezawa mode correlator with -50 dBm efficiency, and we have also constructed the first monolithic Schottky diode storage correlator on silicon.		

DD FORM 1473 JAN 73

EDITION OF 1 NOV 69 IS OBSOLETE
S/N 0102-LF-014-6601

UNCLASSIFIED

SECURITY CLASSIFICATION OF THIS PAGE (When Data Entered)

401640 JK

INDEX

	<u>Page</u>
I. MANAGEMENT REPORT.	1
A. Summary.	1
B. Research Program Plan.	2
C. Major Accomplishments.	2
D. Problems Encountered	3
E. Fiscal Status.	3
F. Action Required by ARPA/ONR.	3
II. TECHNICAL PROGRESS REPORTS	4
A. ZnO Technology Development	4
B. Sezawa Wave Devices.	5
1. Sezawa Wave Delay Lines.	5
2. Sezawa Wave Convolvers	6
3. Sezawa Wave Correlators.	7
C. Monolithic Storage Correlator Theory	8
D. Comparison of Various Systems Based on Bandwidth Considerations	9
E. Schottky Diode Storage Correlator.	10
F. Silicon on Lithium Niobate	12
G. FET Storage Correlator	13
References	15

INDEX (continued)

Page

APPENDICES 18

- A. A Technique for Calculating the Bandwidth-Loss
Relationship for Acoustic Transducers
- B. Theoretical and Experimental Results for Monolithic
SAW Memory Correlators
- C. Dispersion Effects
- D. Broadband Efficient Thin-Film Sezawa Wave Interdigital
Transducers
- E. Adaptive Deconvolution Using an ASW Storage Correlator

Accession For	
NTIS GRA&I	<input checked="" type="checkbox"/>
DTIC TAB	<input type="checkbox"/>
Unannounced	<input type="checkbox"/>
Justification	
By	
Distribution/	
Availability Codes	
Dist	Avail and/or Special
A	

I. MANAGEMENT REPORT

A. Summary

We have continued to improve our ZnO deposition process to the point where the films we are producing are far better than those of which we are aware. The present sputtering rate is 18 μm per hour, a factor of 18 better than we were obtaining two years ago. By carrying out deposition at 500° C, we have obtained x-ray results which show a full width of half maximum of the $\langle 0002 \rangle$ peak of 0.2° and show very clearly that the Cu- α_1 and Cu- α_2 lines are split. RED results are of similar quality, and the x-ray and electron diffraction results are by far the best we have ever seen and indicate that the films must be very nearly single crystals. We have carried out further developments of our Sezawa mode convolvers and correlators. We have made a convolver with an excellent efficiency of -50 dBm with a bandwidth of 25 MHz. We have made low loss delay lines with 32 MHz bandwidth and have designed chirp transducer devices which are presently being constructed with as much as 50 MHz bandwidth.

We have tested Sezawa wave convolvers and correlators to determine the effect of dispersion. This is in agreement with the theory we have worked out. As far as correlators are concerned, the theory indicates that dispersion is far less important than in a convolver, and dispersion should not limit its performance even in very wide bandwidth devices. We have found certain problems in Sezawa mode correlators, which we had not anticipated, but for which we have solutions. One is associated with reflection from the top plate due to the much larger value of $\Delta v/v$ in these devices than that which we had used before. This problem is easily remedied by redesigning the top

plate. Another was associated with stronger excitation of bulk waves than with the Rayleigh wave devices. Again, by bonding the semiconductor with indium to a brass box, we have eliminated the bulk wave excitation. Phase distortion due to the top plate has also been a problem due to the larger value of $\Delta v/v$; again, with redesign of the top plate, we can eliminate this problem.

We have carried out a complete theory of the storage correlator and can predict all its characteristics as regards to storage amplitude as a function of input times and amplitudes. The theory is in excellent agreement with experiment; we have written a paper on the subject which has been accepted for publication. We have constructed the first monolithic Schottky diode storage correlator; with it, we have demonstrated that we can store signals in as short a time as 5 ns for as long as 1 ms. We have managed to make far better quality Schottky diodes than heretofore by carrying out the depositions in a cleaner system to which we have had access at Varian Associates.

We will continue with our work on deposition of Si on LiNbO_3 and have encountered problems with cracking. We have been examining a new concept, the FET storage correlator, and are working out a detailed design for this device.

B. Research Program Plan

We will be constructing very broadband Sezawa mode correlators and working to improve our Schottky diode correlators. It is our intention after constructing broadband Sezawa mode correlators to demonstrate their use in NDE systems.

C. Major Accomplishments

We have demonstrated superb ZnO thin film layers. The films now look virtually like single crystals. Deposition rate is 18 μm per hour. We have constructed the first Sezawa mode correlator and the first monolithic Schottky diode correlator.

D. Problems Encountered

No major problems have been encountered.

E. Fiscal Status

Total amount of contract	\$504,302
Expenditures & commitments through 06/30/80	\$457,705
Estimated funds required to complete work	\$46,597
Estimated date of completion of work	30 September 1980

F. Action Required by ARPA/ONR

Renewal of the program on October 1, 1980

II. TECHNICAL PROGRESS REPORTS

A. ZnO Technology Development

In the last six months, we have been carrying out a series of runs to find the optimum conditions for sputtering ZnO. Our efforts have been very successful as we presently have a set of deposition parameters where the ZnO quality is the best we have done so far, and probably better than anything reported in the open literature. The new set of parameters are:

r-f power	= 1.25 kw
oxygen partial pressure	= 7 μm
target to substrate spacing	= 4.2 cm
substrate temperature	= 500° C
sputtering rate	= 18 $\mu\text{m}/\text{hour}$

The films were evaluated by x-ray diffraction, x-ray rocking curves, scanning electron microscopy, and reflection electron diffraction (RED). A summary of the results and curves is in a paper that was submitted for publication to *Applied Physics Letters* in July. The x-ray results show a full width at half maximum of the (0002) peak of 0.2° and show very clearly that the

Cu- α_1 and Cu- α_2 lines are split. The RED results show a very well defined pattern of spots corresponding to diffraction planes in the film; this indicates an excellent orientation in the films. The x-ray and electron diffraction results are by far the best we have ever seen and indicate that the films are almost single crystalline.

We will be continuing our characterization runs to investigate further the effects of substrate temperature and target to substrate spacing. The

ZnO films will still be evaluated in the same fashion, but we will be adding a few more evaluation tests, namely adhesion by indenting the films with a Vickers indenter, thickness uniformity and surface smoothness with an Alpha-step height profiler, optical transmission of a laser beam, and resistivity.

Measurement on resistivity indicate outstanding resistivities as high as 10^9 ohm-cm . Preliminary adhesion measurements also indicate very uniform adhesion.

B. Sezawa Wave Devices

In the last progress report, we reported on the fabrication of broadband (31 MHz) monolithic Sezawa wave delay lines. During the last six months, we have fabricated delay lines with the same bandwidth, but with 4 dB lower loss (18 dB) . We have also fabricated high efficiency ($F_T = -50$ dBm) broadband (25 MHz) Sezawa wave convolvers and demonstrated them in pulse compression experiments. Finally, we have fabricated Sezawa wave storage correlators and isolated several problems unique to Sezawa wave devices. Solutions to these problems are presented.

1. Sezawa Wave Delay Lines

We have fabricated short (4 mm) Sezawa wave delay lines with very low loss (10 dB) . Of this loss, 6 dB is due to the bidirectionality of each transducer, 1.5 dB is due to ZnO loss¹, .2 dB is due to resistive losses in the 1 mil diameter bonding wire and tuning inductor, and the remaining 2.3 dB is probably due to bulk wave excitation. With the use of the five element tuning circuit shown in Fig. 1, a 3 dB bandwidth of 31.5 MHz was achieved with 18 dB insertion loss (see Fig. 1).

2. Sezawa Wave Convolvers

Sezawa wave convolvers with an excellent efficiency of -50 dBm and a bandwidth of 25 MHz (Fig. 2) were fabricated. Only three elements (Fig. 2) were used for the interdigital transducer (IDT) tuning. The device parameters are given in Table I. The results of 5 bit and 11 bit Barker Code correlation are shown in Fig. 3a and 3b, respectively.

A series of chirp correlation experiments were performed to see if dispersion would limit the usable time-bandwidth product of these devices. The experiments used 3 μ s long chirp signals of variable bandwidths up to a maximum of 23 MHz bandwidth. (A variation of 23 MHz in 3 μ s is the maximum frequency slewing rate obtainable from our chirp generators.) To avoid pulse broadening due to the nonlinearity of the chirp frequency variation with time, one chirp generator was used, and its output was mixed with two cw signals to generate the necessary up and down chirp signals (Fig. 4). Using the input 23 MHz chirp shown in Fig. 5a, the compressed output pulse is shown in Figs. 5b and 5c. The 4 dB pulse width is 44 ns, and the total pulse compression is 68 . The theoretical compression is 3×23 or 69 . The sidelobes are not as small as theoretically expected, nor are they symmetric about the central peak. This is due to the fact that (1) the variation of chirp frequency with time is not linear, and (2) the amplitude of different frequency components of the input chirps varies by as much as 2 dB (Fig. 5a).

The fact that the output pulse width is not limited by dispersion is a remarkable result. The variation in group delay over the 23 MHz bandwidth is $.2$ μ s. Thus, one might expect the minimum output pulse width to be of this order. However, it is shown in Appendix A that dispersion limits Sezawa wave convolvers to a usable time bandwidth product of roughly 100 . In

Appendix A, we also examine the effects of dispersion on correlation and show that in most (but not all) modes of operation, dispersion does not limit the performance of the storage correlator.

3. Sezawa Wave Correlators

A series of storage correlators have been fabricated and used in storage applications; however, their performance is inferior to the best of our Rayleigh wave correlators. A number of these problems have been solved.

The first problem to become apparent was the generation of bulk waves by our IDTs. This is more of a problem than in the past because of the use of 4 finger pair (fp) IDTs rather than 10 fp IDTs. Another factor is that the ZnO films are thicker (8 μm for Sezawa wave devices and 1.6 μm for Rayleigh wave devices), and so bulk waves are more easily excited in the ZnO/Si structure.

This problem has been solved by bonding the Si substrate to a brass carrier box with indium solder. A major portion of the bulk wave power which reaches the back surface of the Si substrate is transmitted into the indium layer and brass box since the impedance of indium and silicon are about the same ($Z_{\text{Si}} = 22$, $Z_{\text{In}} = 19$), and the impedance of brass is slightly higher ($Z_{\text{Br}} = 31$). Using this technique, we have eliminated the problem of spurious bulk waves generated by the interdigital transducers.

A second problem is associated with the fact that our top plates are not rectangles but rhomboids (Fig. 6a). The reason for using slanted ends is that most of the spurious surface wave power generated by the top plate writing or reading signal misses the IDTs. The problem with using this design for Sezawa waves is that the SAW velocity is significantly different in the metallized region and the region without a shorting plane at the surface. If one is only

interested in delay lines, then this is not a problem if both ends of the top plate are slanted the same way (Fig. 6a) and the phase distortion at one end is compensated by the phase distortion at the other end. However, if the device is used as a storage correlator, and it is desired to store charge in diodes, then phase distortion of more than 45° is not acceptable.

For Rayleigh wave devices, this has not been a problem since $\Delta v/v$ is small (i.e., the SAW velocity in the shorted region is about the same as the SAW velocity in the electrically free region). For a 25° angle on the top plate and 1 mm beamwidths, the phase distortion for ZnO/Si Rayleigh wave devices is 2° . For our ZnO/Si Sezawa wave devices, the phase distortion is 87° ! Our proposed solution is shown in Fig. 6b. This eliminates the phase distortion problems and also should decrease our electromagnetic feedthrough problems since there is now a ground plane over most of the device.

C. Monolithic Storage Correlator Theory

In previous progress reports and papers, we have included a great deal of experimental data on the dependence of correlator output on various parameters such as acoustic voltage, writing signal voltage, etc. We have developed a comprehensive theory for the charging and reading processes in the monolithic storage correlator. A complete presentation of the theory is given in a paper accepted for publication in IEEE Transactions on Sonics and Ultrasonics (Appendix B). Experimental and theoretical results are given for the dependence of correlator output on six parameters: acoustic signal duration and amplitude, write signal duration and amplitude, and read signal duration and amplitude. To illustrate this theory, we present two of these results here.

The dependence of correlator output on acoustic signal duration is shown in Fig. 7. Note that the experimental and theoretical results are approximately linear. There is a slight upturn in both the experimental and theoretical results when the acoustic and write signals have approximately the same duration (10 ms). This approximately linear characteristic was surprising when it was first experimentally discovered since the output is very nonlinear when both the write and acoustic signals are varied together. The reason for the linearity is clear from the terms in the theoretical expression. When the write and acoustic durations are varied together, the component of charge with no spatial variation also varies. However, if the write signal duration is fixed (as in Fig. 7), then the component of charge with no spatial variation is constant (and not zero) and the output is proportional to the component of charge with spacing $2\pi/\lambda$, i.e., to the duration of the acoustic signal.

The dependence of correlator output on write signal amplitude is shown in Fig. 8 for several read voltages. The output saturates for write voltages greater than 1.5 V (for 10 ms charging times).

The theory has been used in the design of improved storage correlators. It has also been used to predict the optimum silicon doping density to use for our Sezawa wave devices (Fig. 9). The optimum doping for Sezawa wave devices ($8 \times 10^{14} \text{cm}^{-3}$) is twice the optimum doping for Rayleigh wave devices ($4 \times 10^{14} \text{cm}^{-3}$).

D. Comparison of Various Systems Based on Bandwidth Considerations

In our last progress report, we compared the theoretical maximum bandwidth obtainable (when the optimum tuning circuit is used) for several

different systems such as LiNbO_3 IDTs, ZnO/Si Sezawa wave IDTs, and ZnO/Si Rayleigh wave IDTs. We modelled the IDT as a fixed resistor and capacitor in parallel and used a result derived by Fano to compare the systems.

We have derived a theory based on Fano's work² to predict the optimum bandwidth for an IDT when the IDT is represented by a four element circuit model instead of just two elements. These results are summarized in Appendix C. The differences between the old formulation and our new results are shown in Fig. 10. This figure is a plot of the theoretical maximum bandwidth as a function of the tuning network mismatch loss. As can be seen, the inclusion of a frequency dependent radiation resistance and reactance dramatically limits the theoretically maximum bandwidth (for a given mismatch loss).

A number of systems of interest are compared in Fig. 11. LiNbO_3 IDTs are still the best system to use; however, it can be seen that Sezawa wave IDTs are almost as good. A number of additional comparisons are made in Appendix C such as the dependence of bandwidth on the number of finger pairs, etc.

E. Schottky Diode Storage Correlator

In the past six months, a great deal of progress has been made on the Schottky diode storage correlator. We have demonstrated such a correlator with a correlation efficiency of -77.4 dBm when operating in the acoustic to plate readout mode. More importantly, this efficiency was achieved using a short pulse of approximately 5 ns duration to perform the storage operation. Figure 12 shows the correlation output on the upper trace with a one volt input acoustic signal, a one volt acoustic readout signal, and

63 dB of system gain. Note the second correlation output resulting from the acoustic readout signal reflecting off the transducer at the other end of the device.

The lower trace shows the insertion loss of the system for a one volt amplitude input signal.

Improvements have also been achieved in the storage times of these devices. Whereas our earlier devices have had storage times of the order of 200 μsec , this device displayed a storage time close to 1 msec. Studies we have carried out by depositing ZnO on large area ($750,000 \mu\text{m}^2$) diodes lead us to believe that the ZnO sputtering process degrades the storage time performance of the diodes by a factor of three on the average.

The largest single factor responsible for the increased quality of these devices is the improvement of the PtSi Schottky barrier technology. We have gained access to an extremely clean platinum deposition facility owned by Varian Associates, Inc. This is capable of reducing, quite dramatically, the level of trace impurities at the Schottky barriers, which would tend to increase leakage currents and lower the percentage of good diodes on a particular wafer. We have indeed observed a dramatic improvement in the reliability of the process using the Varian system. The next step to be taken in improving the quality of these devices will be to reduce leakage in the diodes due to the high electric fields at the edges of the diodes, the so-called "edge effect" leakage. In order to do this, we propose to somewhat enlarge the diodes so that it will be possible to encircle the edge of each diode with a p+ diffusion "guard ring," the purpose of which is to increase the radius of curvature at the edges of the diode and hence lower the electric fields in these regions and hence decrease the leakage current in the diodes.

Storage times of the order of 10 ms are expected as a result.

F. Silicon on Lithium Niobate

We have also studied the laser annealing of polysilicon deposited on lithium niobate in hopes of being able to produce semiconductor quality thin silicon films from which convolvers and correlators can be made.

Our studies have been carried out using a 7 watt argon laser with a scan system capable of repeated scans of a 40 μm spot over a large area of a target.

We have attempted the laser annealing on lithium niobate samples with barrier layers of SiO_2 ranging in thickness from .1 micron to 1 micron. The results of these studies indicate that it is indeed possible to anneal the small grain polysilicon in order to obtain "long grain" polysilicon material with grain dimensions of 5 microns wide by 40 microns long. These grain dimensions would prove suitable for fabrication, for example, of a Rayleigh wave amplifier as a monolithic silicon on LiNbO_3 structure.

The major drawback in the use of this technique at the present time is the difficulty in preventing the generation of cracks in the lithium niobate. These cracks are apparently a result of thermal expansion shock in the lithium niobate due to the heat absorbed in the silicon layer.

The situation now presented to us is one of finding the optimum conditions of laser power, SiO_2 layer thickness, and silicon deposition method that will enable us to anneal the silicon without damaging the lithium niobate.

G. FET Storage Correlator

We have carried out theoretical investigations into the possibility of making a device similar in operation to the storage correlator which, like the Schottky diode correlator, will have the advantage of fast signal read in. The basic structure of this device is shown in Fig. 13. With proper geometries of the FET array, this device will be able to store a signal in times less than a nanosecond, which is quite fast enough with which to sample an rf cycle that is 8 ns long.

We are now working with the Integrated Circuits laboratory to design masks and a processing schedule with which this device can be realized.

Table I
Parameters of Sezawa Wave Convolvers

ZnO thickness	7 μm
SiO ₂ thickness	2000 \AA
Silicon thickness	350 μm
IDT and top plate metal thickness	1000 \AA
Beamwidth	1 mm
Length of interaction region	2.3 cm
Silicon orientation	(100)
IDT finger width and spacing	8 μm
Number of finger pairs	4
Convolution efficiency	-50 dBm
Insertion loss	31 dB
Resonant frequency	155 MHz
Bandwidth (3 element tuning circuit)	25 MHz
Group velocity at 150 MHz	4320 m/s

References

1. J. deKlerk, R. W. Weinert, and B. R. McAvoy, "SAW Attenuation in Hydrothermally Grown Single Crystal ZnO," Proc. Ultrasonic Symposium, Cherry Hill, New Jersey, September 1978.
2. R. M. Fano, "Theoretical Limitations on the Broadband Matching of Arbitrary Impedances," J. Franklin Inst., vol. 244, pp. 57 & 139, 1950.

Figure Captions

1. Dependence of insertion loss on frequency for a 4 mm long Sezawa wave delay line. The 5 element IDT tuning circuit is also shown.
2. Variation of convolution efficiency on frequency for a Sezawa wave convolver. The 3 element IDT tuning circuit is also shown.
3. (a) 5 bit Barker Code correlation
(b) 11 bit Barker Code correlation
4. Circuit diagram for chirp compression experiment.
5. Chirp compression
(a) Input chirp
(b) Output pulse (200 nS/div)
(c) Output pulse (20 nS/div)
6. (a) Rayleigh wave top plate metallization
(b) Sezawa wave top plate metallization
7. Dependence of correlator output on acoustic signal duration:
_____ Complete theory; _____ Approximate theory; Experimental
8. Dependence of correlator output on write signal amplitude:
_____ Complete theory; _____ Approximate theory; Experimental
9. The effect of doping level on the acoustic wave attenuation, correlation efficiency (without attenuation) and total correlation efficiency
10. Comparison of bandwidth predictions using the full transducer model (___) and simple R-C model (__) for a Sezawa wave transducer ($f_0 = 165$ MHz , $w = 1$ mm , on (100) Si)
11. Comparison of LiNbO_3 , ZnO/Si Sezawa wave, and ZnO/Si (first $\Delta v/v$ peak Rayleigh wave transducer ($f_0 = 165$ MHz , $w = 1$ mm)

12. Schottky diode correlation with 1 volt input signal level

Top trace: Correlation output 200 mV/div

Bottom trace: Insertion loss 50 mV/div

13. A. FET correlator structure top view

B. FET correlator structure cross-sectional view

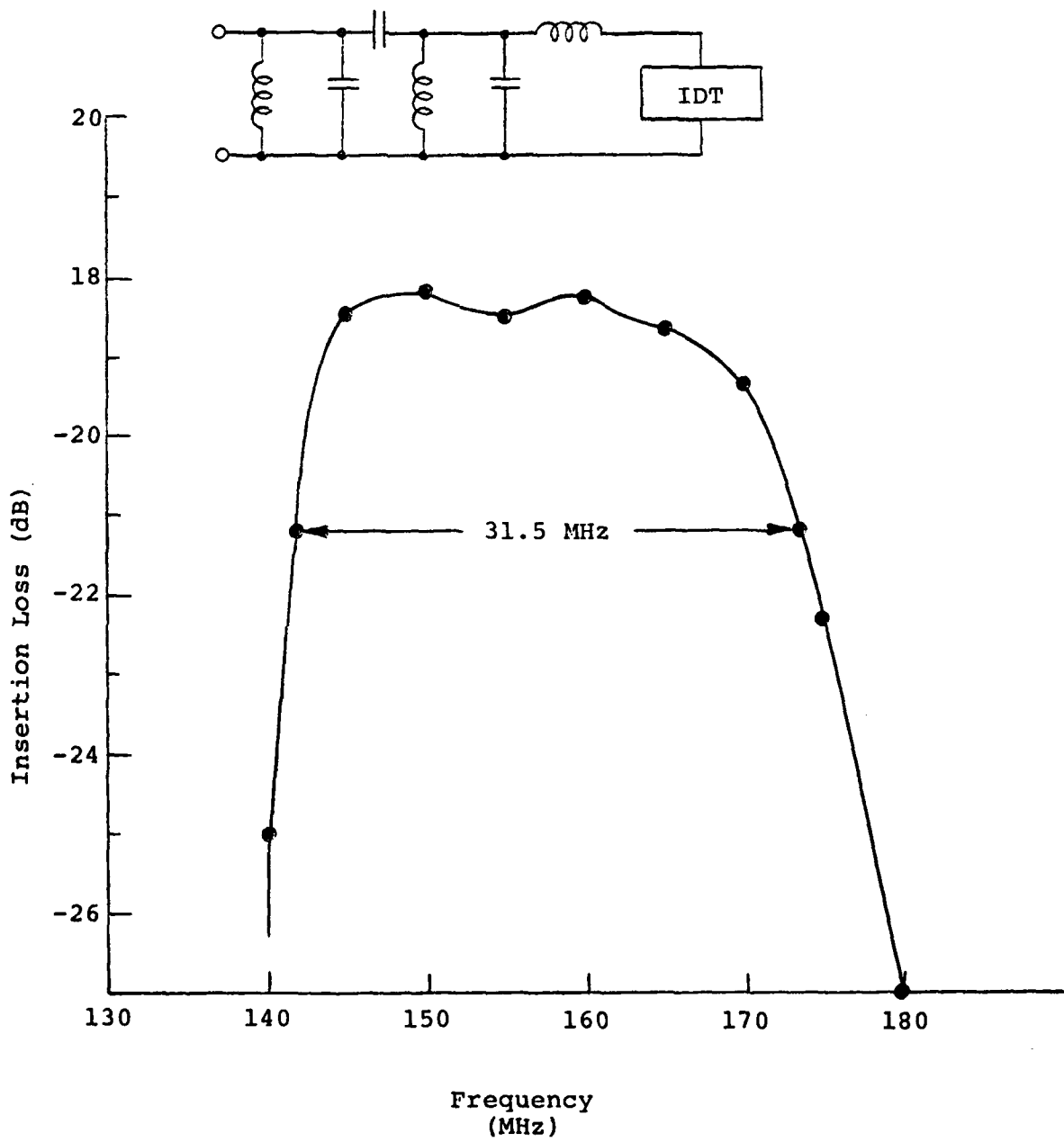
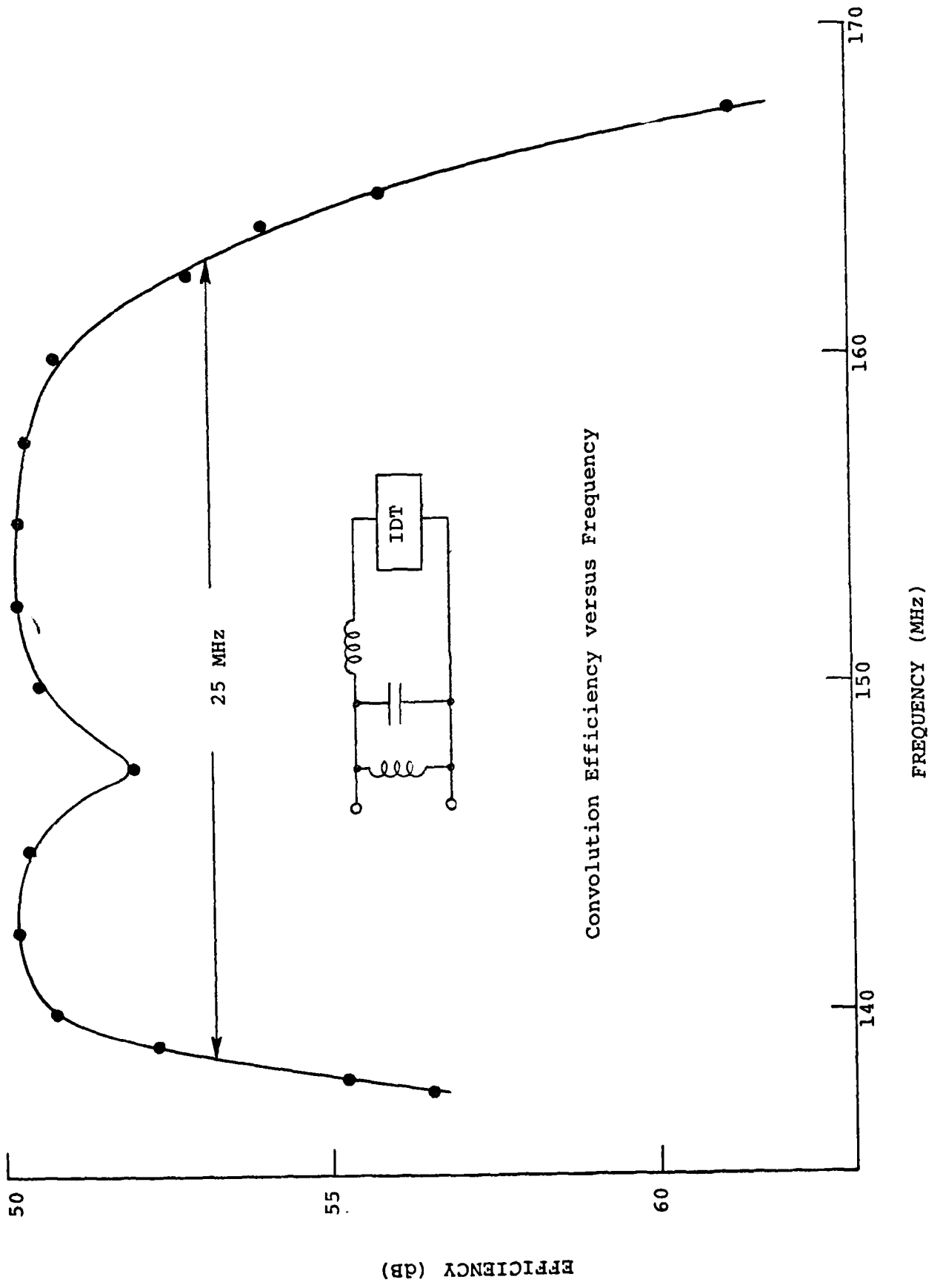


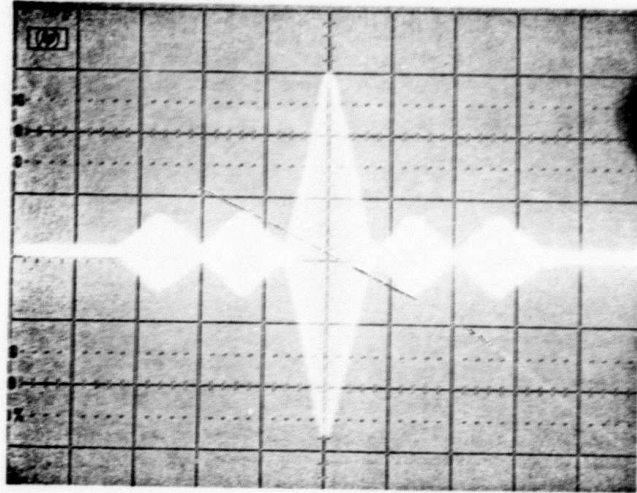
Figure 1



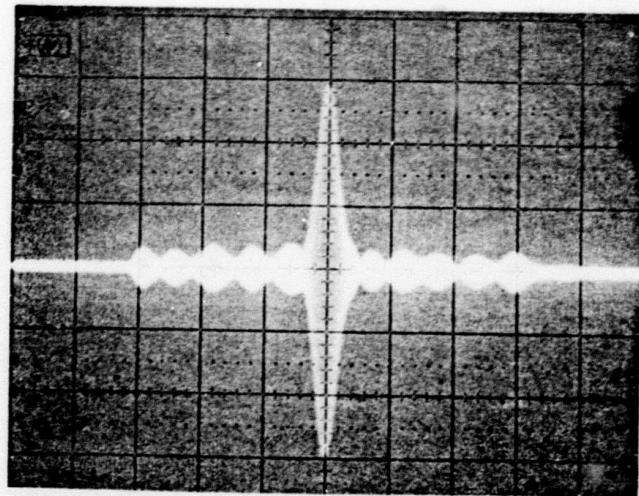
EFFICIENCY (dB)

Figure 2

FREQUENCY (MHz)



(a) $.5 \mu\text{s}/\text{div}$



(b) $.5 \mu\text{s}/\text{div}$

Figure 3

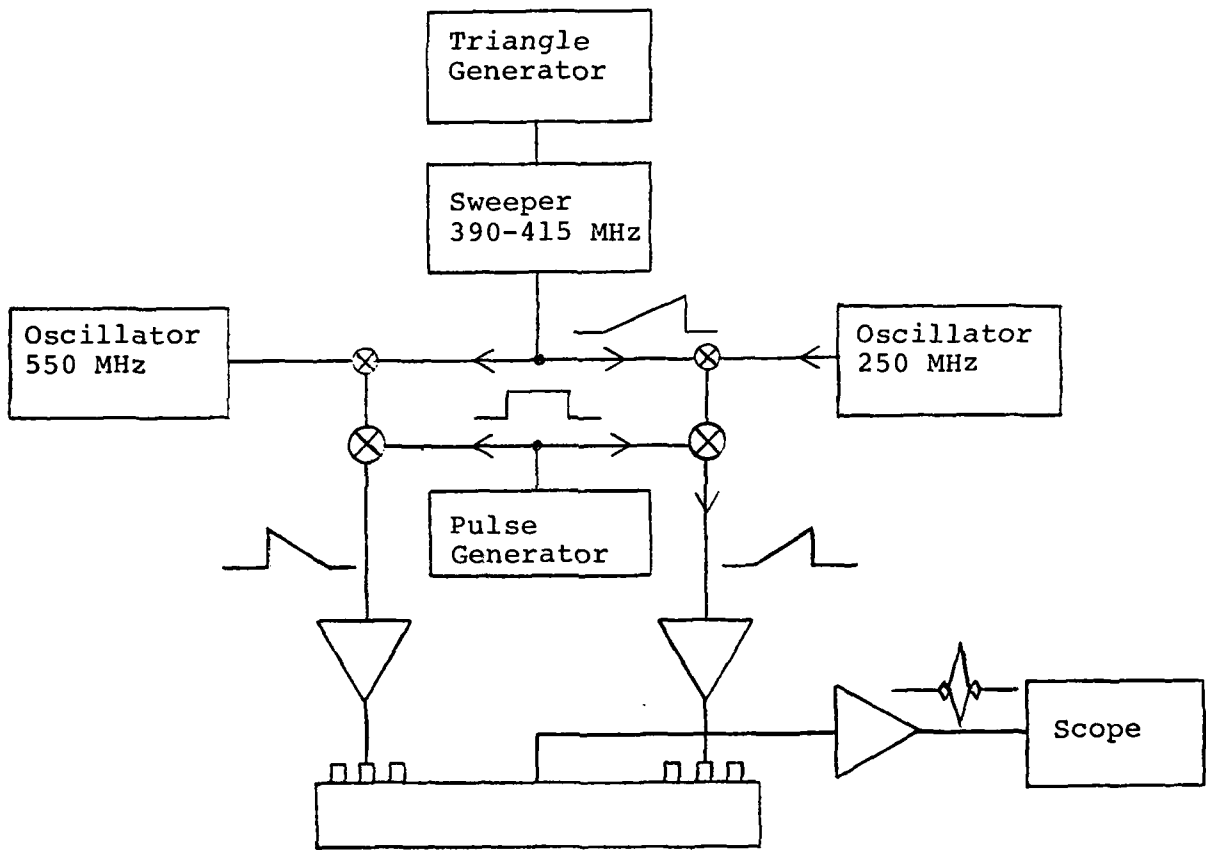
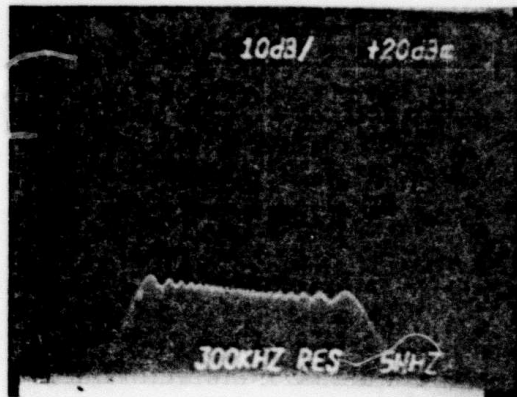
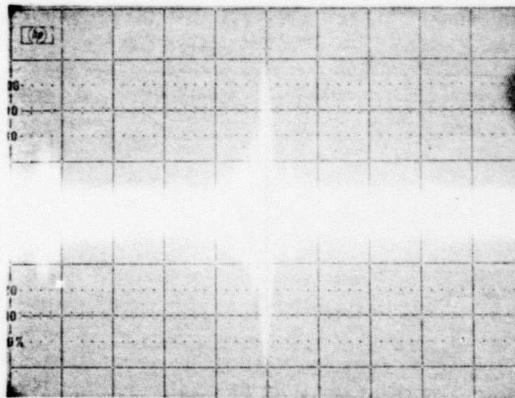


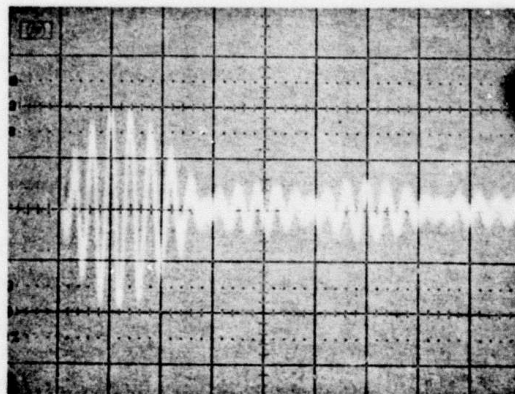
Figure 4



(a) 5 MHz/div



(b) .2 μ s/div



(c) .02 μ s/div

Figure 5

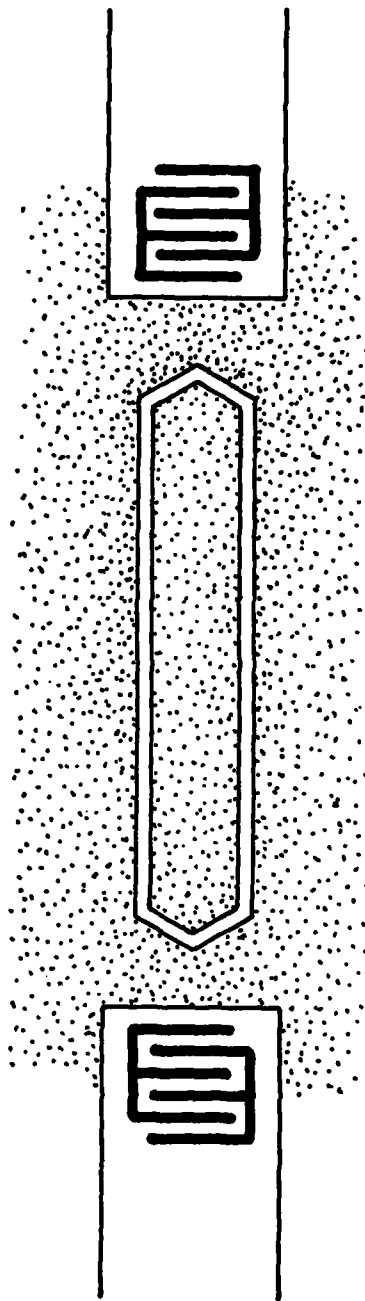
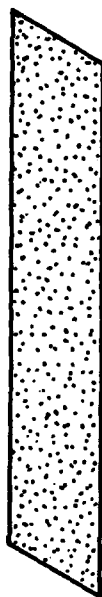


Figure 6

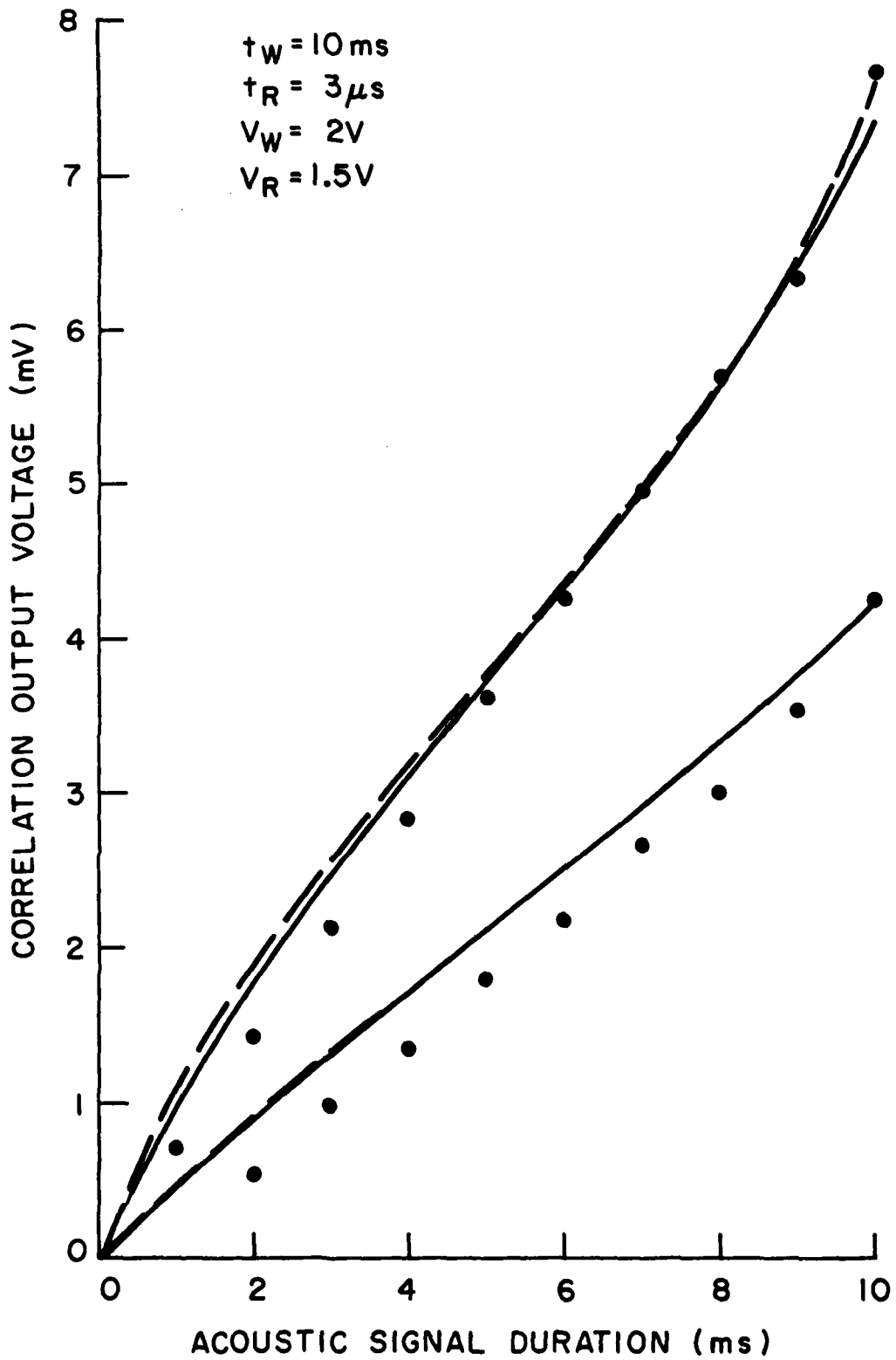


Figure 7

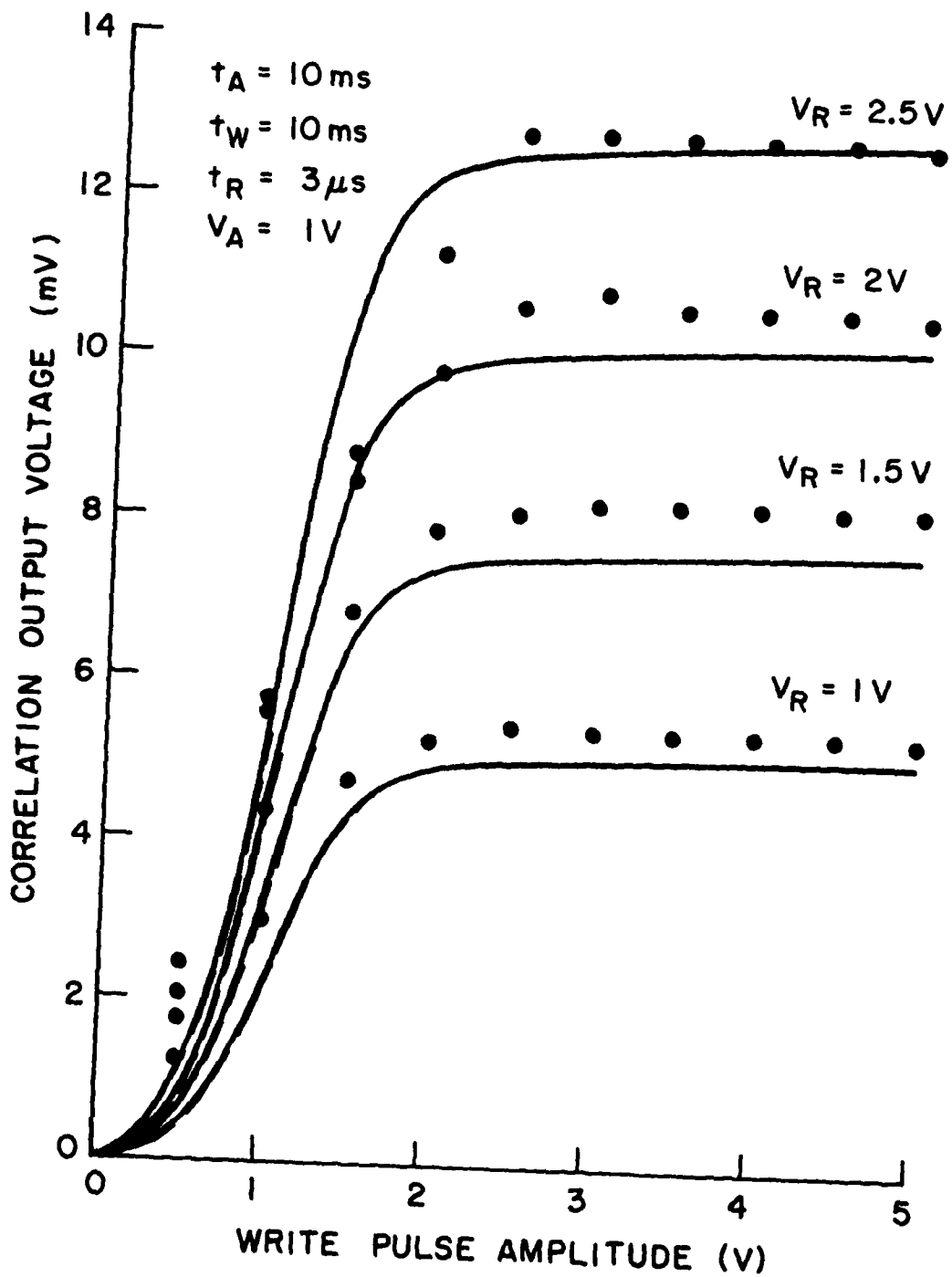


Figure 8

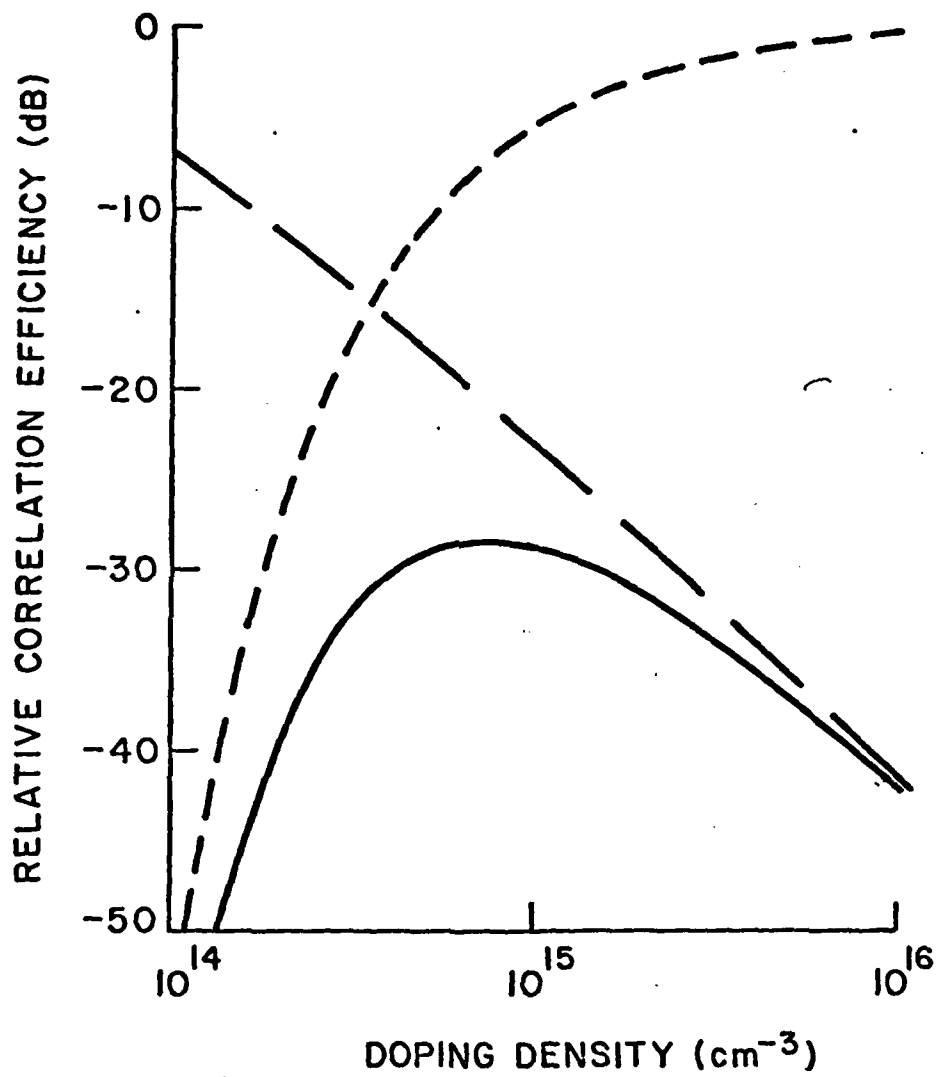


Figure 9

4438.7

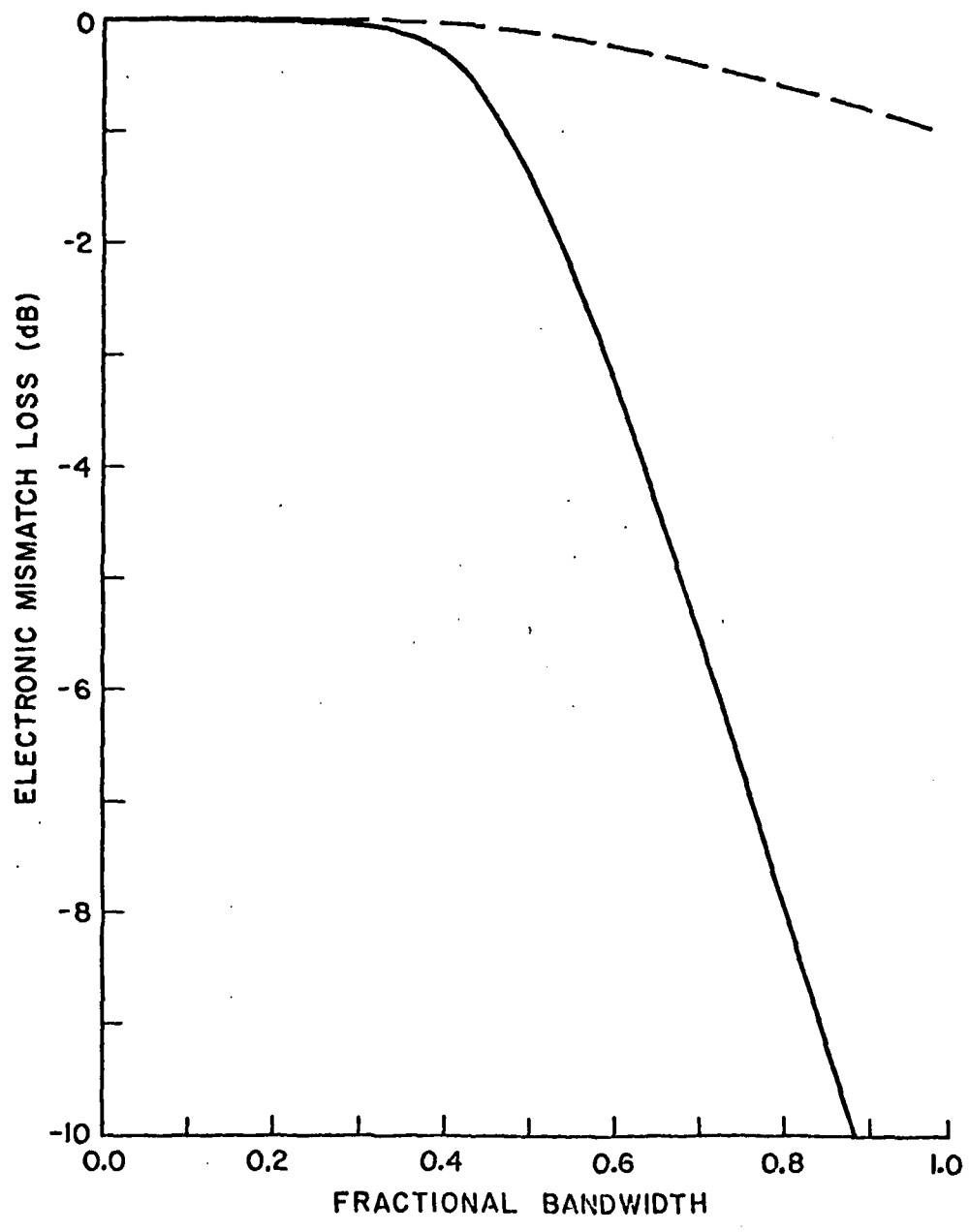


Figure 10

4438-5

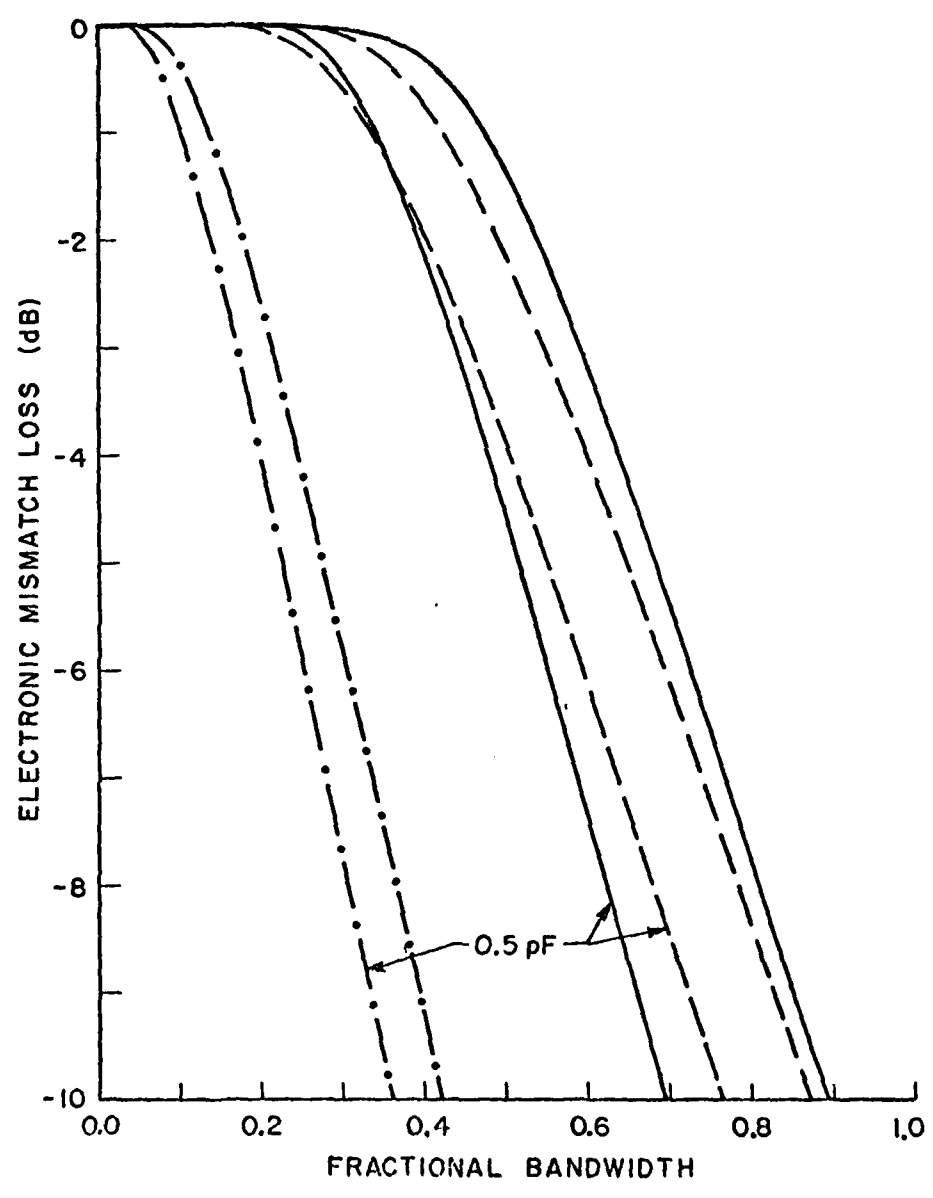
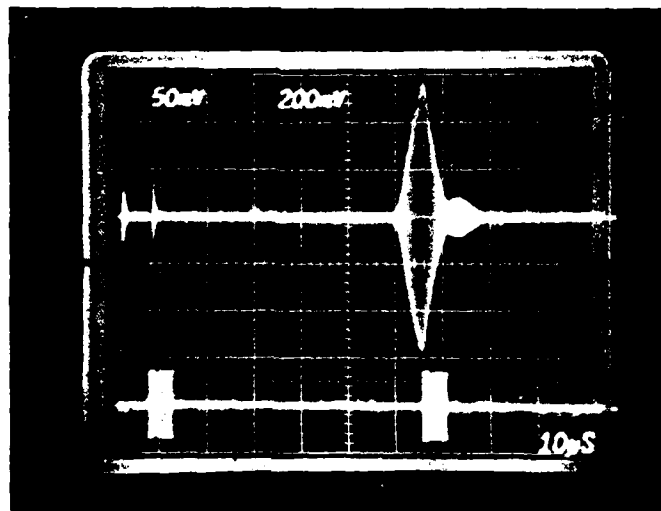
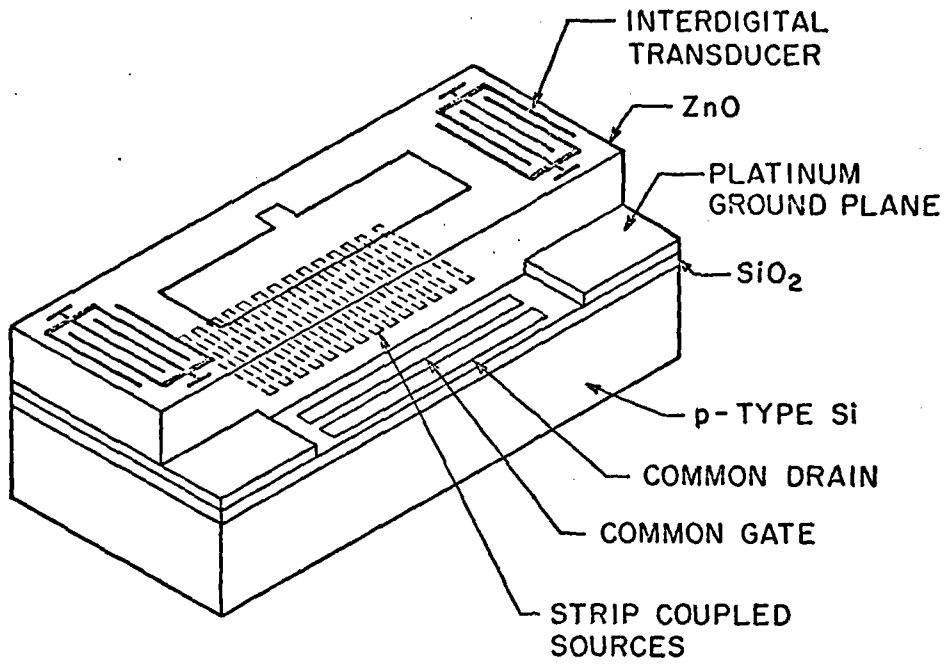


Figure 11



10 μ S/div

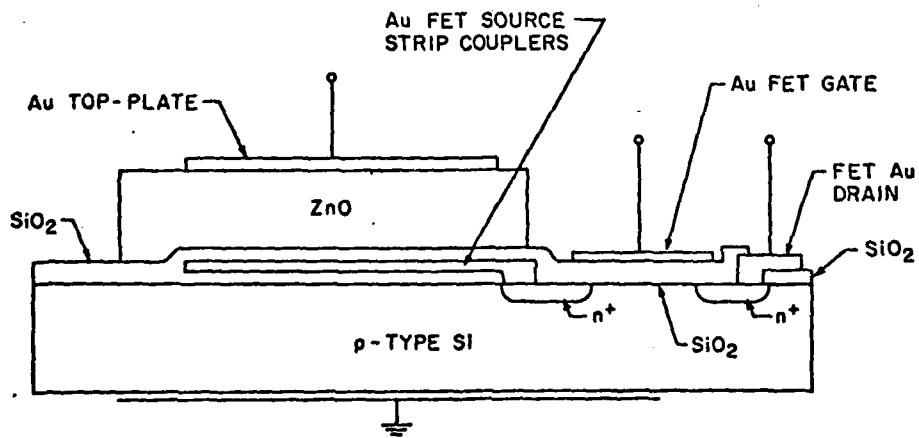
Figure 12



4372-1

4372-2

(a)



(b)

Figure 13

Appendices

- A. J. E. Bowers, "A Technique for Calculating the Bandwidth-Loss Relationship for Acoustic Transducers," Stanford University, unpublished.
- B. H. C. Tuan, J. E. Bowers, and G. S. Kino, "Theoretical and Experimental Results for Monolithic SAW Memory Correlators," accepted for publication, IEEE Trans. on Sonics and Ultrasonics.
- C. J. E. Bowers, "Effects of Dispersion," Stanford University, unpublished.
- D. J. E. Bowers, B. T. Khuri-Yakub, and G. S. Kino, "Broadband Efficient Thin Film Sezawa Wave Interdigital Transducers," Appl. Phys. Lett., vol. 36, no. 10, pp. 806-807, 15 May 1980.
- E. J. E. Bowers, G. S. Kino, D. Behar, and H. Olaisen, "Adaptive Deconvolution Using an ASW Storage Correlator," submitted to Special Issue of IEEE Trans. on Sonics and Ultrasonics, March 1980.

A Technique for Calculating the Bandwidth-Loss Relationship for Acoustic Transducers

Ginzton Laboratory
Stanford University
Stanford, CA 95305

Abstract

A technique is developed to determine the maximum bandwidth obtainable from a transducer matched through the optimum matching network to an ideal source. The transducer is modeled by four elements. This technique can be applied to surface acoustic wave (SAW) transducers or bulk acoustic wave transducers. The technique was used 1) to compare SAW IDTs on various materials such as LiNbO_3 and ZnO/Si , 2) to compare different modes such as the Rayleigh and Sezawa modes in ZnO/Si structures, and 3) to compare different substrate orientations. It is found that Sezawa wave IDTs in $\text{ZnO}/(100)\text{Si}$ offers the best performance of the monolithic structures considered, and that these transducers are as good as LiNbO_3 IDTs for obtaining broad bandwidth. The design of transducers for maximum bandwidth is also considered using this technique.

I. Introduction

A major problem in the design of SAW devices is obtaining the broadband operation necessary for many applications, such as utilization in spread spectrum systems. There has been a major effort in developing monolithic versions of many SAW devices such as delay lines, convolvers, and storage correlators. These devices have been narrowband, and consequently, there was a search for other monolithic systems which had broader bandwidth such as Sezawa wave IDTs and edge bonded transducers. These systems have been compared by considering the SAW coupling coefficient or transducer Q ; however, the transducer bandwidth (for a given loss) is a function of several of these parameters, and it is not always evident which system is best. In this paper, a technique is developed to theoretically compare such alternatives on the basis of bandwidth considerations. After a choice of transducer is made, the technique described here can be used to determine the optimum design criteria. Smith et. al. [1] and Khuri-Yakub[2] have addressed the problem of transducer design and heuristically argued that the acoustic Q should be equal to the electronic Q for optimum bandwidth. This is an approximate result which is only valid for small mismatch losses and series inductor tuning. This rule is not applicable to more sophisticated tuning circuits. The technique described in this section determines the optimum transducer parameters assuming the best matching network for these parameters is used. In particular, balanced and unbalanced operation can be compared, and the optimum width and number of finger pairs can be determined.

II. Theory

1. History

Bode[3] recognized that a source can be matched to a load consisting of a capacitor and a resistor in parallel (Fig. 1) only over a limited frequency range. He obtained the limitation on the bandwidth

$$\int_0^{\infty} \ln \frac{1}{|\rho(\omega)|} d\omega \leq \frac{\pi}{RC} \quad (1)$$

where ρ is the input reflection coefficient.

$$\rho(\omega) = \frac{Z(\omega) - 1}{Z(\omega) + 1} \quad (2)$$

where $Z(\omega)$ is the impedance of the matching network and load. If ρ is constant (ρ_m) over the desired bandwidth (ω_B) and equal to 1 over the rest of the frequency spectrum, then Eq. (1) becomes

$$\omega_B \ln \frac{1}{\rho_m} \leq \frac{\pi}{RC} \quad (3)$$

As expected, the price of broader bandwidth is higher loss.

As a first approximation the circuit model of an IDT can be represented as a fixed value resistor and capacitor in parallel, and Eq. (1) can then be used to determine the relationship between bandwidth and loss. This has been done by Reeder[4] and Schellenberg[5].

The problems with this approximation (see Fig. 2a) are 1) the acoustic conductance is not at all constant, and 2) the acoustic susceptance is nonzero:

$$G(\omega) = G_{ao} \left(\frac{\sin X}{X} \right)^2 \quad (4)$$

$$B(\omega) = G_{ao} \frac{\sin(2X) - 2X}{2X^2} \quad (5)$$

where

$$X = \frac{N\pi(\omega - \omega_0)}{\omega_0} \quad (6)$$

and ω_0 is the resonant frequency and N is the number of finger pairs.

Fano[6] extended the work of Bode by considering the matching of a source to an arbitrary passive load. He then applied his results to the case of a resistor and inductor in parallel (the dual network of Bode's network) and rederived Eq. (1).

In the next section, we shall demonstrate that a passive circuit composed of four circuit elements with frequency independent values can represent the IDT admittance represented by Fig. 2a and then use this model with Fano's theory to obtain the bandwidth-loss relationship in the general case for an acoustic transducer.

2. Circuit Model

The circuit model shown in Fig. 2b has been used to model bulk wave transducers[7]; however, this is the first instance the author is aware of that the model has been applied to SAW transducers.

The relation between the parallel circuit for the IDT (Fig. 2a) and the model (Fig. 2b) can be found by expanding the expressions for the transducer admittance Eq. (4) and (5) about the transducer center frequency, and expanding the model admittance about the same frequency. If the zero and first order terms in $(\omega - \omega_0)$ for the real and the imaginary parts of the transducer admittance are equated, then there are four equations to determine the four model parameters: R, C_0, L and C_1

$$R = \frac{1}{G_{ao}} \quad (7)$$

$$C_0 = C_T + C_P \quad (8)$$

$$L = \frac{N\pi}{3\omega_0 G_{ao}} - \frac{C_0}{2G_{ao}^2} \quad (9)$$

$$C_1 = \frac{1}{L\omega_0^2} \quad (10)$$

where C_T is the transducer finger capacity and C_P is the pad and stray capacity. For most SAW transducers, $\Delta v/v$ is small enough ($\Delta v/v < .03$) that the imaginary part of the admittance is predominantly due to the parallel capacitor, and a better match between the transducer and model admittances is obtained if the first three terms in the expansion of the real part of the admittance are equated, and only the first term of the imaginary parts is equated. The model relations in this case are the same as Eqs. (7) to (10) except that the expression for L becomes

$$L = \frac{\pi N}{2\sqrt{3}\omega_0 G_{ao}} \quad (11)$$

For the case of a ZnO/Si Sezawa wave transducer the real and imaginary parts of the transducer admittance are shown in Fig. 3. Also shown in these figures are the model predictions. Note that the agreement is good near the resonant frequency, but for larger bandwidths, the real part of the model admittance does not drop as rapidly as the transducer admittance. Hence, the predictions made in the next section will be optimistic for large bandwidths. This was the case for all of the types of transducers studied. For the sake of comparison, the transducer and model parameters were determined for 1) Sezawa wave IDTs: ZnO/ (100)Si and (111) Si, 2) First order Rayleigh wave IDTs: ZnO/ (100)Si and (111)Si for the first and second peaks in $\Delta v/v$ and 3) Rayleigh wave IDTs on YZ LiNbO₃. These parameters are tabulated in Table 1 for use in a later section of this paper. The capacity of the bonding pads C_P is negligible for transducers on a semi-infinite LiNbO₃ substrate. However, all of the ZnO/Si monolithic transducers considered here have either IDTs at the top surface and a shorting plane at the interface (Sezawa wave, Rayleigh

wave (first $\Delta v/v$ peak)) or IDTs at the interface and a shorting plane at the top surface (Rayleigh wave (second $\Delta v/v$ peak)). Consequently, the bonding pad capacity cannot be neglected for monolithic devices.

3. Integral Equations

Consider the system in Fig. 4a. Any physically realizable load can be represented by a reactive two terminal network terminated by a resistance. This resistance can be made equal to the source resistance by incorporating a transformer in the reactive network (Fig. 4b). It is obvious from Fig. 4b that the transducer network will limit the power transmission from the source to the load resistor; independent of what the matching network (N_m) is. Fano's analysis is more tractable, if the two networks are flipped (Fig. 4c) so the source is driving the transducer network N_T . Fano considers the function $\ln 1/\rho$ where ρ is the reflection coefficient of the matching network and load, and shows that for each zero in the right half plane of the load transmission coefficient t_1 , an integral equation is obtained relating

- ρ (reflection coefficient of the load plus matching network)
- ω (angular frequency)
- λ_i (zeros of the matching network that lie in the right half plane.)

In particular, he obtained the relations

$$\int_0^{\infty} \omega^{-2(k+1)} \ln \frac{1}{|\rho|} d\omega = (-1)^k \frac{\pi}{2} F_{2k+1}^0 \quad (12)$$

for a zero of order k at the origin, and

$$\int_0^{\infty} \omega^{2k} \ln \frac{1}{|\rho|} d\omega = (-1)^k \frac{\pi}{2} F_{2k+1}^{\infty} \quad (13)$$

for a zero of order k at infinity. A_j^i is the i th coefficient of the Taylor series

expansion of $\ln 1/|\rho_1|$ about the point j and

$$F_{2k+1}^0 = A_{2k+1}^0 - \frac{2}{2k+1} \sum_i \lambda_i^{-(2k+1)} \quad (14)$$

$$F_{2k+1}^\infty = A_{2k+1}^\infty - \frac{2}{2k+1} \sum_i \lambda_i^{2k+1} \quad (15)$$

The performance of the system is given by the left hand side of the integral equations and the limitations on the performance is given by the right hand side. The transducer characteristics enter through A_j^i and the matching network characteristics enter through the positions of the zeros of the matching network λ_i .

4. Application to Acoustic Transducers

The impedance of the model shown in Fig. 2b is

$$Z_T = \frac{1}{R} \frac{1 + s(C_1 + C_0) + s^2 LC_1 + s^3 LC_1 C_0}{sC_1 + s^2 C_1 C_0} \quad (16)$$

where $s = j\omega$. All impedances have been normalized to R_s . The reflection coefficient is

$$\rho_1 = \frac{Z_T - 1}{Z_T + 1} \quad (17)$$

The transmission coefficient is

$$t_1 = \frac{2(sRC_1 + s^2 RC_1 C_0)}{1 + s(C_1 + C_0 + RC_1) + s^2(LC_1 + RC_1 C_0) + s^3 LC_1 C_0} \quad (18)$$

There is one zero of t_1 at the origin and two zeros at infinity. The function of interest is

$$F = \ln \frac{1}{|\rho_1|} = \ln \frac{1 + s(C_1 + C_0 + RC_1) + s^2(LC_1 + RC_1 C_0) + s^3 LC_1 C_0}{1 + s(C_1 + C_0 - RC_1) + s^2(LC_1 - RC_1 C_0) + s^3 LC_1 C_0} \quad (19)$$

Expanding F about the origin yields

$$F = A_1^0 \omega + A_3^0 \omega^3 + \dots \quad (20)$$

Thus,

$$A_1^0 = \left. \frac{dF}{d\omega} \right|_{\omega=0} = 2RC_1 \quad (21)$$

Expanding F about infinity is equivalent to expanding F about $q = 1/\omega$ as $q \rightarrow 0$.

$$F = A_1^\infty q + A_3^\infty q^3 + \dots \quad (22)$$

Thus,

$$A_1^\infty = \left. \frac{dF}{dq} \right|_{q=0} = \frac{2R}{L} \quad (23)$$

$$A_3^\infty = \left. \frac{1}{6} \frac{d^3 F}{d^3 q} \right|_{q=0} = -\frac{2R}{L^2 C_3} \left(1 - \frac{R^2 C_3}{3L}\right) \quad (24)$$

where

$$\frac{1}{C_3} = \frac{1}{C_1} + \frac{1}{C_0} \quad (25)$$

Note that $C_3 \approx C_1$ and from Eqs. (7) to (10),

$$\frac{C_1}{L} \approx \frac{1}{(NR)^2} \quad (26)$$

so

$$A_3^\infty \approx -\frac{3R}{L^2 C_3} \left(1 - \frac{1}{3N^2}\right). \quad (27)$$

For an IDT, the number of finger pairs N is at least one; hence, A_3^∞ is negative.

This is in general true, and as we shall see, this is important for a solution to these equations to exist.

Using Eqs. (12),(13),(21),(23) and (27) we obtain the results

$$\int_0^\infty \frac{1}{\omega^2} \ln \frac{1}{|\rho|} d\omega = \frac{\pi}{2} (2RC_1 - 2 \sum_i s_i^{-1}) \quad (28)$$

$$\int_0^{\infty} \ln \frac{1}{|\rho|} d\omega = \frac{\pi}{2} \left(\frac{2R}{L} - 2 \sum_i s_i \right) \quad (29)$$

$$\int_0^{\infty} \omega^2 \ln \frac{1}{|\rho|} d\omega = \frac{\pi}{2} \left[\frac{3R}{L^2 C_3} \left(1 - \frac{1}{3N^2} \right) + \frac{2}{3} \sum_i s_i \right] \quad (30)$$

Examine first Eq. (29). This equation is the dual of the equation obtained by Bode when $s_i = 0$. Good matching occurs when $\rho \approx 0$ and $\ln 1/|\rho|$ is large. Thus, the left hand side of Eq. (29) is the area under a matching versus frequency plot. The value for the area depends on the transducer parameters and will be largest when $s_i = 0$. However, since Eq. (28) and Eq. (30) must also be satisfied, there will have to be several nonzero roots s_i . For the applications of interest in this paper, a flat frequency response over a given bandwidth is desired. According to Eq. (29), the best transmission over this bandwidth will occur when the transmission outside the bandwidth is zero and no "area" is wasted outside the desired bandwidth. Thus the ideal frequency dependence of the reflection coefficient is

$$\ln \frac{1}{|\rho|} = \begin{cases} \frac{\pi}{2} K & \text{when } \omega_1 \leq \omega \leq \omega_2 \\ 1 & \text{otherwise} \end{cases} \quad (31)$$

Eqs. (28) to (30) become

$$\frac{K}{2} \left(\frac{1}{\omega_1} - \frac{1}{\omega_2} \right) = RC_1 - \frac{1}{s_1} - \frac{1}{s_2} - \dots \quad (32)$$

$$\frac{K}{2} (\omega_2 - \omega_1) = \frac{R}{L} - s_1 - s_2 - \dots \quad (33)$$

$$\frac{K}{2} (\omega_2^3 - \omega_1^3) = \frac{3R}{L^2 C_3} - \frac{R^3}{L^3} + s_1^3 + s_2^3 + \dots \quad (34)$$

For the matching network to be realizable, the zeros in the right half plane will be symmetric about the real axis. Thus the s_i are real or occur in complex conjugate pairs. We shall assume that the transducer parameters (R, L, C_1, C_0) and the desired passband frequencies (ω_1 to ω_2) are known

and that it is desired to find the matching parameter K . At least three variables K, s_1, s_2 are needed to solve the three equations. Are more zeros needed for the optimum match? If N additional zeros are included and N additional minimizing equations are used; then it is easily shown that K is a monotonically decreasing function of N . In other words, the best match occurs when only enough zeros are included to simultaneously solve the three equations (34) to (36). In our case two zeros are needed.

If we recall that the real parts of s_i are positive and that these zeros are either both real or complex conjugate pairs, then it can be seen that Eq. (32) and Eq. (33) set maximum values for K

$$K_{max} = \frac{2R}{L(\omega_2 - \omega_1)} \text{ when } s_1 = s_2 = 0 \quad (35)$$

$$K'_{max} = \frac{2RC_1\omega_1\omega_2}{\omega_2 - \omega_1} \text{ when } s_1 = s_2 = \infty \quad (36)$$

Similarly, Eq. (34) provides the minimum for K

$$K_{min} = \frac{\frac{6R}{L^2C_2} - \frac{2R^3}{L^3}}{\omega_2^3 - \omega_1^3} \quad (37)$$

The value of K which satisfies all three equations is between these limits. Using Eq. (7) to Eq. (10), it can be seen that K'_{max} is slightly smaller than K_{max}

$$\frac{K'_{max}}{K_{max}} = LC_1\omega_1\omega_2 \approx 1 - \left(\frac{B}{2}\right)^2 \leq 1 \quad (38)$$

where B is the fractional bandwidth. A solution for K can only exist if $K_{min} < K'_{max}$:

$$1 \leq \frac{K'_{max}}{K_{min}} = \frac{\frac{C_2}{C_1}(1 - \frac{B^2}{6})}{1 - \frac{1}{2N^2}} \approx (1 + \frac{1}{3N^2} - \frac{B^2}{2})(1 - \frac{C_1}{C_0}) \approx 1 - \frac{6B^2}{N^2} \quad (39)$$

Thus,

$$B < \frac{\sqrt{6}}{N} \quad (40)$$

This is equivalent to the intuitive argument that

$$B < \frac{1}{N} \quad (41)$$

i.e. the bandwidth is approximately the frequency range between the 3dB points of the conductance of the transducer. As might be expected, the maximum bandwidth is larger than this value by $\sqrt{6}$ times this value. A simultaneous solution to the three Eqs. (32) to (34) was obtained using a computer. The results are given in the next section for a number of different situations.

Three comments regarding bulk acoustic wave transducers are in order. First, the expressions for the model parameters are different. If $R_B + 1/j\omega_0 C_B$ is the transducer impedance at center frequency, then the model parameters are [8,9]

$$R = \frac{1}{R_B(\omega_0 C_B)^2} \quad (42)$$

$$C_0 = C_B \quad (43)$$

$$C_1 = C_0 \frac{k_{eff}^2}{1 - k_{eff}^2} \quad (44)$$

$$L = \frac{1}{\omega_0^2 C_1} \quad (45)$$

where

$$k_{eff}^2 = \frac{8k_T^2}{\pi^2} \quad (46)$$

Secondly, unlike the result with SAW transducers, it is found that for bulk transducers $K'_{max} > K_{max}$. Finally, in some cases a flat frequency response is not important; rather, a good pulse response is desired. Thus, a gaussian frequency response is a better choice, and a relation between the minimum loss and the width of the gaussian is desired. An interesting result is obtained in this case, namely that the left hand side of two of the integrals diverge. In

other words, it is not possible to match a transducer for a gaussian bandpass over either of the ranges ω_1 to ∞ or ω_2 to 0 (dc) where $\omega_1 \leq \omega_0 \leq \omega_2$. If a finite cutoff is assumed on both ends of the response, then two of the integrals can be carried out exactly, and a good approximate closed form expression can be obtained for the third integral. The analysis for bulk acoustic wave transducers can then be carried out just as for SAW IDTs.

III. Results and Discussion

Has all of this formalism done any good, or should we just have used Bode's result? The difference in Bode's result and our result is shown in Fig. 5 for Rayleigh and Sezawa wave transducers. Obviously, Bode's result is not very applicable to SAW transducers. A number of different systems and transducer designs will now be compared.

Interdigital transducers using 1) 1st Rayleigh mode (hereafter referred to as Rayleigh wave) on YZ LiNbO₃, 2) Rayleigh waves on ZnO/(100)Si and (111)Si, and 3) Sezawa waves on ZnO/(100)Si are compared in Fig. 6. ZnO/Si Sezawa wave IDTs are theoretically slightly superior to LiNbO₃ IDTs due to the higher value for $\Delta v/v$ (.023 versus .024). In practice, the full bandwidth for Sezawa wave IDTs may be difficult to achieve due to the significant problems with stray capacity. It is important for broadband matching to any transducer to keep the stray capacity much smaller than the IDT series capacity. The series capacity of ZnO/Si Sezawa wave IDTs is much smaller than LiNbO₃ IDTs (.45 pF versus 1.3 pF for the geometry considered here) since the dielectric constant of ZnO is five times smaller than LiNbO₃. Consequently, .5 pF stray capacity in the connecting leads is much more detrimental for ZnO/Si IDTs. This result is shown in Fig. 6, where it

can be seen that LiNbO_3 IDTs are superior for mismatch losses greater than 1dB.

Another important prediction is that the use of (100)Si instead of (111)Si for Rayleigh wave monolithic devices should produce broader bandwidth devices. Traditionally, (111)Si has been used for monolithic SAW devices at Stanford; however, as these results show, broader bandwidth devices can be obtained on (100)Si. The physical reasons for the superiority of (100)Si are 1) $\Delta v/v$ is larger (.0046 versus .0039) and 2) the peak in $\Delta v/v$ occurs at a smaller value of hk (.31 versus .37) and consequently, the series capacity is larger, and stray capacities are less significant.

Six kinds of monolithic transducers are compared in Fig. 7. Sezawa wave transducers are slightly better than second peak Rayleigh wave transducers. In practice, the performance of the second $\Delta v/v$ peak Rayleigh wave transducers will be significantly degraded since the transducer is at the ZnO/SiO_2 interface, and the calculation for the series and pad capacities assumed an infinitely thick SiO_2 layer. Actually, the layer would only be several microns thick, and a larger parallel capacity would be present due to conduction in the silicon. Note that this is parallel capacity (shorting the radiation resistance), not series capacity since this capacity is due to fields between fingers which does not generate acoustic stress since SiO_2 and Si are not piezoelectric.

Balanced and unbalanced operation is compared in Fig. 8. As expected from calculations of electronic Q , balanced operation is better. However, it is interesting to note that unbalanced operation is better for large bandwidths (and high loss). Also, the increase in bandwidth when switching from unbalanced to balanced operation is not 2:1 as expected from the increase of a factor of 2 in electronic Q . This is well verified experimentally.

The physical reason for the results listed in the above paragraph is the tradeoff between 1) electronic limitations to the bandwidth due to the size of

the finger capacity, and 2) acoustic limitations. As a rough approximation[2], we can equate the acoustic and electronic Q's to determine the optimum number of finger pairs:

$$Q_a = N \quad (47)$$

$$Q_e = \frac{1}{\omega C_T R_{ao}} = \frac{\nu}{2.13 \frac{\Delta v}{v}} N \quad (48)$$

where $\nu = 1$ for balanced operation, and $\nu = 2$ for unbalanced operation. Equating Q's

$$N = \left(\frac{\nu}{2.13 \frac{\Delta v}{v}} \right)^{\frac{1}{2}} \quad (49)$$

For ZnO/Si Sezawa wave balanced transducers, the optimum N according to this argument is 4 while for LiNbO₃ IDTs the optimum N is 4.5. The prediction of the theory based on Fano's work is shown in Fig. 9. It can be seen that the optimum N is 3.5 for both ZnO/Si Sezawa wave and LiNbO₃ IDTs.

IV. Conclusions

A powerful and versatile technique has been developed in this paper for comparing different transducer systems. Sixty per cent bandwidth with low mismatch loss (<3dB) is predicted for Sezawa wave IDTs. This technique can be used for transducer design, and the optimum number of finger pairs, optimum width, and optimum finger width to spacing can be determined.

Acknowledgment

The author wishes to acknowledge many valuable discussions with B. T. Khuri-Yakub and G. S. Kino. This work was supported by the Defense Advance Research Projects Agency and monitored by the Office of Naval Research under Contract N0014-76-c-0127.

REFERENCES

- [1] W. R. Smith, H. M. Gerard, J. H. Collins, T. M. Reeder, H. J. Shaw, "Analysis of interdigital surface wave transducers by use of an equivalent circuit model", IEEE Trans. Microwave Theory and Tech., MTT-17, pp. 856-864, 1969.
- [2] B. T. Khuri-Yakub and G. S. Kino, "A detailed theory of the monolithic zinc oxide on silicon convolver", IEEE Trans. Sonics, Ultrasonics, SU-24, 34, (1977).
- [3] H. W. Bode, "Network Analysis and Feedback Amplifier Design", Sec. 16.3, Van Nostrand, New York, 1945.
- [4] T. M. Reeder, W. R. Shreve, and P. L. Adams, "A New Broadband Coupling Network for Interdigital Surface Wave Transducers", IEEE Trans. Sonics, Ultrasonics, SU-19, 466(1972).
- [5] J. M. Schellenberg, "Broadband Matching to SAW transducers by active immittance transforming", 1974 Ultrasonics Symposium Proc., pp. 437-449.
- [6] R. M. Fano, "Theoretical Limitations on the broadband matching of arbitrary impedances", J. Franklin Inst., 244, p.57 and p. 139 (1950).
- [7] L. J. Augustine and J. Anderson, "An algorithm for the design of transformerless broadband equalizer of ultrasonic transducers", J. Acous. Soc. 66 pp. 629-635.
- [8] G. S. Kino, "Theory of Acoustic Devices", Prentice-Hall, New York, 1981.
- [9] C. H. Chou, personal communication, 1980.

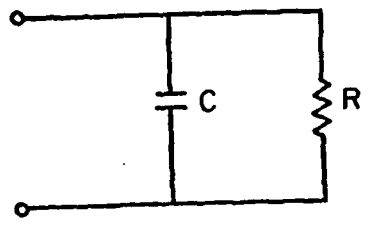
• **List of Figures**

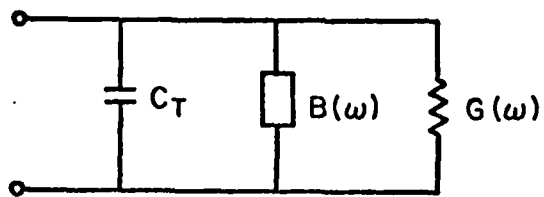
- [1] R-C Circuit analyzed by Bode.
- [2] a) parallel model for SAW IDT, b) Passive, fixed component model used by author.
- [3] Real and imaginary parts of the transducer admittance (transducer - model - -).
- [4] a) Schematic drawing of source, matching network, and load, b) Equivalent circuit, c) Equivalent (but inverted) circuit for analysis.
- [5] Comparison of bandwidth predictions using the full transducer model (-) and simple R-C model (- -) for a Sezawa wave transducer ($f_0=165$ MHz, $w=1$ mm, balanced, on (100)Si).
- [6] Comparison of LiNbO₃, ZnO/Si Sezawa wave, and ZnO/Si (first $\Delta v/v$ peak Rayleigh wave transducer ($f_0 = 165$ MHz, $w= 1$ mm, balanced).
- [7] Comparison of Sezawa wave IDTs, first and second $\Delta v/v$ peak Rayleigh wave IDTs ($f_0=165$ MHz, $w= 1$ mm, 4 fp, balanced)
- [8] Comparison of balanced and unbalanced operation for a Sezawa wave transducer on (100)Si ($f_0=165$ MHz, $w=1$ mm, 4 fp, balanced).
- [9] Dependence of bandwidth (for 4dB mismatch loss) on number of finger pairs N for Sezawa wave IDTs, LiNbO₃ IDTs, and Rayleigh wave ZnO/(100)Si ($f_0= 165$ MHz, $w=1$ mm, balanced).

• **List of Tables**

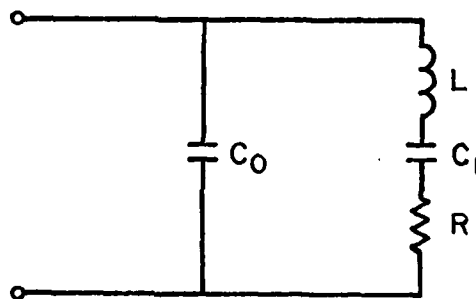
- [1] Transducer and Model Parameters for several systems of interest.

4438-1



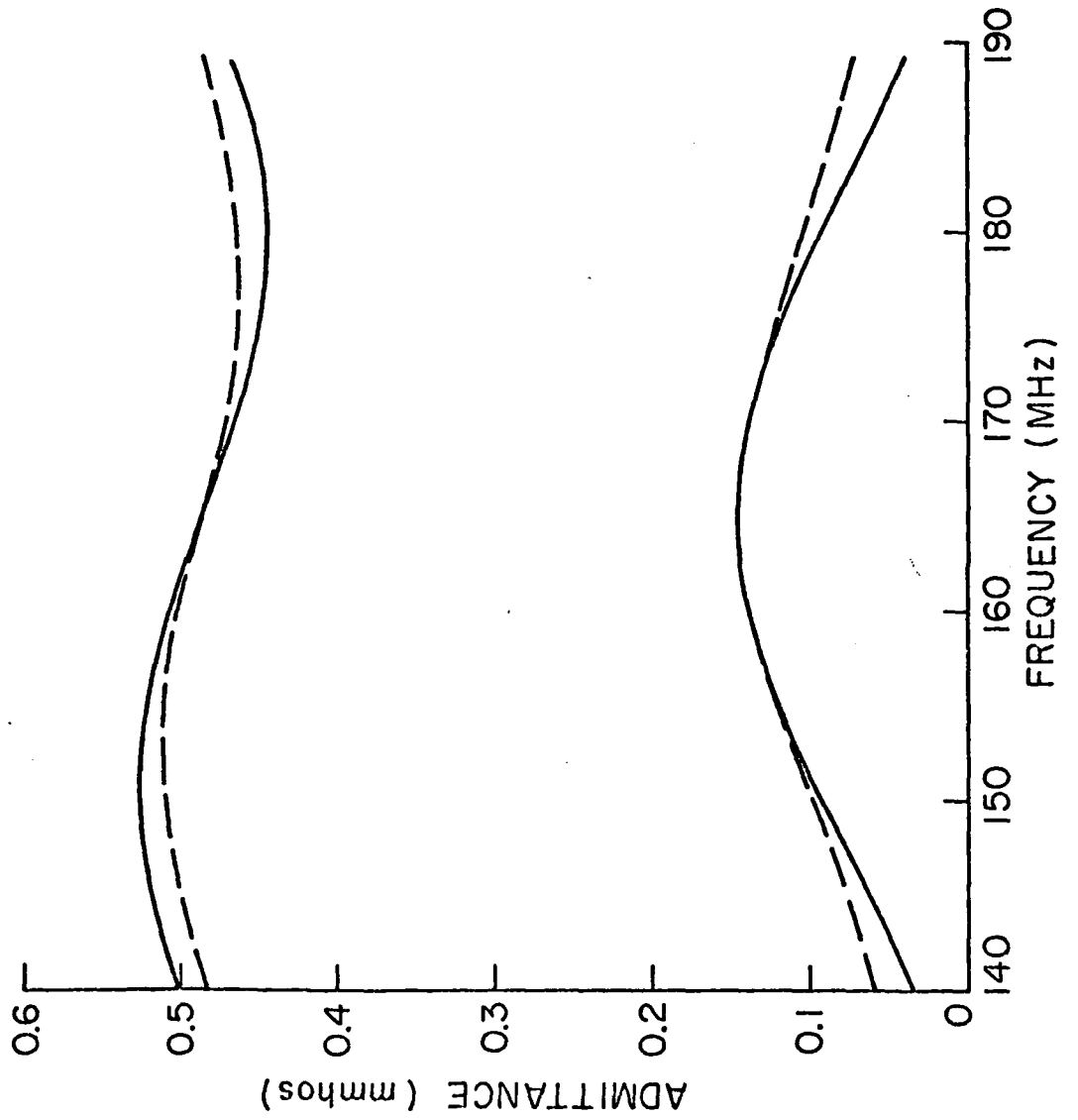


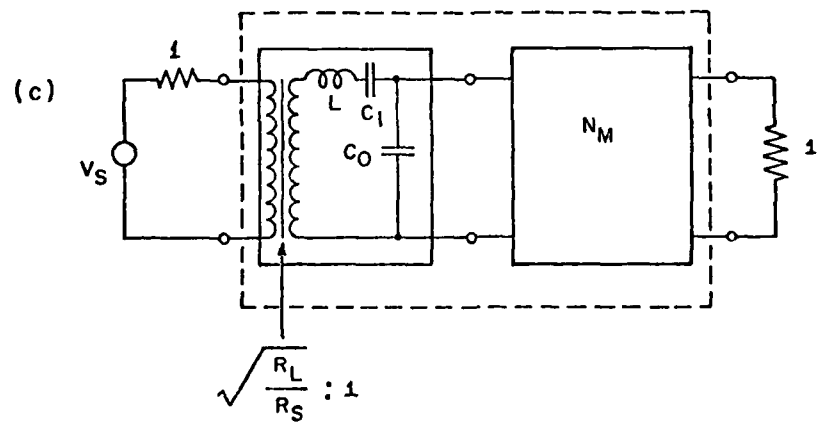
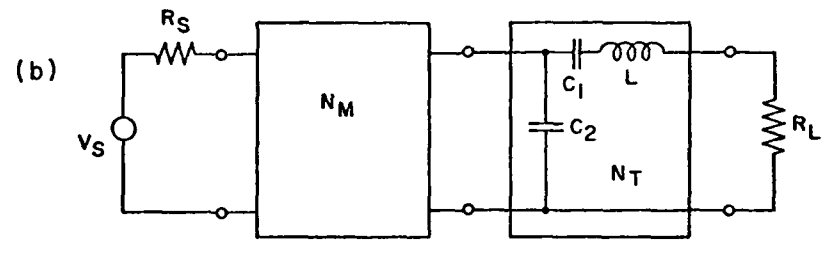
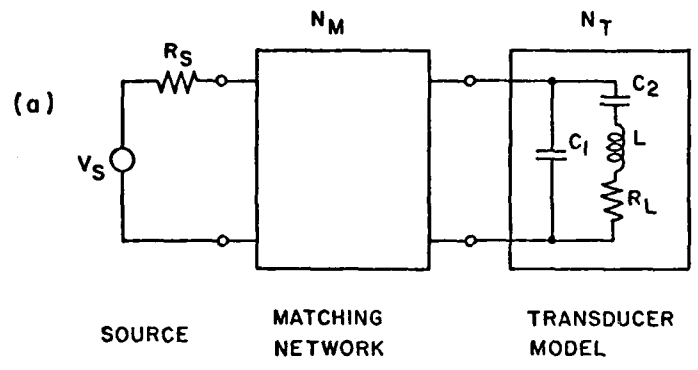
(a)

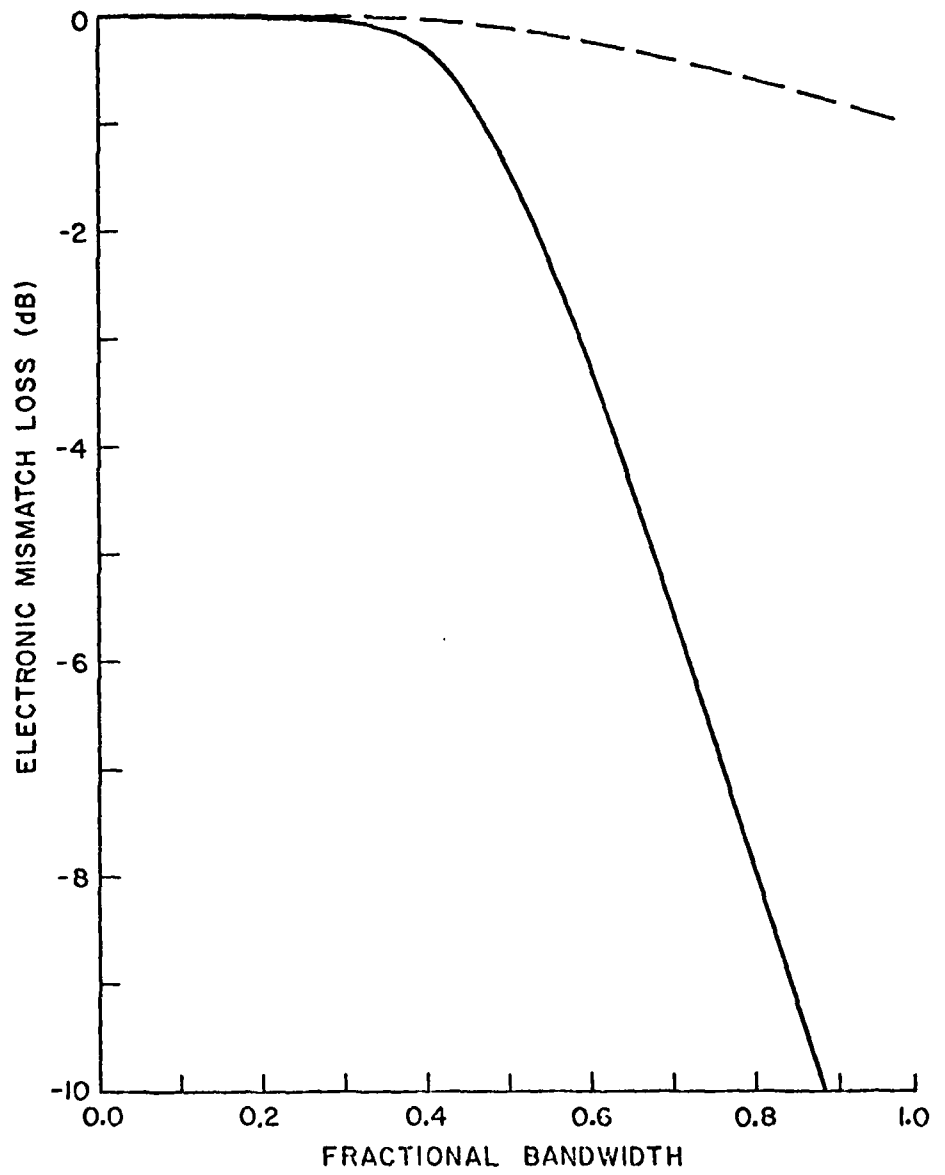


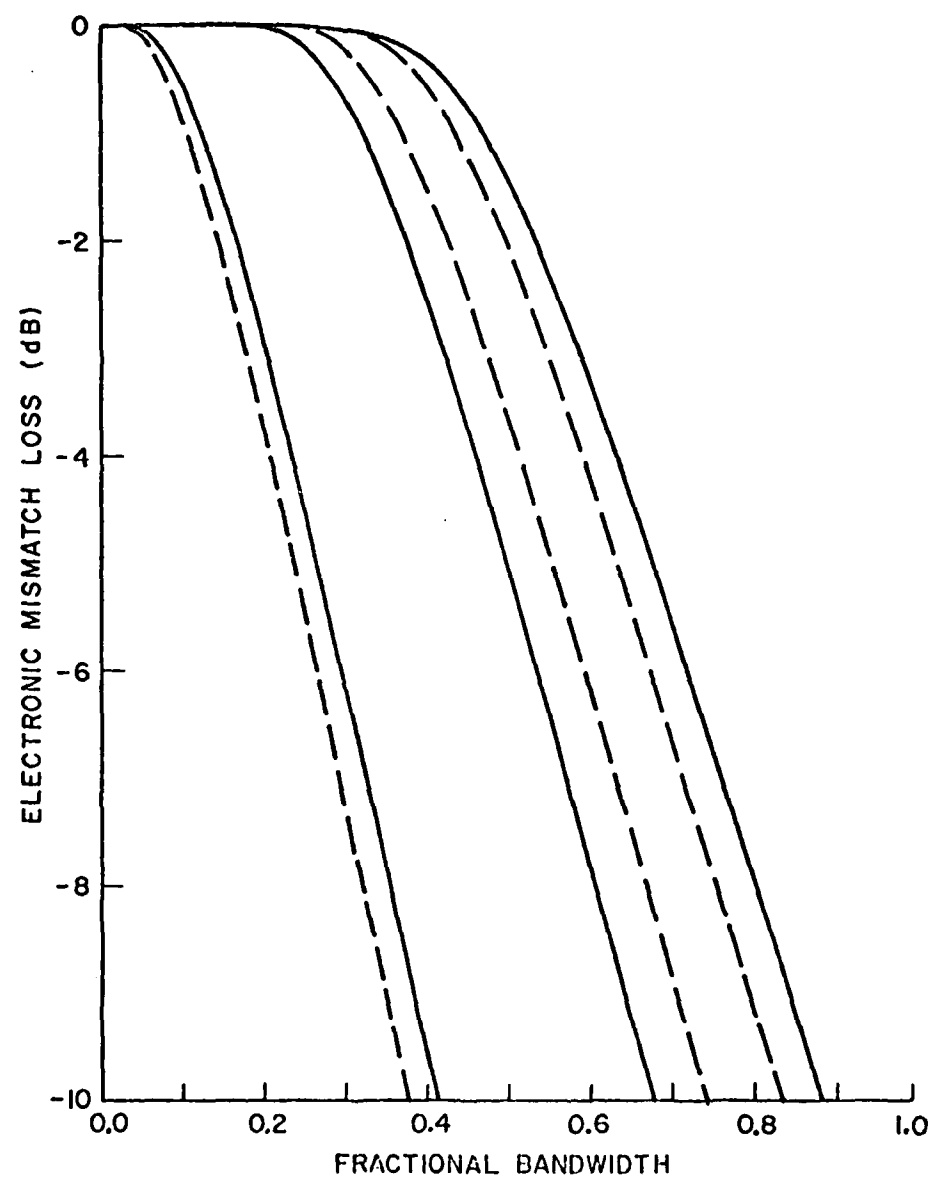
(b)

4438-3

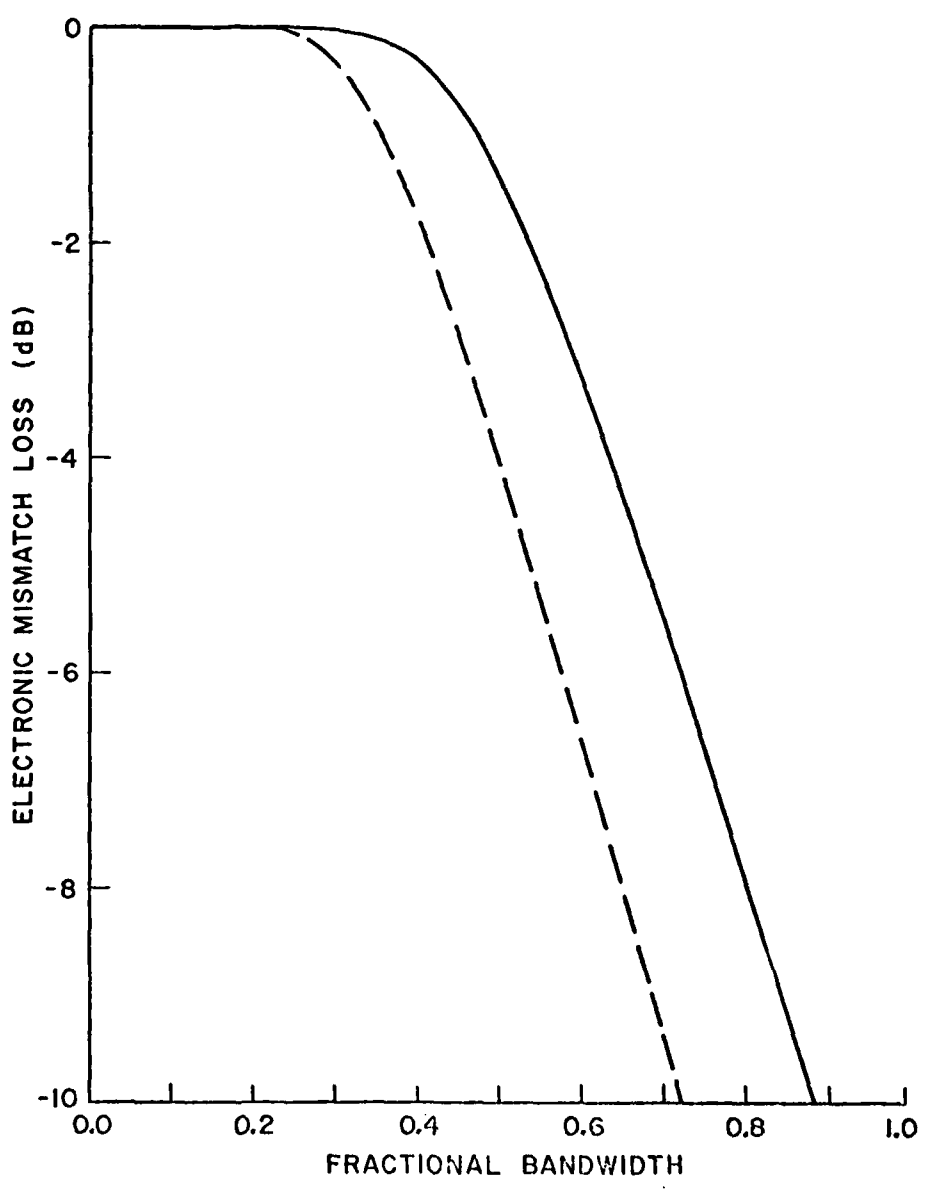








44-38-6



4438-8

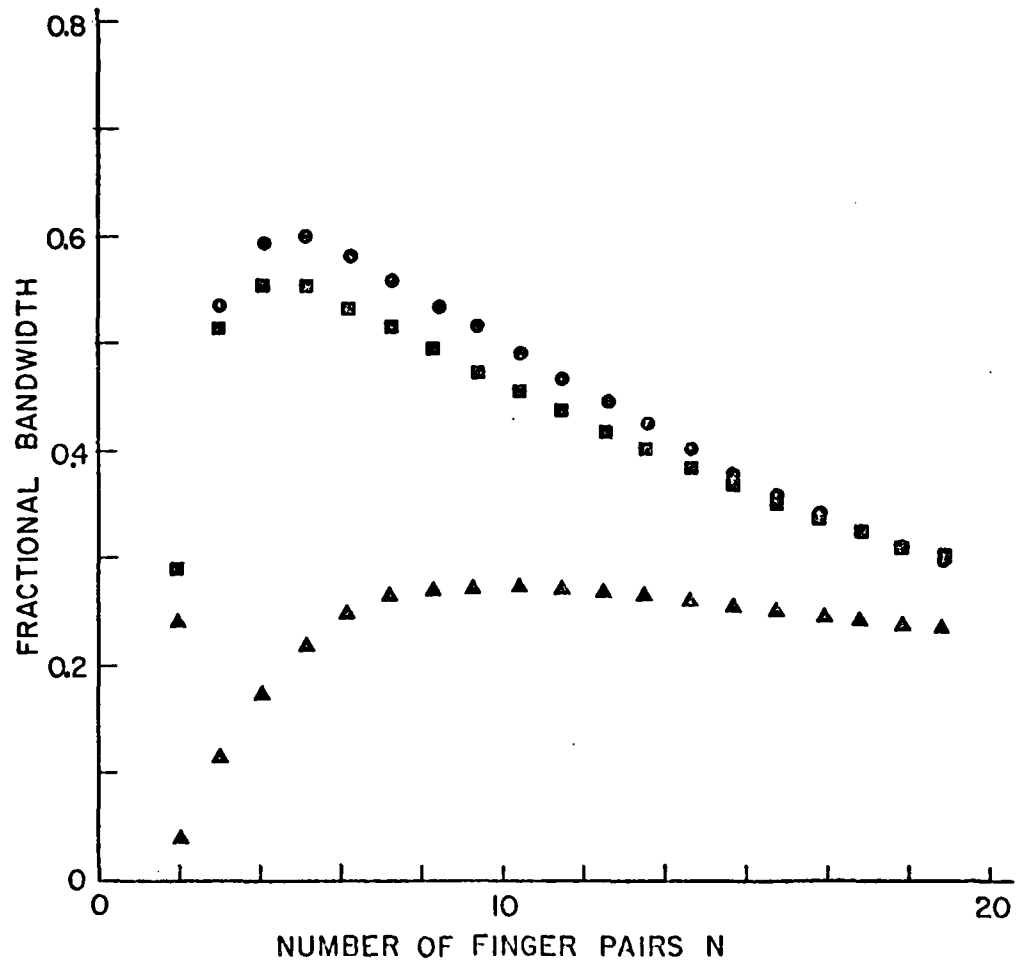


Table 1. Parameters of Systems Considered in this Paper

System	Mode	$G_{\alpha 0}$ (mmho)	C_T (pF)	C_P (pF)	R (Ω)	C_0 (pF)	C_1 (pF)	L (μH)
ZnO/(100)Si	Sezawa	.145	.401	.1	6890.	.501	.0386	24.1
ZnO/(111)Si	Sezawa	.114	.388	.08	8770.	.468	.0303	30.7
ZnO/(100)Si	Rayleigh *	.0834	1.40	.42	12000.	1.82	.0222	42.0
ZnO/(111)Si	Rayleigh *	.0591	1.16	.35	16900.	1.51	.0157	59.2
ZnO/(100)Si	Rayleigh +	.0758	.485	.063	13200.	.548	.0201	46.2
ZnO/(111)Si	Rayleigh +	.0954	.478	.065	10500.	.543	.0253	36.7
YZ LiNbO ₃	Rayleigh	.222	1.29	0.	4500.	1.29	.0787	11.8

* First Δ_{ν}^z peak

+ Second Δ_{ν}^z peak

APPENDIX B

THEORETICAL AND EXPERIMENTAL RESULTS FOR MONOLITHIC SAW MEMORY CORRELATORS

H. C. Tuan, J. E. Bowers, and G. S. Kino

ABSTRACT

A detailed theory is presented for the writing and reading processes in the monolithic surface acoustic wave (SAW) storage correlator. Theoretical and experimental results are presented on the dependence of the correlation output on the duration of the acoustic, write, and read signals. The dependence of the output on the amplitudes of the acoustic, write, and read signals is also given. The theoretical predictions are in good agreement with the experimental results in all of these cases. Suggestions are provided for the design of improved monolithic storage correlators.

I. Introduction

The diode storage correlator was first implemented using an air-gap structure where the surfaces of a LiNbO_3 and a Si substrate were placed a few thousand Angstroms apart.^{1,2} A comprehensive theoretical and experimental study of this device was undertaken by Borden and Kino^{3,4} and Loh et al.⁵ El-Nokali and Adler⁶ extended the portion of the theory dealing with the charging process to apply to diodes with minority carrier lifetimes longer than the rf period.

The air-gap correlator has a number of problems such as spurious bulk wave generation, air-gap uniformity, and the necessity for large voltages to store and read out signals. Consequently, Tuan, Khuri-Yakub, and Kino^{7,8} developed the monolithic storage correlator which used the first order Rayleigh mode propagating in a ZnO-on-Si structure. This reduced or eliminated the problems described above. However, a limitation of this approach is that narrower bandwidths are obtained than with LiNbO_3 devices. Monolithic devices with broader bandwidths may be obtained through the use of the second Rayleigh mode.⁹⁻¹¹ The results presented in this paper are from a device which used the first Rayleigh mode.

A complete theory of the monolithic storage correlator is presented here. The results of this theory are compared to a comprehensive set of data on the dependence of the correlator output on six parameters: acoustic signal duration and amplitude, write signal duration and amplitude, and read signal duration and amplitude. Results are presented for both the normal correlation mode, when the acoustic and plate signal durations are of the order of the top plate duration (typically several microseconds), and for the input correlation

mode where the acoustic and plate signal durations are of the order of the storage time of the diode (typically hundreds of milliseconds). Only the correlation of two square pulses is considered here. Other applications such as the use of chirp or phase shift keyed¹² signals involve simple calculations of compression gains.

II. Description of SAW Memory Correlator

A schematic drawing of the monolithic storage correlator is shown in Fig. 1. The operation of the correlator is a two-step operation where the correlation $Q(z)$ of the acoustic signal $V_A(t)$ from the left transducer and the writing signal $V_W(t)$ are first stored in the diode array in the form of a spatially-varying charge pattern. Then a second reading signal $V_R(t)$ is applied to the center (or plate) port. As a result of the interaction of the stored charge pattern and the plate signal, the correlation and convolution of the stored signal $Q(z)$ and the read signal $V_R(t)$ are obtained at the left and right interdigital transducers (IDT's), respectively. A second method of reading, called acoustic-to-plate reading, is a simple extension of the theory presented below.

The parameters of the device used in the experiments described here are given in Table I. The parameters in the first part of the table are measured parameters, and the second part of the table contains calculated parameters such as the equivalent acoustic capacitance.¹³ The definitions of the variables used in this paper are also given in Table I. In particular, the capacity of the diode at zero bias is C_d , the capacity of the region in between the diodes is C_d' , the total silicon capacity is $C_0 = C_d + C_d'$,

the capacity of the ZnO and SiO₂ layers is C_{ox} , and the total capacity of the plate is $C_p = C_{ox}C_0/(C_{ox} + C_0)$. All of the capacitances and charges are per unit area. Capital subscripts are used to designate external voltages such as V_A , and the internal voltage is given by lower case subscripts (v_a).

The equivalent circuit model used in the writing process is given in Figs. 2a and 2b. This model has been changed from that used earlier for the air-gap correlator^{1,3,6} for two reasons. The substrate resistance cannot be neglected for devices which use silicon with resistivities of the order of 10 Ω cm, unless epitaxial layers on highly conducting substrates are used. Secondly, it is important to realize that the acoustic wave does not interact directly with the plate circuit so that neither part of the circuit loads the other. It is, therefore, more correct to use two separate circuits for the two branches, as shown in Fig. 2a and 2b.

Because of the high density of diodes, the resistance of the plate circuit can be calculated without including the effects of spreading resistance.

When the dc bias on the plate is varied, the MOS capacity of the region in between the diodes C_d' also varies, and the rf coupling of the plate and acoustic ports to the diode changes. Due to charge injection in the ZnO, the dependence of the MOS capacity on the dc bias is complicated. This effect has been studied by Pierret et al.¹⁴

The model shown in Fig. 2a is for a single diode, and the source voltage V_p is the voltage at the top plate. The external driving voltage V_w is connected to the top plate through a short lead. The rf impedance of a

short lead (~ 1 cm) can easily be of the same order of magnitude as the impedance of the plate capacitor, and thus this inductance L cannot be neglected.

The values of the electrical half of the circuit (R , L , and C_p) can be determined by measuring the plate impedance as a function of frequency (Fig. 3). The impedance of the circuit in Fig. 2a matches the measured impedance quite well. The values used in the fit (see Fig. 3) agree with the component values expected from calculations of R , L , and C_p (see Table I).

The circuit models used for the diode (Fig. 2b) and the read-out process (Fig. 2c) are the same as the models used for the air-gap correlator.³ In the read-out process, the capacitance of an individual diode is regarded as being changed by the writing process. When an rf signal is applied to the plate, it develops a potential across this reverse biased diode capacity, which depends on its capacity and on the capacity in series with the diode.

III. Theory

We shall initially consider the writing process and calculate the component of stored charge with wave number k . Then, the read-out process is considered, and the output voltage is calculated.

Writing

The model shown in Fig. 2a is essentially just a sample and hold circuit, and the effect of the resistances, inductance, and parallel capacitance C_d is to reduce the voltage at the diode V_d .

In the first few cycles of operation, when the rf potential becomes positive, the diode potential rises to approximately 0.5V . During the negative half of the cycle, the potential across the diode becomes negative, and some of the injected charge initially stored in the neutral region of the diode returns to the driving circuit. However, for devices where the minority carrier lifetime is much longer than the rf period, it can be shown that during the negative half cycle, the charge returning to the external circuit is much less than that injected, and it would take a period corresponding to several rf cycles for most of the charge to leave the diode. Consequently, on the next cycle, when the applied potential becomes positive, the voltage across the diode does not reach as large a positive potential as in the first cycle. It therefore follows that after a few cycles, when the applied potential becomes positive, only a very small amount of excess charge is injected into the diode on each positive half cycle. Consequently, the potential across the diode can be estimated easily by regarding it as a simple capacitor and neglecting the conduction current. It is therefore convenient to model the diode as a simple capacitor to determine the rf voltage present at the plate, and from this information calculate the charge that recombines in the diode.

The rf voltage across the diode is

$$V(t,z) = \gamma_w V_w \cos \omega t + \gamma_a V_a \cos (\omega t - kz) \quad (1)$$

where

$$\gamma_w = \left[\left(1 + \frac{C_o}{C_{ox}} - \omega^2 LC_o \right)^2 + (\omega R_p C_o)^2 \right]^{-1/2} \quad (2)$$

and

$$\gamma_a = \left[\left(1 + \frac{C_o}{C_a} \right)^2 + (\omega R_a C_o)^2 \right]^{-1/2} \quad (3)$$

where

$$C_o = C_d + C'_d \quad (4)$$

Only the magnitudes of γ_w and γ_a have been used here since any phase change associated with the phases of γ_w and γ_a can be removed through appropriate definitions of the zeros of t and z . Using the values in Table I, $\gamma_w = .14$. Equation (1) can be rewritten as

$$V(t,z) = V \cos(\omega t - \phi) \quad (5)$$

where

$$V = \left[(\gamma_w V_w + \gamma_a V_a \cos kz)^2 + (\gamma_a V_a \sin kz)^2 \right]^{1/2} \quad (6)$$

and

$$\phi = \tan^{-1} \left(\frac{\gamma_a V_a \sin kz}{\gamma_w V_w + \gamma_a V_a \cos kz} \right) \quad (7)$$

To first order in $\gamma_a V_a / \gamma_w V_w$, Eqs. (6) and (7) become

$$V = \gamma_w V_w + \gamma_a V_a \cos kz \quad (8)$$

and

$$\phi = \frac{\gamma_a V_a}{\gamma_w V_w} \sin kz \quad (9)$$

These expressions will be used to calculate the recombined charge. Note that we expect the theory to break down for small plate voltages where Equations (8) and (9) are not valid and also for small times (i.e., the first few rf cycles) where the calculation for γ_w and γ_a is not valid since a significant portion of the diode current is charge flowing into the neutral region.

The minority carrier density $p_n(x,t)$ in the diode obeys the diffusion equation:

$$-D_p \frac{\partial^2 p_n}{\partial x^2} + \frac{\partial p_n}{\partial t} = -\frac{p_n}{\tau_p} \quad (10)$$

where x is the distance into the neutral n region, D_p is the diffusion coefficient for the holes, and τ_p is the recombination time of the holes. It can be shown that the total excess minority carrier charge in the neutral region Q_p is given by the solution of Eq. (9) in the form

$$Q_p(t) = q\sqrt{D_p/\pi} \int_0^t \frac{p_n(\tau) e^{-(t-\tau)/\tau_p}}{(t-\tau)^{1/2}} d\tau \quad (11)$$

where $p_n(\tau)$ is the excess minority carrier density at a time τ at the plane $x = 0$. The charge that recombines in the diode (Q_R) is given by the differential equation

$$\frac{dQ_R}{dt} = \frac{Q_p}{\tau_p} \quad (12)$$

Just as in a sample and hold circuit, the charge which recombines in the diode Q_R is charge stored on the external capacitor. This produces a change in voltage across the diode

$$V_R = -Q_R / (C_o + C_{ox}) \quad (13)$$

Since

$$p_n(\tau) = p_{no} e^{\beta V_D(\tau)} \quad (14)$$

where $\beta = q/(kT)$ and p_{no} is the equilibrium hole concentration on the n side of the junction, it follows that

$$Q_p = qp_{no} \sqrt{\frac{D_p}{\pi}} \int_0^t \left[e^{\beta V \sin(\omega\tau + \phi)} e^{-\beta Q_R / (C_{ox} + C_o)} - 1 \right] \frac{e^{-(t-\tau)/\tau_p}}{(t-\tau)^{1/2}} d\tau \quad (15)$$

We shall consider the case where the minority carrier lifetime τ_p is much longer than an rf period. Then, the most rapid variation occurs in the exponential term containing the rf dependence, and we obtain the approximate result

$$Q_p \approx q p_{no} \sqrt{\frac{D_p}{\pi}} \int_0^t [I_0(\beta V) e^{-\beta Q_R / (C_{ox} + C_o)} - 1] \left[\frac{e^{-(t-\tau)/\tau_p}}{(t-\tau)^{1/2}} \right] d\tau \quad (16)$$

where I_0 is the modified Bessel function of order zero. For slow charging, the first term in brackets is a slowly varying function, and the second term in brackets is only significant for $\tau \approx t$. Thus, evaluating the first term at $t = \tau$

$$Q_p \approx q p_{no} \sqrt{\frac{D_p}{\pi}} [I_0(\beta V) e^{-\beta Q_R(t) / (C_{ox} + C_o)} - 1] \int_0^t \frac{e^{-(t-\tau)/\tau_p}}{(t-\tau)^{1/2}} d\tau \quad (17)$$

or

$$Q_p \approx q p_{no} \sqrt{D_p \tau_p} [I_0(\beta V) e^{-\beta Q_R / (C_{ox} + C_o)} - 1] \operatorname{erf} (t/\tau_p)^{1/2} \quad (18)$$

where

$$\operatorname{erf} x = \frac{2}{\sqrt{\pi}} \int_0^x e^{-u^2} du$$

Using Eq. (11), we obtain a simple differential equation for Q_R

$$\frac{dQ_R}{dt} = q p_{no} \sqrt{\frac{D_p}{\tau_p}} I_0(BV) (e^{-\beta Q_R / (C_{ox} + C_o)} - 1) \operatorname{erf} \left(\frac{t}{\tau_p} \right)^{1/2} \quad (19)$$

This has the solution

$$\ln \left[\frac{I_0 - e^{\beta Q_R / (C_{ox} + C_o)}}{I_0 - e^{\beta Q_{R0} / (C_{ox} + C_o)}} \right] = \frac{\beta q p_{no}}{2(C_{ox} + C_o)} \sqrt{D_p \tau_p} f(t) \quad (20)$$

where

$$f(t) = \left(\frac{t}{\tau_p} - \frac{1}{2} \right) \operatorname{erf} \left(\frac{t}{\tau_p} \right)^{1/2} + \frac{1}{\sqrt{2\pi}} \sqrt{\frac{t}{\tau_p}} e^{-t/\tau_p} \quad (21)$$

and Q_{R0} is the charge previously stored in the array. In some of the figures in the next section, the writing signal is on for a longer period than the acoustic signal. Consequently, we need to calculate the charge stored when only the writing signal is present Q_{R0} and then calculate the final charge Q_R after both the writing and acoustic signals are present. Thus,

$$Q_R = \frac{C_{ox} + C_o}{\beta} \ln \left[I_0(BV) - e^{-A f(t)} (I_0(BV) - e^{\beta Q_{R0} / (C_{ox} + C_o)}) \right] \quad (22)$$

where

$$A = \frac{\beta q p_{no} \sqrt{D_p \tau_p}}{2(C_{ox} + C_o)} \quad (23)$$

When $Q_{RO} = 0$, Eq. (22) is equivalent to the result obtained in ref. 6 for the air-gap correlator.

The derivation given here has neglected the recombination of the injected charge Q_p , which occurs after the pulse has been turned off. This effect is negligible for writing times long compared to the minority carrier lifetime τ_p .

It is interesting to note that if a Schottky characteristic had been assumed

$$I_o = I_s (e^{qV_D/(kT)} - 1) \quad (24)$$

then the same result as Eq. (22) would have been obtained, except that the argument of the exponential term would have been

$$\frac{\beta}{C_{ox} + C_o} I_s t$$

instead of

$$Af(t) \approx \frac{\beta}{C_{ox} + C_o} \frac{q p_{no}}{2} \sqrt{\frac{D_p}{\tau_p}} t \quad (25)$$

for $t/\tau_p \gg 1$. Assuming a typical value for Schottky diodes

($I_s = 10^{-4}$ amps/cm²), the charging rate is 15 times faster than for p-n diodes. However, the assumptions of the theory are questionable for such fast charging times.

The recombined charge given in Eq. (22) is essentially the charge across the plate capacitor when the diode voltage is at its rf peak. However, after the plate signal is removed, the charge redistributes between the diode and plate capacitors. If the variable capacity of the diode under reverse bias is taken into account, then the relation between the total recombined charge Q_R and the final charge on the diode itself Q_{RD} after redistribution is

$$Q_{RD} = Q_0 \left(1 + \frac{C_o}{C_{ox}}\right) \left[\left(1 + \frac{2C_o C_{ox}}{(C_{ox} + C_o)^2} \frac{Q_R}{Q_0}\right)^{1/2} - 1 \right] \quad (26)$$

where Q_0 is the depletion layer charge at thermal equilibrium. In our case, $Q_R \ll Q_0$ for all of the charging voltages considered in the next section. In this case, Eq. (26) becomes

$$Q_{RD} = \frac{C_o}{C_{ox} + C_o} Q_R \quad (27)$$

This is exactly what one would calculate if the diode capacity were assumed to be constant.

If we now include the spatial variation of the acoustic wave, Eq. (8), then the redistributed charge is

$$Q_{RD} = \frac{C_0}{\beta} \ln [I - e^{-Af(t)} (I - e^{\beta Q_{R0}/(C_{ox} + C_0)})] \quad (28)$$

where

$$I = I_0 [\beta(\gamma_w V_w + \gamma_a V_a \cos kz)] \quad (29)$$

The charging time of the diode in the theory was taken to be t . Since the plate voltage is generally much larger than the internal acoustic voltage, this charging time is determined by the duration of the write-in signal to the plate t_w . If the acoustic signal is present at the diode during the entire charging time, then the stored charge is given by Eq. (23) with $t = t_w$. However, if the plate signal is present, either before or after the acoustic signal is present, then there is an additional component of charge with no spatial variation. Using the fact that $Af(t) \ll 1$, and using Eq. (22) to obtain Q_R and Q_{R0} , then the following result is obtained

$$Q_{RD} = \frac{C_0}{\beta} \ln \left\{ [1 + Af(t_w - t_A) I_0 (\beta \gamma_w V_w) + Af(t_A) I_0 [\beta(\gamma_w V_w + \gamma_a V_a)]] \right\} \quad (30)$$

for $t_w > t_A$, and

$$Q_{RD} = \frac{C_0}{\beta} \ln \left\{ 1 + Af(t_A) I_0 [\beta(\gamma_w V_w + \gamma_a V_a)] \right\} \quad (31)$$

for $t_w < t_A$.

This is the expression for the total stored charge. For the read-out process, we are only concerned with the component of stored charge at the acoustic spatial wave number k .

$$Q_k(t) = 1/2\pi \int_0^{2\pi} Q_{RD}(t,z) \cos(kz) d(kz) \quad (32)$$

This integral is calculated numerically for the figures in the next section. However, a good approximate relation may be found by assuming that the second and higher harmonics are all negligible, and writing

$$Q_k(t) \approx \frac{Q_k^{\max}(t) - Q_k^{\min}(t)}{2} \quad (33)$$

For $t_w > t_A$,

$$Q_k = \frac{C_0}{2\beta} \ln \frac{1 + A f(t_w - t_A) I_0(\beta \gamma_w V_w) + A f(t_A) I_0[\beta(\gamma_w V_w + \gamma_a V_a)]}{1 + A f(t_w - t_A) I_0(\beta \gamma_w V_w) + A f(t_A) I_0[\beta(\gamma_w V_w - \gamma_a V_a)]} \quad (34)$$

For $t_w < t_a$,

$$Q_k \approx \frac{C_0}{2\beta} \ln \frac{1 + A f(t_w) I_0[\beta(\gamma_w V_w + \gamma_a V_a)]}{1 + A f(t_w) I_0[\beta(\gamma_w V_w - \gamma_a V_a)]} \quad (35)$$

Several results are clear from this expression. Suppose the plate signal is on for a fixed time ($t_w = 10$ ms for example) and the acoustic signal length t_A is varied from 0 - 10 ms. In Eq. (34), the third term in the numerator and denominator is small compared to the first two terms. Putting

$f(t) = t/\tau_p$, and carrying out a Taylor expansion, we see that Q_k is linear with respect to t_A , except in the region where $t_A = t_w$. This is basically because the presence of fixed charge due to the applied plate potential over the period of 10 ms does not affect the spatial modulation due to the acoustic term.

Suppose instead that the duration of the acoustic signal is fixed (10 ms for example), and the duration of the signal on the plate is varied from 0 - 10 ms. Using Eq. (35), it can be seen that the second term in the numerator and denominator is initially smaller than 1, and later much larger than 1. The net effect is a very nonlinear characteristic. Put another way, the variation of the plate signal also affects the spatial modulation of the stored charge due to the acoustic signal, as the uniform charge stored is no longer invariant with time.

From the form of Eqs. (30) and (31), (or even from the approximate result of Eqs. (34) and (35), it is not obvious that the output should be linear with respect to V_a , except for the case when $\beta\gamma_w V_w \gg 1$ and the expressions for I_0 and the logarithm may be expanded and a linear dependence on V_a is obtained. Using computer calculations, it will be shown in the next section that the theoretical dependence of Q_k on V_a is linear, and consequently, we shall express our relations for $Q_k = h(V_w)V_a$. For large V_w , Eqs. (34) and (35) are independent of V_w .

$$\frac{Q_k}{Q_0} = \frac{C_0 \gamma_a V_a}{Q_0} = \frac{\gamma_a V_a}{2V_{bi}} \quad (36)$$

where V_{bi} is the built-in voltage of the diode.

The Readout

Plate to acoustic read-out is treated in this section. In this case, an rf modulated signal is applied to the plate port and interacts with the spatially-modulated capacity of the diode array to generate two acoustic waves which travel towards each transducer. We shall assume that the amplitude of the stored charge is constant across the diode array and that the read signal is a square pulse of duration t_R . For more complicated signals, it is straightforward to show that the envelopes of the two acoustic waves are the correlation and convolution of the stored signal and the read signal.

We shall assume that the read voltage is never large enough to forward bias the diodes; if the read voltage were that large, the stored charge pattern would be altered during the read-out process, and the analysis is more complicated.

The voltage at the diode due to the read voltage will be calculated first. Then a normal mode approach will be used to calculate the amplitude of the excited wave.

Using the circuit model in Fig. 2c, the relation between the plate voltage and the diode voltage is

$$V_D(z) = \frac{1 + j\omega R C_0(z)}{1 + j\omega R C_0(z) + C_0(z)/C_{ox}} V_P \quad (37)$$

where $C_0(z) = C_d(z) + C'_d$. Due to the plate lead inductance, the voltage at the plate V_P is different from the externally measured read voltage V_R .

$$|V_p| = \alpha |V_R| \quad (38)$$

and

$$\alpha = \left[\frac{1 + \omega^2 R^2 C_p^2}{(1 - \omega^2 L C_p)^2 + \omega^2 R^2 C_p^2} \right]^{1/2} \quad (39)$$

where C_p is the series combination of C_{ox} and C_o .

The diode capacity, $C_d(z)$ is easily found in terms of the stored charge $Q_R(z)$.

$$\frac{1}{C_d(z)} \approx \frac{1}{C_o} + \frac{1}{C_{ox} + C_o} \frac{Q_R(z)}{Q_o} \quad (40)$$

This expression is valid to first order in Q_R/Q_o . When Eq. (40) is substituted into Eq. (37), the spatially-varying component of $V_d(z)$ is found to be

$$V_{Dk} = \frac{\frac{C_{ox}}{C_o + C_{ox}}}{1 + \frac{C_{ox}}{C_o} + j\omega R C_{ox}} \frac{Q_k}{Q_o} V_p \quad (41)$$

The amplitude of the surface acoustic wave which is excited by this potential can be found using the normal mode analysis of Auld and Kino.¹⁵

$$\phi_a = \left(kL \frac{\Delta v}{v} \right) \left(\frac{\delta}{2\ell} \operatorname{sinc} \frac{k\delta}{2} \right) V_{Dk} \frac{t_R}{T} \quad (42)$$

where k is the wave number of the acoustic wave, L is the total length of the diode array, δ is the diode spacing, λ is the diode period, and t_R/T is the ratio of the durations of the read and stored signals. For $t_R/T > 1$, the ratio should be replaced by 1.

Correlator Output

To express the output in terms of external parameters, we need to relate the internal acoustic voltages V_a and ϕ_a to the external input and output electrical voltages V_A and V_{out} , respectively.

$$V_a = 10^{-IL/40} \sqrt{\frac{Z_a}{R_s}} V_A \quad (43)$$

and

$$V_{out} = 10^{-IL/40} \sqrt{\frac{R_s}{Z_a}} \phi_a \quad (44)$$

where IL is the insertion loss in dB, Z_a is the acoustic impedance, and R_s is the source impedance.

The external output voltage of the correlator can now be calculated in terms of external parameters

$$V_{out} = \epsilon h(V_w) \left(\frac{t_R}{T}\right) V_R V_A \quad (45)$$

where

$$\epsilon = \left(\frac{\delta}{2\ell} \operatorname{sinc} \frac{k\delta}{2} \right) \left(\frac{\frac{C_{ox}}{C_o + C_{ox}}}{[(1 - \omega^2 LC_p)^2 + \omega^2 R^2 C_p^2]^{1/2}} \right) \left(10^{-IL/20} \right) \left(kL \frac{\Delta v}{v} \right) \quad (46)$$

IV. Results and Discussion

Correlator Efficiency

The dependence of the output on V_A and V_R is linear; however, the output saturates as V_w is increased (Eq. 35). Consequently, the terminal efficiency F_T shall be defined as the output power divided by the available powers associated with the two linear parameters. The terminal efficiency (dBm) is

$$F_T = 10 \log \frac{P_{out}}{P_A P_{RE}} \quad (47)$$

$$F_T = 20 \log (.32\epsilon h_{max} \gamma_R) \quad (48)$$

where

$$h_{max} = \frac{\gamma_a}{2V_{bi}} \quad (49)$$

and γ_R is the power loss which results when the plate is not tuned to 50 Ω . Assuming the amplifier is well represented by an ideal voltage source in series with a source resistor R_s ,

$$\gamma_R = 2 \left[\frac{(1 - \omega^2 C_p L)^2 + \omega^2 C_p^2 R^2}{(1 - \omega^2 L C_p)^2 + \omega^2 C_p^2 (R + R_s)^2} \right]^{1/2} \quad (50)$$

Using the parameters given in Table 1, $\gamma_R = .5$. Experimentally, it is found that γ_R is closer to 1, although the exact value depends on the type of amplifier and power levels used. The maximum terminal efficiency is therefore

$$F_T = 20 \log \left(\frac{.16 \gamma_a}{V_{bi}} \right) \left(\frac{\delta}{2\ell} \operatorname{sinc} \frac{k\delta}{2} \right) \left(10^{-IL/20} \right) \left(kL \frac{\Delta v}{v} \right) \left(\frac{\gamma_R \frac{C_{ox}}{C_o + C_{ox}}}{[(1 - \omega^2 L C_p)^2 + (\omega C_p R_p)^2]^{1/2}} \right) \quad (51)$$

We shall examine each of these terms, and evaluate the terms using the values listed in Table 1.

The first term is essentially the diode built in voltage normalized to dBm. A 50 Ω load on the acoustic port was assumed. This term has the value .04. The second term is the reduction in output due to the use of discrete diodes. In our case, the diode width and spacing are both 4 μ , so this term has the value .24. Decreasing the diode widths and spacing while keeping the width equal to the spacing only negligibly increases this term to .25. However, if the diode spacing is reduced, this term can be increased to .5. The limit of .5 is due to the fact that either the forward or backward travelling wave is used, not both.

The third term is due to the insertion loss and has the value .16 . The fourth term is a modified coupling coefficient, and has the value 5.83 . The last term results from the conversion of a charge variation to a capacitance variation, and the conversion of plate voltage V_p to V_{RE} . This term has the value .069 . Decreasing the length of the plate wire so that the proper tuning is obtained only slightly increases this term to .071 .

If an epitaxial layer on a low resistivity substrate is used to decrease R , then the first term increases to .12 and increases the fourth term to .077 .

The first and last terms are monotonically increasing functions of C_0 and $1/R$ and consequently a low resistivity substrate is suggested. However, since the insertion loss also increases with decreasing resistivity, there is an optimum value. This trade-off is shown in Fig. 4. For our device configuration, the optimum resistivity is $5 \times 10^{14} \text{ cm}^{-3}$.

Using the values given above, we predict a correlator efficiency of -64 dBm . We experimentally observed an efficiency of -56 dBm . Note that if all of the above suggestions are incorporated, the efficiency can in principle be improved by 17 dB .

V. Experimental Results

A series of experimental results were compared with theory using the device described in the introduction. Most of the experimental measurements were carried out using Hewlett Packard calibrated attenuators and a Hewlett Packard oscilloscope. The accuracy of such measurements is, at best, 1 dB , and is subject to further errors at low signal levels due to noise.

In each of the figures, the theoretical results, Eqs. (30) to (32), are represented by a solid line. The approximate results, Eqs. (34) and (35), are represented by a dashed line. The same parameters were used in the calculations for all the figures.

Time Dependence

The dependence of the output on the acoustic signal duration when the plate signal duration is kept constant at time $t_w = 10 \text{ ms}$ is shown in Fig. 5. As anticipated in Section III, the dependence is linear except when $t_A \approx t_w$. In this case, both the experimental and theoretical results indicate a slight deviation from a linear curve. It can be seen that the approximate formula is accurate enough for most purposes.

The dependence of the output on the write signal duration for short times ($< 1 \text{ } \mu\text{s}$) is shown in Fig. 6. As expected, the agreement is good except for the initial charging period when our expressions for γ_w and γ_a are not valid.

For the slow charging input correlation mode (Fig. 7), the charging dependence is similar to the dependence for fast charging, except that the time scale is larger by a factor of roughly 50,000. The effect of having the write signal on for times longer than the acoustic signal (4 ms) is also shown in Fig. 7. The output decreases due to the increase in the component of stored charge with no spatial variation.

The dependence of the output on the read signal duration was experimentally and theoretically found to be linear.

The dependence of the correlator output on the number of times a given correlation is written into the diode array is shown in Fig. 8. The form of the dependence is important for applications such as adaptive filtering^{16,17} where multiple correlations are added together. For most applications, it would be desirable to have a linear dependence, however, as shown in Fig. 8, this is not the case. For adaptive filter applications,¹⁷ the feedback gain should be decreased as a function of time (equivalently, the number of writing pulses) and consequently the dependence shown in Fig. 8 is desirable.

Amplitude Dependence

The dependence of the output amplitude on the acoustic input signal amplitude is shown in Fig. 9. It can be seen that the output is very nearly linear over a range of 35 dB .

The dependence of the output on the writing signal on the plate is shown in Fig. 10 for four different read voltages. It can be seen that the agreement between experimental and theoretical results is good except for small write voltages and large read voltages where our approximations are no longer valid. The charging period is very long ($t_p = t_a = 10$ ms) in Fig. 10 and the output saturates for voltages greater than 2V . For short charging periods (.2 μ s), as shown in Fig. 11, the output does not saturate until the write signal reaches 3V . The error in the write amplitude range between 2 and 3V is due to the fact that the I-V characteristic of the diode follows an exponential curve of the form $\exp qV/kT$. Hence, very slight errors in estimating V show up as large errors in the curve.

The dependence of output voltage on the read-out voltage is shown in Fig. 12 for three different acoustic voltages. It can be seen that the agreement with theory is good except for large read-out voltages where the variation in diode capacitance is no longer linear with voltage as approximated in the theory.

VI. Conclusions

We have given here a comprehensive quantitative theory which predicts the output of a monolithic acoustic surface wave correlator as a function of the important external variables. An extensive set of experimental measurements confirms the predictions of the theory. The theory can therefore be employed for accurate design of monolithic acoustic surface wave storage correlators. Suggestions are given for improving the efficiency of the device by as much as 17 dB .

Acknowledgment

The authors would like to thank B. T. Khuri-Yakub, P. Grant, and R. Thornton for many helpful discussions of this work.

This work was supported by the Defense Advanced Research Projects Agency and monitored by the Office of Naval Research under Contract N00014-76-C-0129 and through the National Institute of Health under Grant GM17940-10.

References

1. K. A. Ingebritsen, R. A. Cohen, and R. W. Mountain, "A Schottky Diode Acoustic Memory and Correlation," *Appl. Phys. Lett.*, 26, pp. 296-598, 1975.
2. C. Maerfeld and Ph. Defranould, "A Surface Wave Memory Device Using pn Diodes," *Proc. IEEE Ultrasonics Symp.*, pp. 209-211, 1975.
3. P. G. Borden and G. S. Kino, "An Analytic Theory for the Storage Correlator," *Proc. IEEE Ultrasonics Symp.*, pp. 485-491, 1977.
4. P. G. Borden, "The Storage Correlator: Theory and Signal Processing Applications," Ph.D. thesis, Stanford University, 1978.
5. K. W. Loh, D. K. Schroeder, and P. R. Emtage, "Control of Storage and Writing Times in the Diode Storage Correlator," *Appl. Phys. Lett.*, 33, pp. 555-556, 1978.
6. M. El-Nokali and E. L. Adler, "A Modified Theory for SAW Memory Correlators," *IEEE Trans. Sonics and Ultrasonics*, SU-27, pp. 38-42, 1980.
7. H. C. Tuan, B. T. Khuri-Yakub, and G. S. Kino, "A New Zinc Oxide on Silicon Monolithic Storage Correlator," *Proc. IEEE Ultrasonics Symp.*, pp. 496-499, 1977.
8. H. C. Tuan and G. S. Kino, "A Monolithic Zinc Oxide on Silicon pn Diode Storage Correlator," *Appl. Phys. Lett.*, 31, pp. 641-643, 1977.
9. G. A. Armstrong and S. Crampin, "Piezoelectric Surface Waves in Zinc Oxide Layered Substrates," *Electr. Lett.*, 9, pp. 322-323, 1973.
10. F. C. Lo, R. L. Gunshor, and R. G. Pierret, "Monolithic (ZnO) Sezawa Mode pn Diode Array Memory Correlator," *Appl. Phys. Lett.*, 34, pp. 725-726, 1979.

11. J. E. Bowers, B. T. Khuri-Yakub, and G. S. Kino, "Broadband Efficient, Thin Film Sezawa Wave Interdigital Transducers," Appl. Phys. Lett., 36, 1980.
12. H. C. Tuan, P. M. Grant, and G. S. Kino, "Theory and Application of Zinc Oxide on Silicon Monolithic Storage Correlator," Proc. IEEE Ultrasonics Symp. Proc., pp. 38-43, 1978.
13. G. S. Kino, and R. S. Wagers, "Theory of Interdigital Couplers on Nonpiezoelectric Substrates," J. Appl. Phys., 44, pp. 1480-1488, 1973.
14. R. F. Pierret, R. L. Gunshor, and M. E. Cornell, "Charge Injection in Metal ZnO-SiO₂-Si Structures," J. Appl. Phys., 50, pp. 8112-8124, 1979.
15. B. A. Auld, and G. S. Kino, "A Normal Mode Theory for Acoustic Surface Waves and Its Application to the Interdigital Transducer," IEEE Trans. Electr. Dev., ED-18, pp. 898-908, 1971.
16. D. Behar, G. S. Kino, J. E. Bowers, and H. Olaisen, "Storage Correlator as an Adaptive Inverse Filter," Electr. Lett., 16, pp. 130-131, 1980.
17. J. E. Bowers, G. S. Kino, D. Behar, and H. Olaisen, "Adaptive Deconvolution Using an SAW Storage Correlator," IEEE Trans. Sonics and Ultrasonics, to be published.

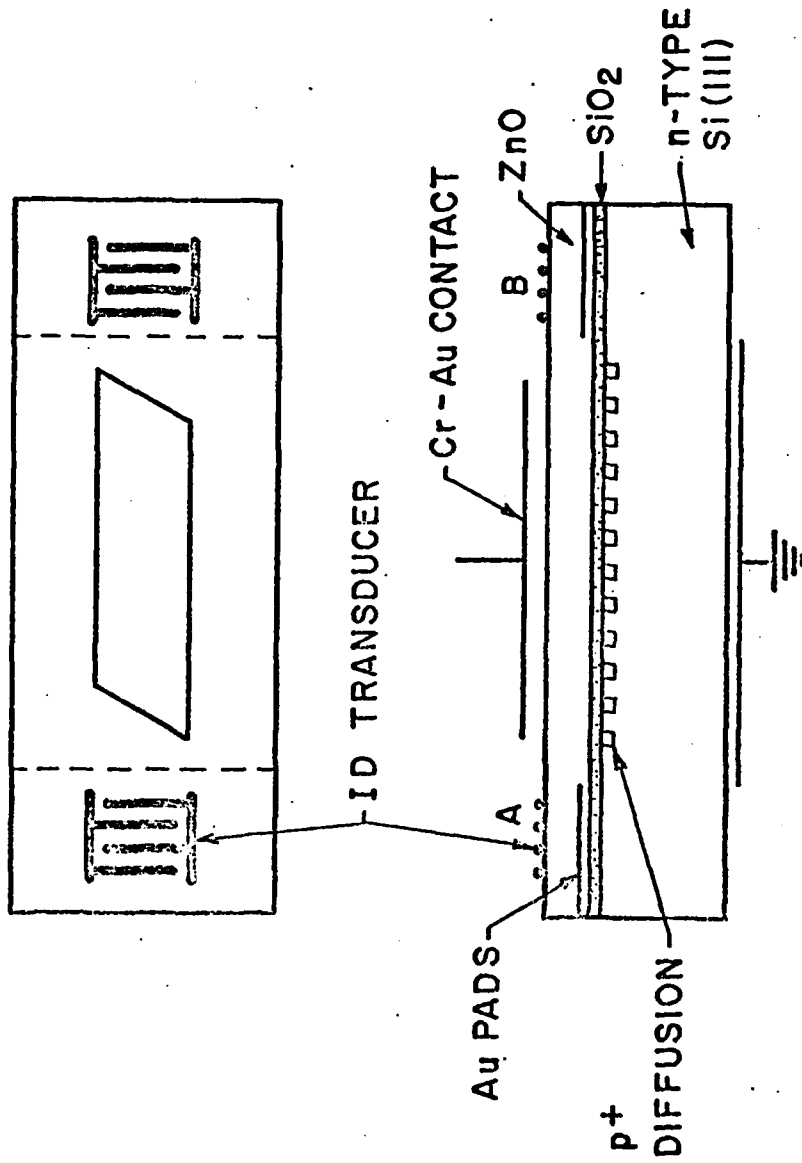
FIGURE CAPTIONS

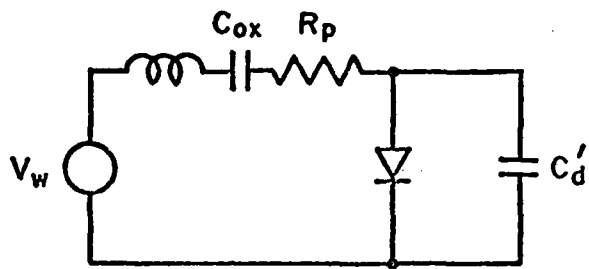
1. Schematic drawing of the monolithic storage correlator.
2. Circuit models: (a) writing process; (b) diode model; and (c) reading process.
3. Experimental measurement (•) of the top plate impedance as a function of frequency and theoretical fit (-) to the data using the model of Fig. 2a.
4. The effect of doping level on the acoustic wave attenuation correlation efficiency and total correlation efficiency, including attenuation for short pulses.
5. Dependence of correlator output on the duration of the acoustic signal.
6. Dependence of correlator output on the duration of the write signal for short pulses (0-1 μ s).
7. Dependence of correlator output on the duration of the write signal for long pulses (0-10 ms).
8. Dependence of correlator output on the number of correlations.
9. Dependence of correlator output on acoustic power.
10. Dependence of correlator output on writing signal voltage for four reading voltages and 10 ms input correlation times.
11. Dependence of the correlator output on writing signal voltage for two acoustic power levels and .2 μ s input correlation times.
12. Dependence of output correlation on the readout voltage for three different acoustic voltages.

TABLE I: Parameters of the Storage Correlator Used in the Experiments

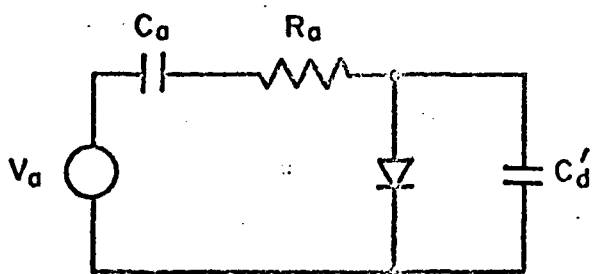
Measured Parameters		
L	Length of diode array	1.1 cm
l	Diode periodicity	8.0 μm
δ	Diode spacing	4.0 μm
λ	Acoustic wavelength	32.0 μm
	Substrate thickness	350.0 μm
	SiO ₂ thickness	.1 μm
	ZnO thickness	1.6 μm
$\Delta v/v$	Coupling coefficient	.0027 (.0036*)
R _p	Substrate resistance	5.0 Ω (5.2*)
L	Top plate lead inductance	22 nH (20 nH*)
C _p	Series capacitance of ZnO and SiO ₂	364.0 pF (326 pF*)
	Top plate area	.11 cm ²
	Type of substrate	N-type
Calculated Parameters		
ω	Angular frequency	7.8 x 10 ⁸ rad/s
C _{ox}	ZnO and SiO ₂ capacity	5850 pF/cm ²
C _a	Acoustic capacity	7950 pF/cm ²
C _d	Diode capacity	6030 pF/cm ²
C _o	Silicon capacity (C _d + C _d ')	6030 pF/cm ²
N _p	Substrate doping density	3.5 x 10 ¹⁴ cm ⁻³
Estimated Parameters		
τ_p	Minority carrier lifetime	.1 μs
C _d '	Capacity between the diodes	6030 pF/cm ²

* Theoretical calculation.

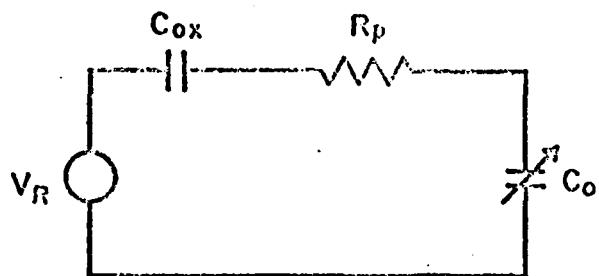




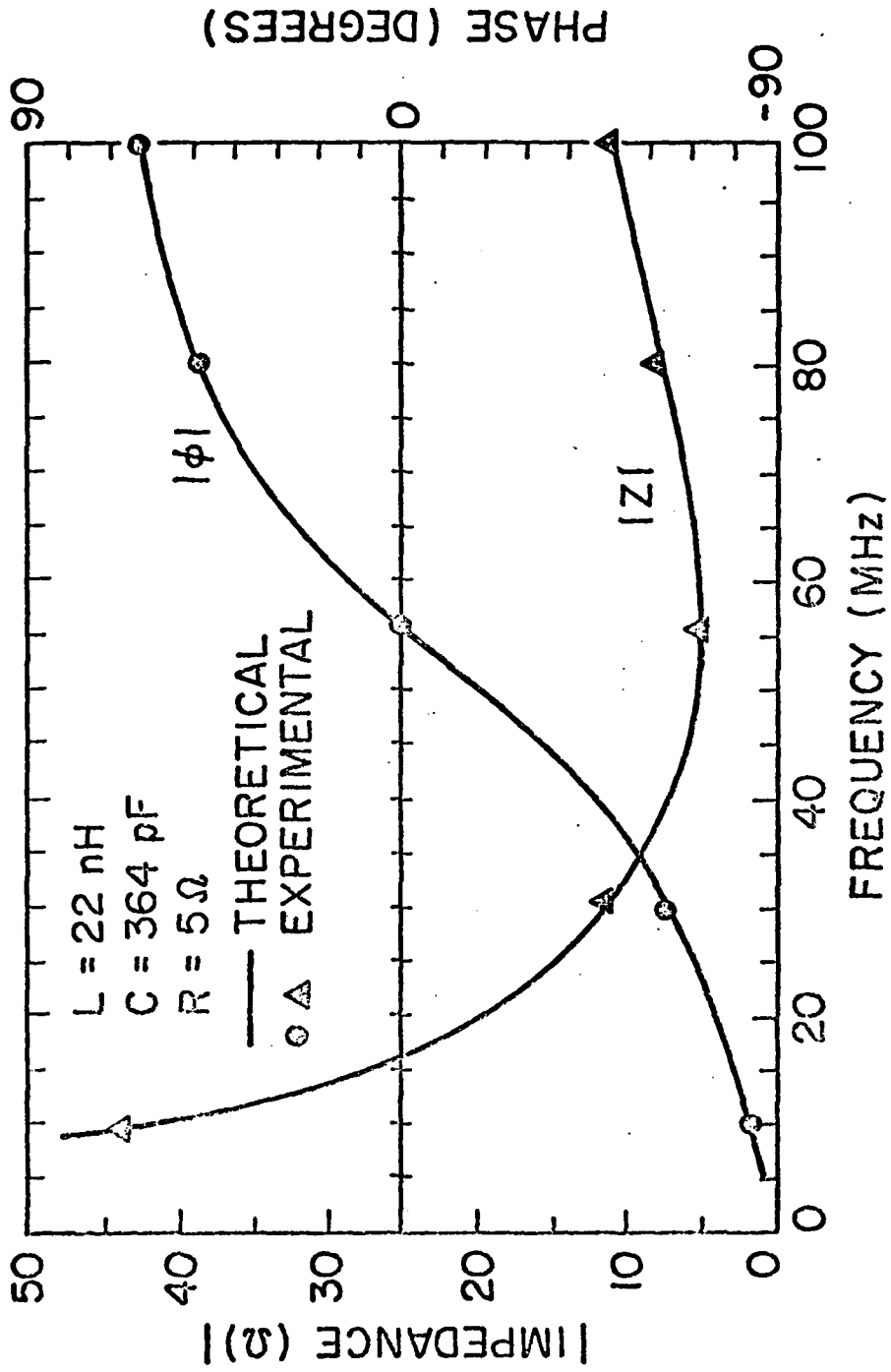
(a)

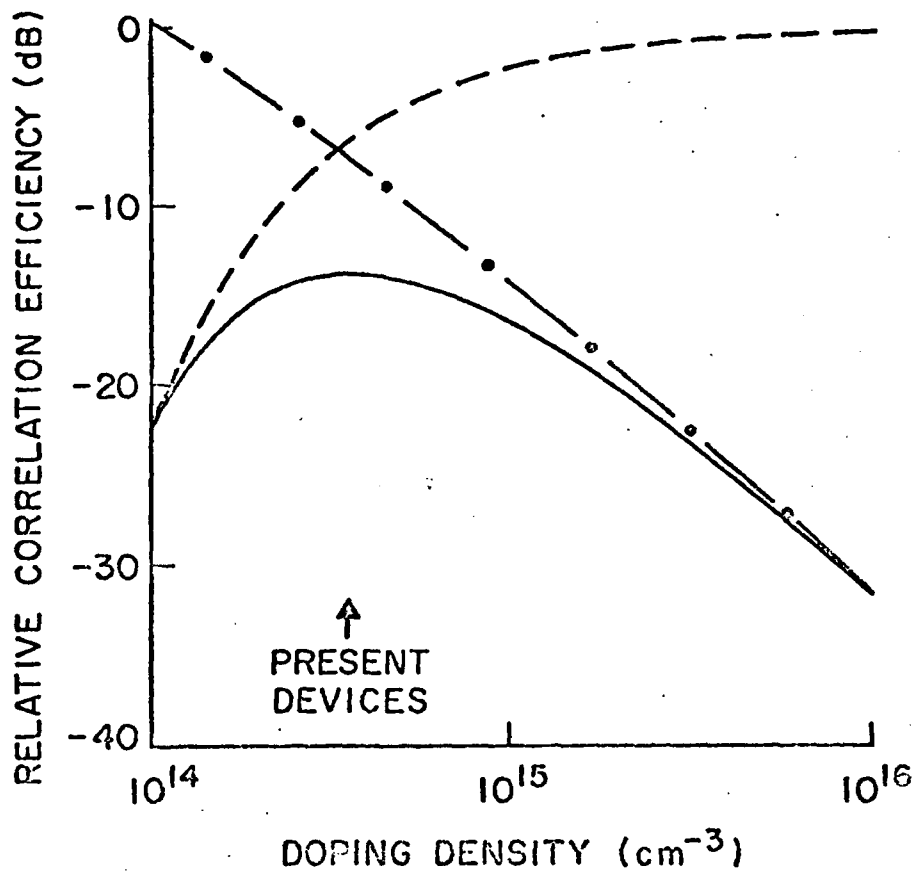


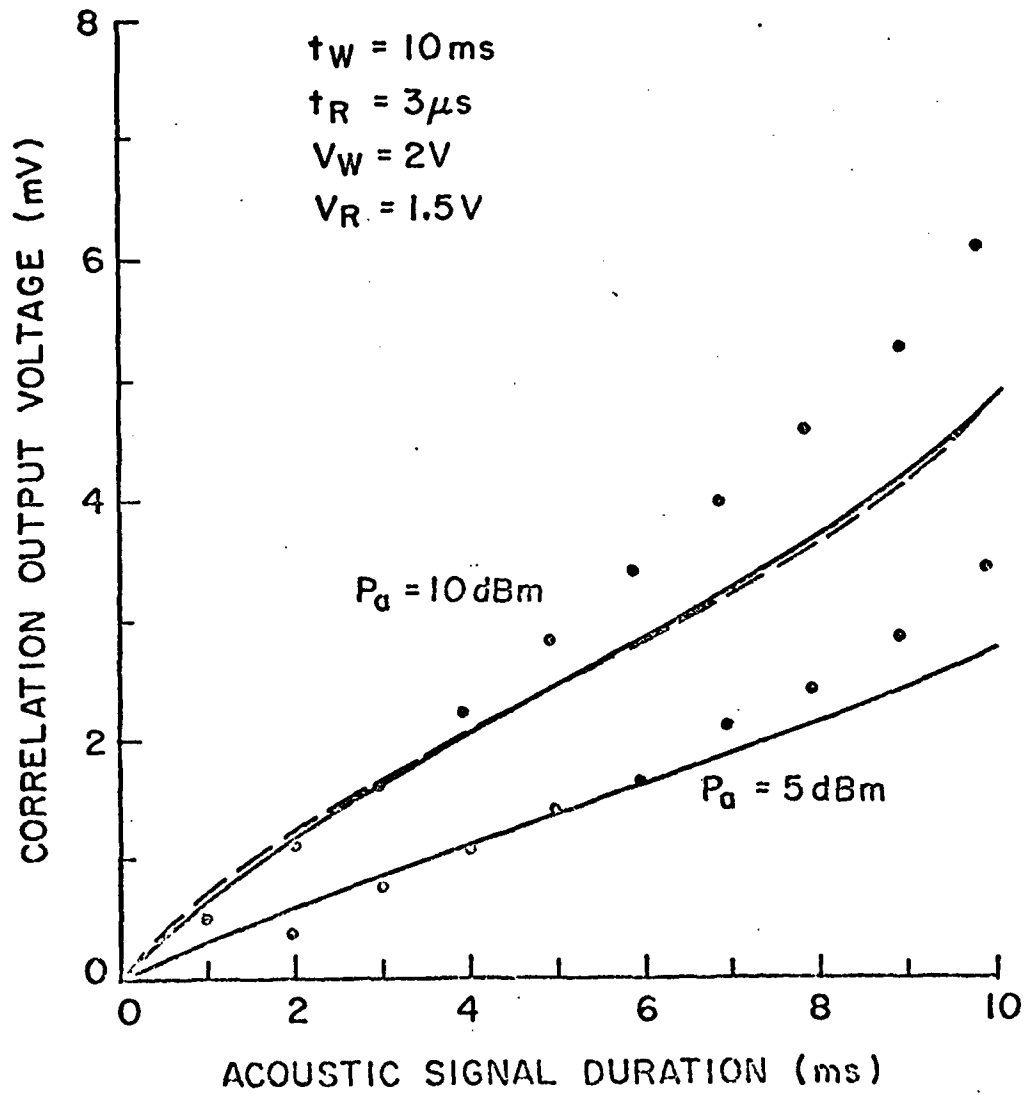
(b)

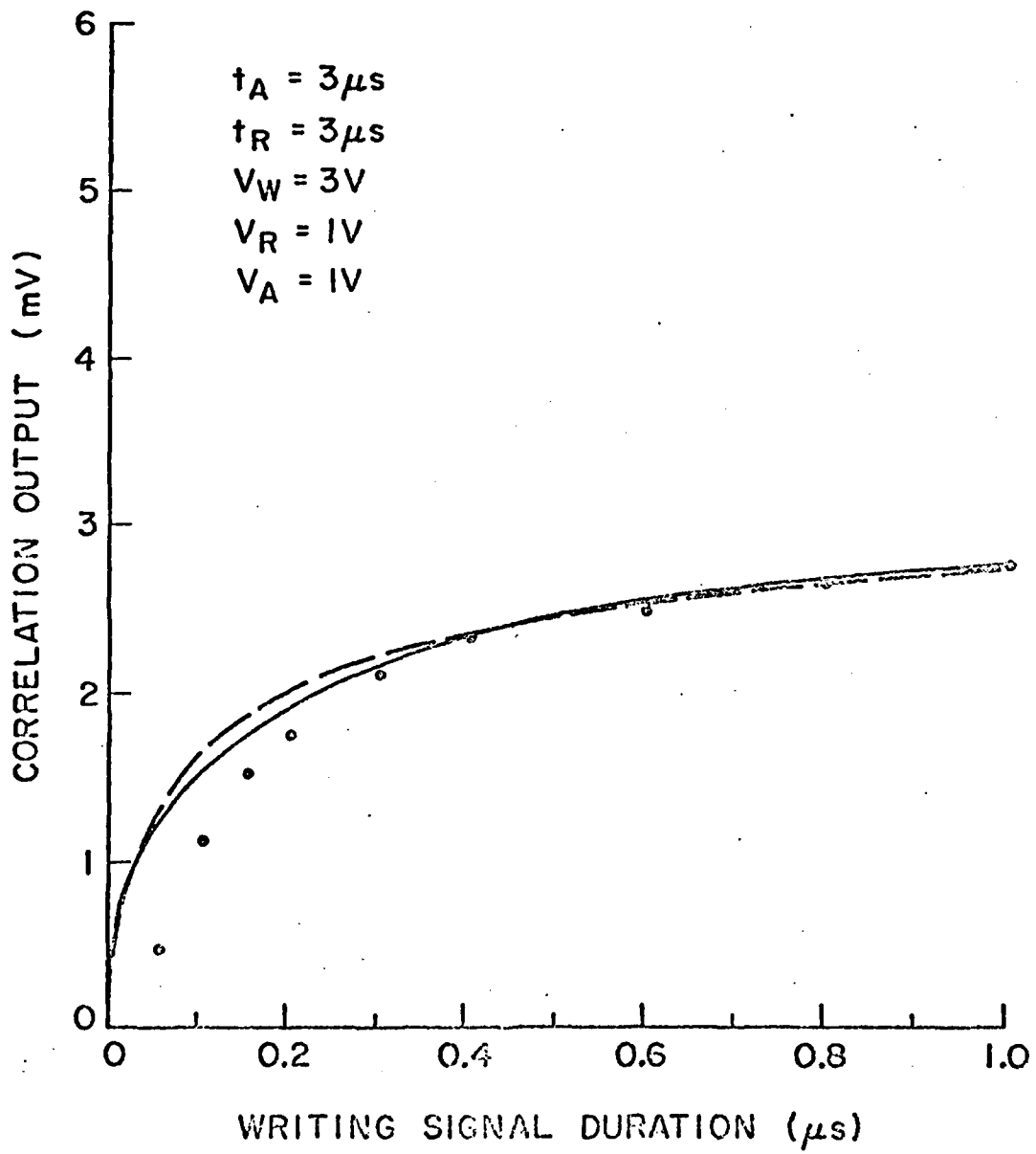


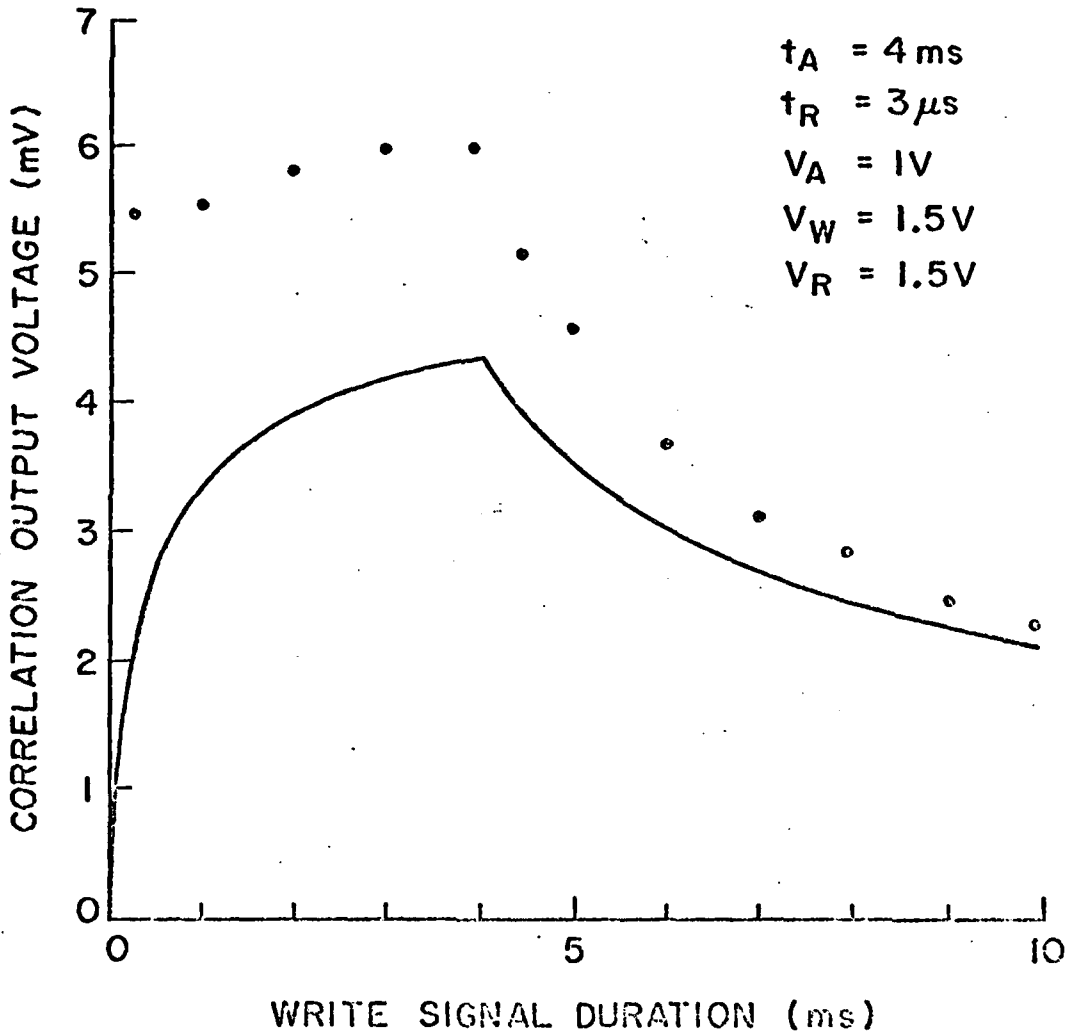
(c)

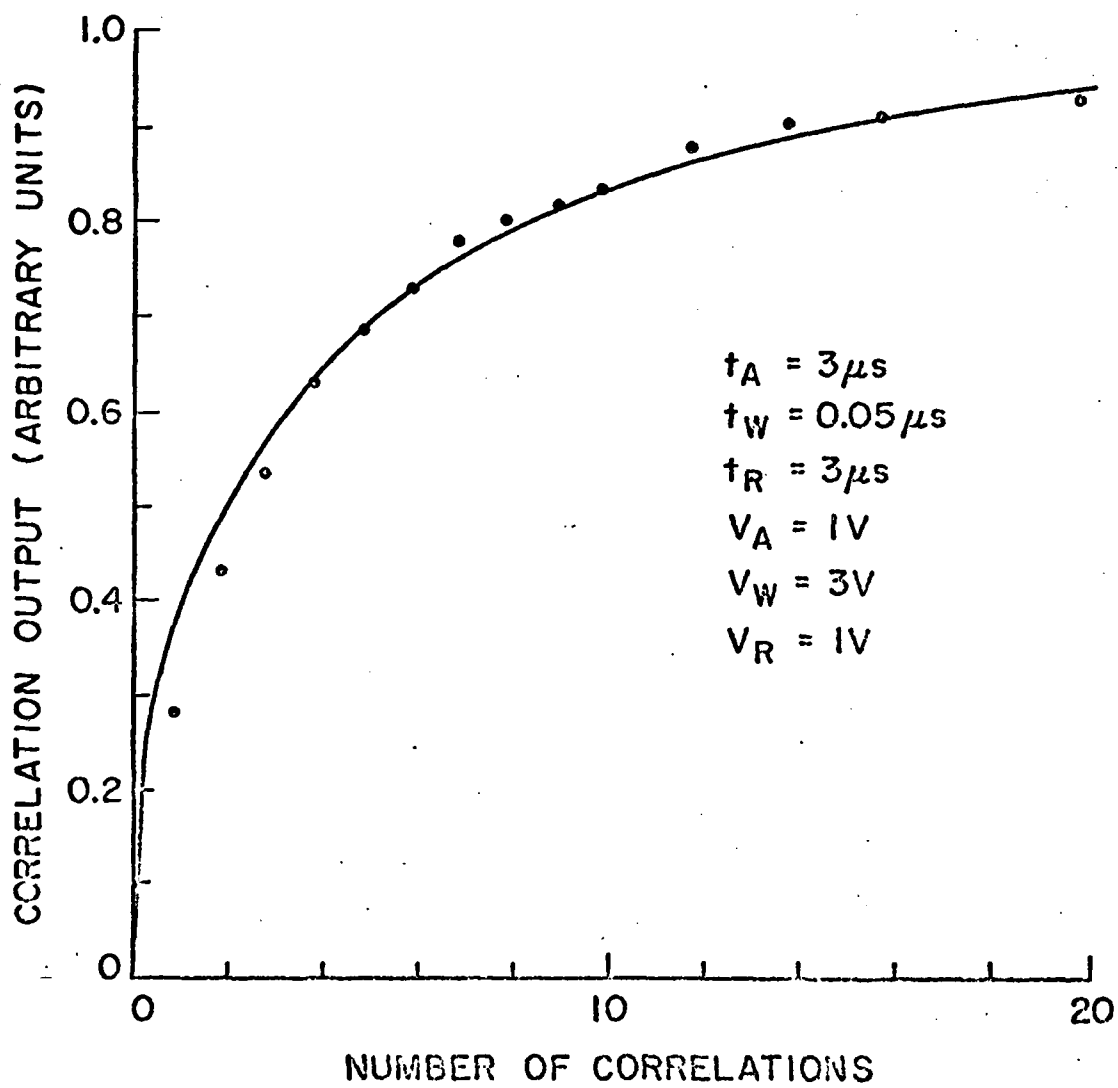


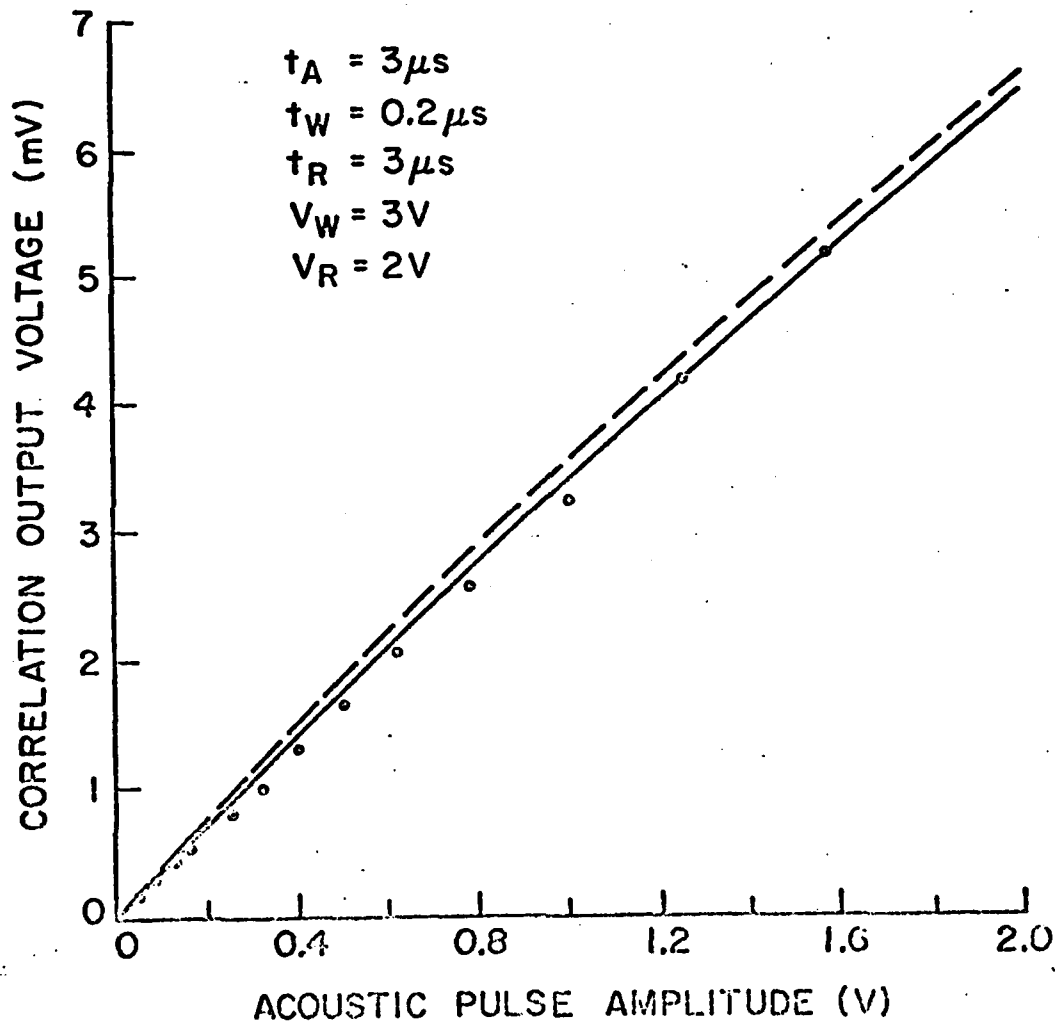


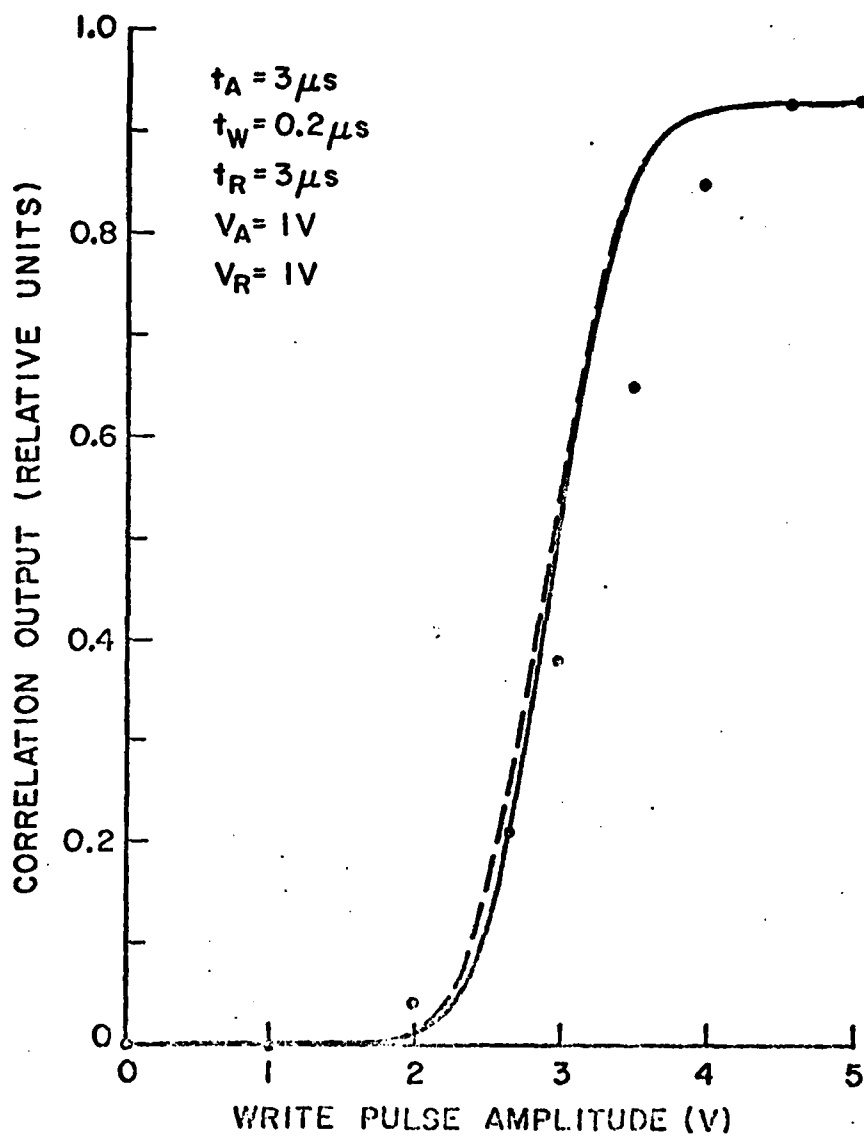


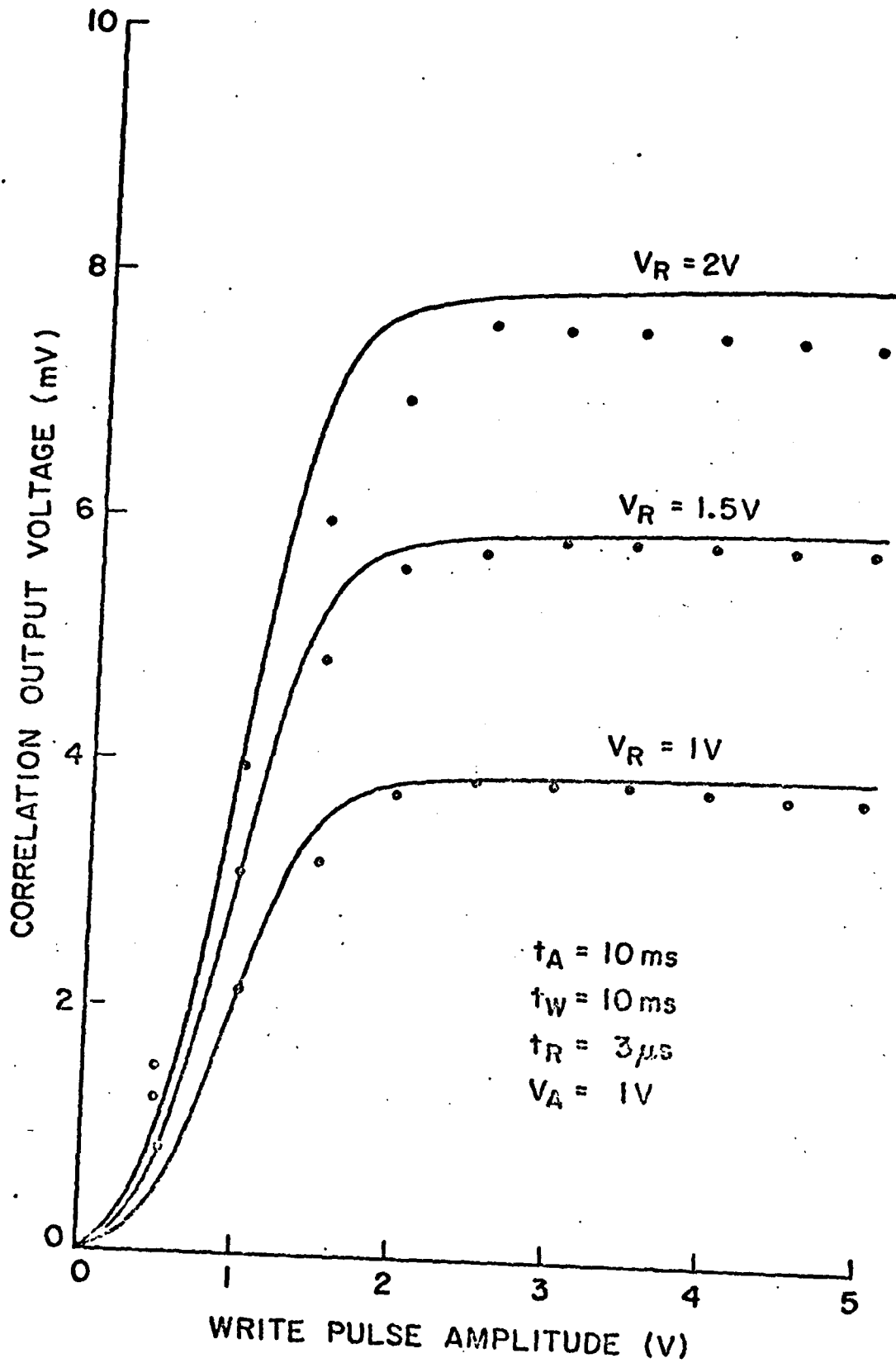


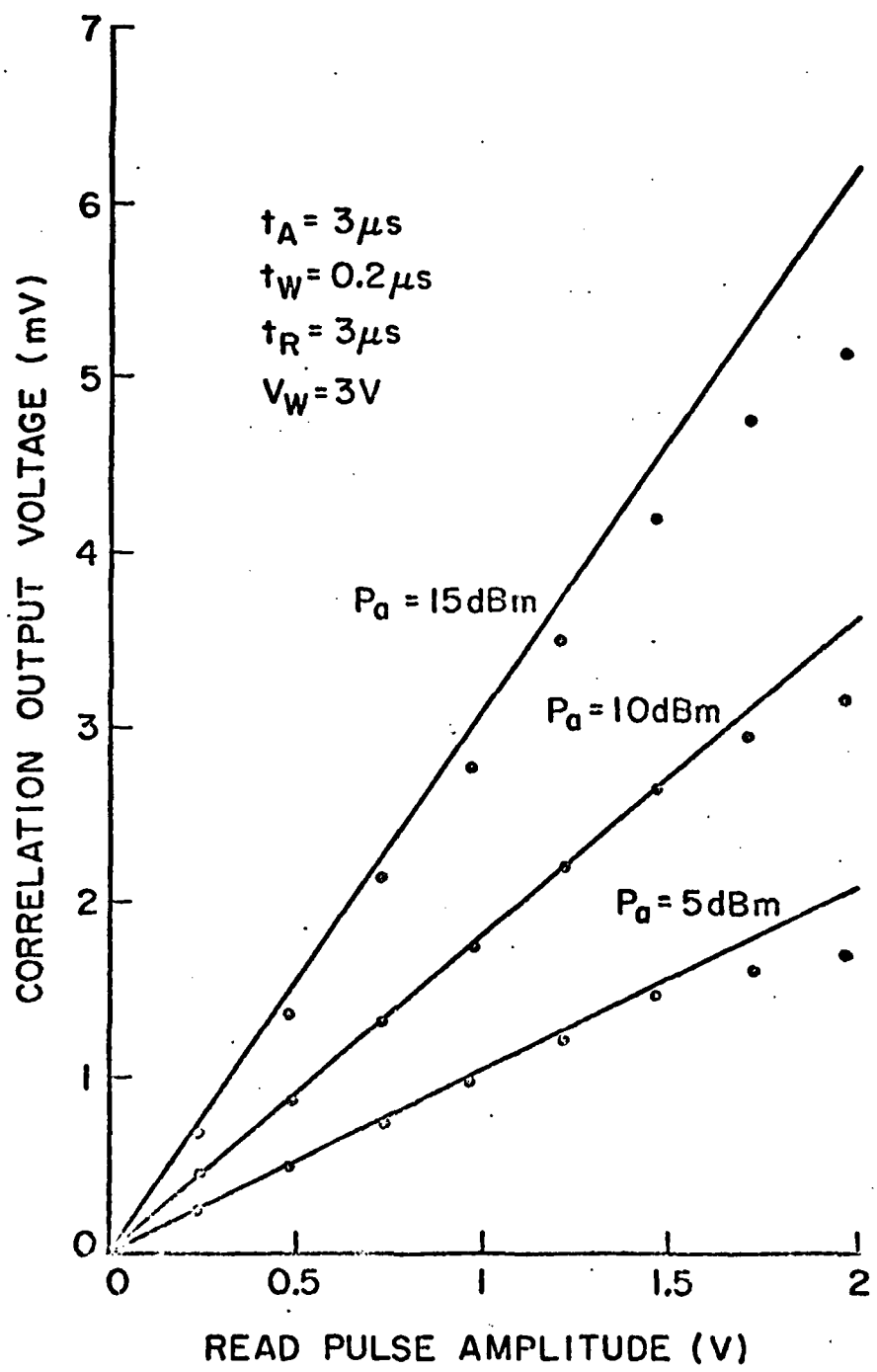












DISPERSION EFFECTS

1. Introduction

Any SAW device that utilizes a layered substrate will be dispersive i. e. the velocity of propagation will depend on the frequency of the wave. The SAW velocity of the material used for the substrate will in general be different than the SAW velocity of the material used for the layer. Consequently, the SAW velocity of the layer/substrate system will depend on the relative amounts of energy in the layer and in the substrate. As the frequency of the wave decreases, the decay depth of the surface wave increases and the SAW velocity approaches the SAW velocity of the substrate. Dispersion will thus be minimized when the SAW velocities of the substrate and layer are almost equal. Thus systems like ZnO ($v_R = 2639$) on GaAs ($v_R = 2600$) are not very dispersive while systems like ZnO on silicon ($v_R = 4920$) or ZnO on sapphire ($v_R = 5600$) are very dispersive.

Dispersion is of course not a problem in narrow band systems since the velocity does not change very much over the frequency range. However, dispersion causes phase distortions of the wave, and in broadband systems, dispersion can limit the usable bandwidth to much less than the IDT bandwidth.

In this section we shall present results on the variation of group velocity with frequency and compare the amount of dispersion in the different systems discussed in the previous section. Then we shall analytically examine the effects of dispersion on correlation and convolution.

2. Group Velocity

The dependences of the group and phase velocities on normalized wave number hk for the Rayleigh mode in ZnO on (100)Si and (111)Si are given in Fig. 2.1. The position of the two peaks in $\Delta v/v$ are indicated in the figure. Note that the second $\Delta v/v$ peak occurs at the optimum value of hk , namely the point where the group velocity goes through a minimum. The curves for (100)Si and (111)Si have the same amount of dispersion at the position of the second $\Delta v/v$ peak; however, at the first $\Delta v/v$ peak the slope of the group velocity curve for the (111)Si system is half the slope of the (100)Si system.

The same data for Sezawa waves on (100)Si is presented in Fig. 2.2. In this case, the horizontal axis is multiplied by the phase velocity to obtain $h\omega$ which unlike hk is an experimentally measurable quantity. This is done so that the experimental data could be included. It can be seen that the agreement is very good.

These systems can be numerically compared by tabulating the slope of the group velocity curve at the desired operating point (Table 1). This parameter will be used for the analysis in the next section; however, a better physical grasp of the situation can be obtained by calculating how much spreading occurs to a $.04 \mu s$ pulse after it has traveled 1 cm (column 2, Table 1) or after it has traveled 1 μs (column 3, Table 1). The magnitude of the dispersion problem is now apparent. For instance, suppose it was desired to delay a digital code (25 MHz bit rate) by 1 μs . The output would be hopelessly distorted by any of the monolithic systems considered here. The

maximum bit rate that could be used with a Sezawa wave 1 μs delay line is 14 MHz. Thus, the usable bandwidth is entirely limited by dispersion, not the IDT bandwidth.

For systems like ZnO/Si Sezawa wave or Rayleigh wave (first $\Delta v/v$ peak), the variation of group velocity is linear. Thus, a chirp transducer with linear phase dispersion can be used to compensate for the material dispersion. This will work for any delay line with a fixed delay. The technique is only approximate for devices like convolvers and correlators where the delay to different points in the interaction region varies from typically 0 to 4 μs . However, as we shall see in the next section, compensation can be obtained for many systems utilizing correlators or convolvers.

3. Effect of Dispersion on Correlation and Convolution

It is useful to qualitatively consider the effects of dispersion on 1) correlation and input correlation in the storage correlator, and 2) convolution in the SAW convolver. We shall then analytically examine the effects of dispersion on these processes.

Qualitative Dispersion Effects

We shall use a chirp signal for our discussion since its use has important signal processing applications and since the different frequency components are clearly distinguishable.

The correlation of a chirp is shown in Fig. 2.3. For the ZnO/Si system, the group velocity decreases with increasing frequency (for $h\omega < 10^4$) so for a down chirp, the initial high frequency components travel the slowest, and the chirp contracts. This signal is stored by applying a short signal to the topplate. A second signal is sent to the same acoustic port; it undergoes the same distortion and the correlation is obtained at the topplate port.

The output is compressed from the initial width by the full time bandwidth product of the device. However, for times before and after the time of chirp coincidence, the distortions on the two signals are different, and thus, the sidelobe pattern of a dispersive device will be different than the sidelobe pattern of a nondispersive device. Thus, *the width of the output pulse is not increased but the sidelobe pattern will change.* This change is usually unimportant. Note that these conclusions are true for any compression experiment. The code can be a chirp, PSK (phase shift keyed), or frequency hopped, and the maximum bit rate allowed by the transducer bandwidth can be used.

For input correlation in a device without dispersion, two long chirps are sent into the device, and a narrow peak builds up in the center of the interaction region. Much larger compression ratios can be obtained using the input correlation mode (30,000 for a ZnO/Si correlator[1]) since the duration of the codes is only limited by the storage time of the diodes. However, the dynamic range is limited because all of the charge is stored in just a few diodes, and the full interaction region is not being utilized.

Consider now a dispersive correlator. Only one of the two chirp signals is distorted, unlike the regular correlation mode. The effect of distorting only one chirp is that as the correlation proceeds, the position of the narrow pulse changes (it shifts from left to right in Fig. 2.3). The total peak shift is given by the change in group velocity over the chirp frequency range times the time delay to the center of the interaction region. This width is .45 cm for a typical Sezawa wave device. Fortunately, the phase relations in the broadened pulse are such that when an rf read pulse is applied to the acoustic port, the full compression should be obtained. Furthermore, the dynamic range should be better than for a nondispersive device since much more of the interaction region is utilized in the dispersive device. Thus, dispersion does not degrade

the storage correlator performance in compression experiments.

In a convolver, two counterpropagating waves are sent into the device (Fig. 2.4). The effect of dispersion is to compress one chirp and expand the other. Thus, the output pulse width will be broadened by dispersion. Note, however, that in a device with a linear change in group velocity that the full compression can be obtained by appropriately changing one of the slopes, either by using a chirp transducer or by using two chirp generators with different slopes.

Analytic Effects of Dispersion

Consider first a correlator operating in the regular correlation mode. A signal $a_1(t) \cos \omega_0 t$ is sent into the acoustic port. If the Fourier transform of this signal is $A_1(\omega)$ i. e.

$$a_1(t) \cos \omega_0 t = \frac{1}{\sqrt{2\pi}} \int_{-\infty}^{\infty} d\omega A_1(\omega) e^{j\omega t} \quad 2.49$$

After this signal has propagated for a time t_0 , a short pulse is applied to the topplate, and the signal $q(z)$ is stored

$$q(z) = \frac{1}{\sqrt{2\pi}} \int_{-\infty}^{\infty} d\omega A_1(\omega) e^{j(\omega t_0 - k(\omega)z)} \quad 2.50$$

For acoustic to plate readout, a second signal $a_2(t) \cos \omega_0 t$ with Fourier transform $A_2(\omega)$ is sent to the acoustic port, and the time and spatial dependence of the propagating signal is

$$a_2(z, t) = \frac{1}{\sqrt{2\pi}} \int_{-\infty}^{\infty} d\omega' A_2(\omega') e^{j(\omega' t - k(\omega')z)} \quad 2.51$$

The output is

$$V(t) = \int_0^L dz a_2(z, t) q(z) \quad 2.52$$

$$V(t) = \frac{1}{2\pi} \int d\omega d\omega' A_1(\omega) A_2(\omega') \int e^{jz(k(\omega) - k(\omega'))} dz \quad 2.53$$

$$V(t) = \int d\omega d\omega' A_1(\omega) A_2(\omega') e^{j(\omega't - \omega t_0)} \delta(k(\omega) - k(\omega')) \quad 2.54$$

Since[2]

$$\int_{-\infty}^{\infty} g(x) \delta(f(x)) dx = \sum_i g(x_i) \frac{1}{\left| \frac{df}{dx} \right|_{x_i}} \quad 2.55$$

where x_i are the zeros of $f(x)$, and since

$$|V_g| = \frac{1}{\left| \frac{dk}{d\omega} \right|_{\omega=\omega'}} \quad 2.56$$

then

$$V(t) = \frac{1}{2\pi} \int_{-\infty}^{\infty} d\omega |V_G(\omega)| A_1(\omega) A_2(-\omega) \quad 2.57$$

For no dispersion, $V_G(\omega)$ is a constant (V_{G0}) and the output is just the correlation of the two inputs:

$$V_0(t) = V_{G0} \int_{-\infty}^{\infty} d\omega A_1(\omega) A_2(-\omega) = V_{G0} [a_1(t) \cos \omega_0 t] \otimes [a_2(t) \cos \omega_0 t] \quad 2.58$$

where \otimes stands for correlation. When dispersion is present, then the output is the convolution of 1) the correlation output in the absence of dispersion $V_0(t)$ with 2) the Fourier transform of the group velocity

$$V(t) = V_0 * F(|V_G(\omega)|) \quad 2.59$$

For the case of linear dispersion, this transform is

$$F(|V_G(\omega)|) = \frac{\pi}{\tau} V_{G0} \left(\frac{\sin \frac{\tau}{2}}{\frac{\tau}{2}} \right)^2 \quad 2.60$$

where

$$\tau = \left| \frac{1}{V_{G0}} \frac{dV_G}{d\omega} \right|_{\omega_0} \quad 2.61$$

Thus, the output is broadened; however, for any of the monolithic devices discussed here, τ is so small that the broadening is not detectable. For instance, for a ZnO/Si Sezawa wave device at 165 MHz, $\tau = 5 \times 10^{-14}$ s.

For input correlation, the analysis is the same except that the stored charge is

$$q(z) = \int A_1(\omega)A_2(\omega)e^{-j\omega z/V_{G0}}e^{j\omega^2\tau zV_{G0}} \quad 2.62$$

where τ is defined in Eq. 2.61. If τ is nonzero, then there is a nonzero distorting term. If a delta function read pulse is assumed, then Eq. 2.58 is obtained. Thus, even if τ is nonzero, the correlation output is not significantly broadened by dispersion.

The case of dispersion in a convolver has been treated by Morgan[3]. The analysis is similar to the correlation analysis. The two traveling waves are

$$a_1(z, t) = \frac{1}{\sqrt{2\pi}} \int_{-\infty}^{\infty} d\omega A_1(\omega) e^{j(\omega t - k(\omega)z)} \quad 2.63$$

$$a_2(z, t) = \frac{1}{\sqrt{2\pi}} \int_{-\infty}^{\infty} d\omega' A_2(\omega') e^{j(\omega' t + k(\omega')z) - k(\omega')L} \quad 2.64$$

The output is

$$V(t) = \int_0^L dz a_1(z, t) a_2(z, t) \quad 2.65$$

$$V(t) = \int_{-\infty}^{\infty} d\omega |V_{G0}(\omega)| A_1(\omega) A_2(\omega) e^{j(2\omega t - k(\omega))L} \quad 2.66$$

Using the expansion for k

$$k \approx \frac{\omega}{V_{G0}} + \frac{d}{d\omega} \left(\frac{1}{V_G} \right) \omega^2 = \frac{\omega}{V_{G0}} + \frac{\tau}{V_{G0}} \omega^2 \quad 2.67$$

and changing the transform variable to $t_1 = 2t - L/V_{G0}$ yields

$$V(t) = \frac{V_{G0}}{2} \int_{-\infty}^{\infty} d\omega A_1(\omega) A_2(\omega) e^{j\omega t_1} e^{-jL\tau\omega^2/V_{G0}} \quad 2.68$$

The important difference between this expression and the expression we obtained for correlation is the rapidly varying phase term $\exp(-jL\omega^2\tau/V_{G0})$. For correlation, the total effect of dispersion entered through the frequency variation of $V_G(\omega)$. For convolution, this relatively slow variation can be neglected. Since the Fourier transform of $\exp(-\alpha\omega^2)$ is $1/\alpha \exp(-t_1^2/\alpha)$ then the convolution output is convolved with the distorting factor

$$F(e^{-j(L\omega^2\tau/V_{G0})}) = \frac{-j}{\tau'^2} e^{jt^2/\tau'^2} \quad 2.69$$

where $\tau' = \sqrt{L\tau/V_{G0}}$. For a Sezawa wave, $\tau' = .03\mu s$. Consequently, the maximum usable bandwidth is on the order of 30 MHz.

REFERENCES

- [1] H. C. Tuan and G. S. Kino, *El. Lett.*
- [2] R. Bracewell, "The Fourier Transform and Its Applications", McGraw-Hill, New York, 95(1965).
- [3] D. P. Morgan, "Effect of Dispersion in Surface Acoustic Wave Convolver", *IEEE Trans. Sonics, Ultrasonics*, SU-22, 274(1975).

• **List of Figures**

- [1] Dependence of group and phase velocities on normalized wave number hk for the first Rayleigh mode on (100)Si and (111)Si.
- [2] Dependence of group and phase velocities on normalized frequency $h\omega$ for the Sezawa mode (theory -, experiment .).
- [3] Schematic drawing of chirp correlation experiment a) regular correlation mode, b) input correlation mode.
- [4] Schematic drawing of chirp convolution (one chirp inverted).

• **List of Tables**

- [1] Dispersion characteristics for several systems of interest.

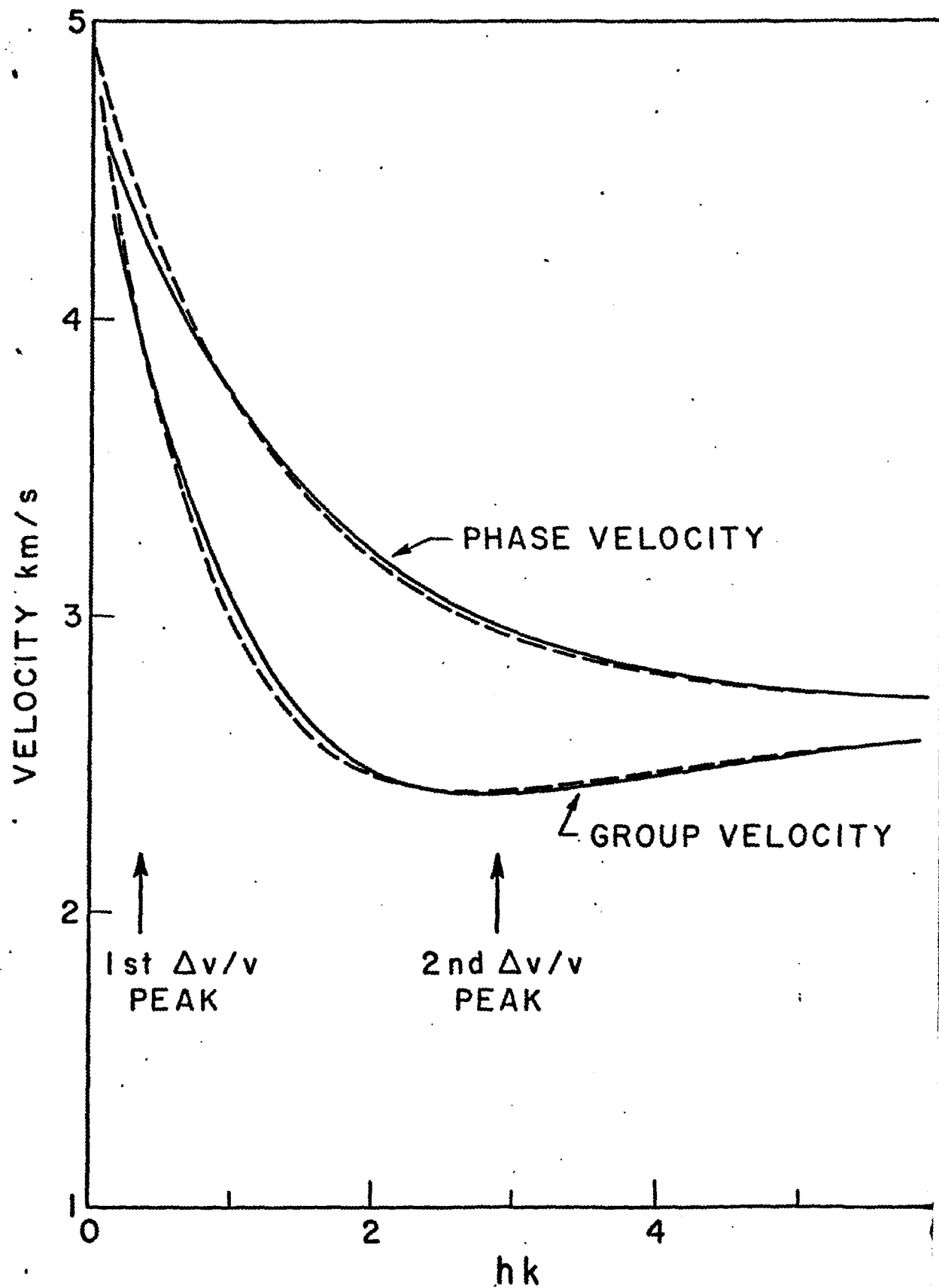


Fig. C-1

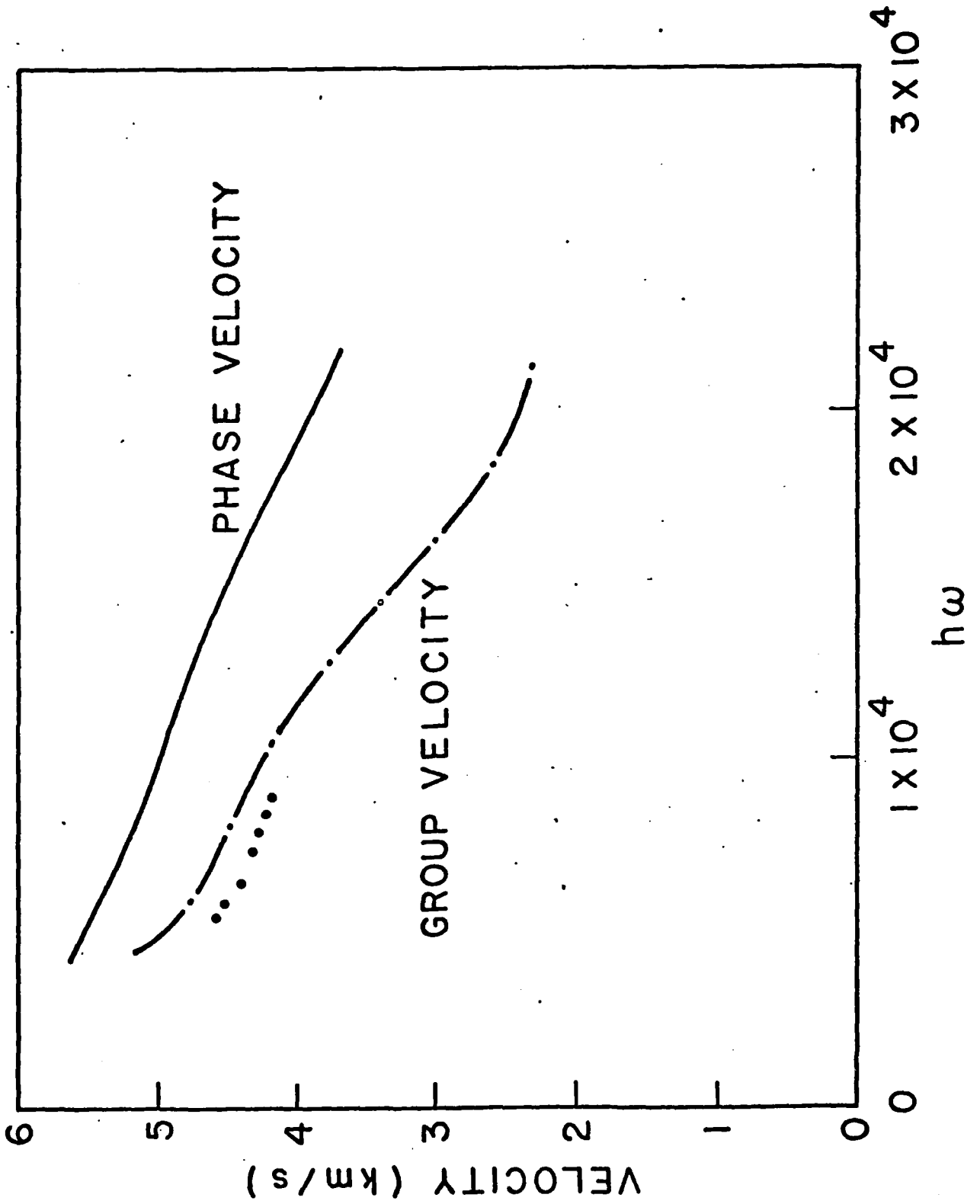
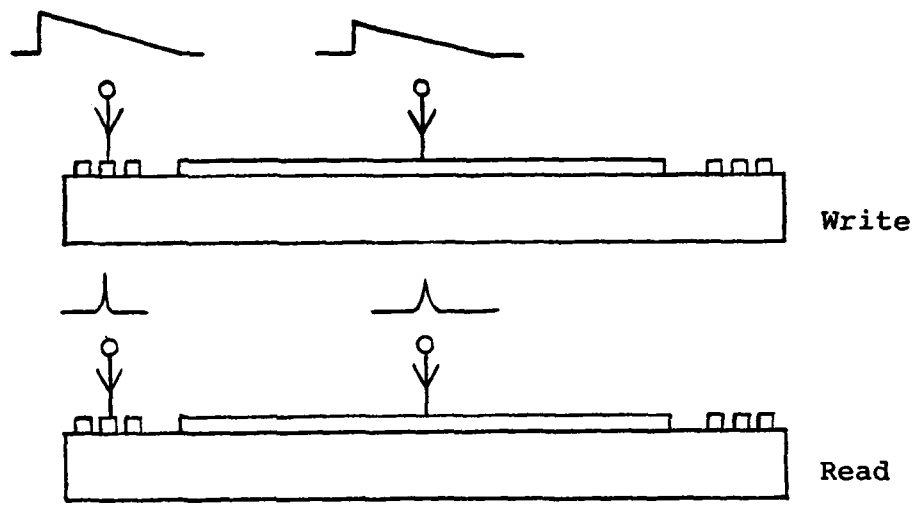
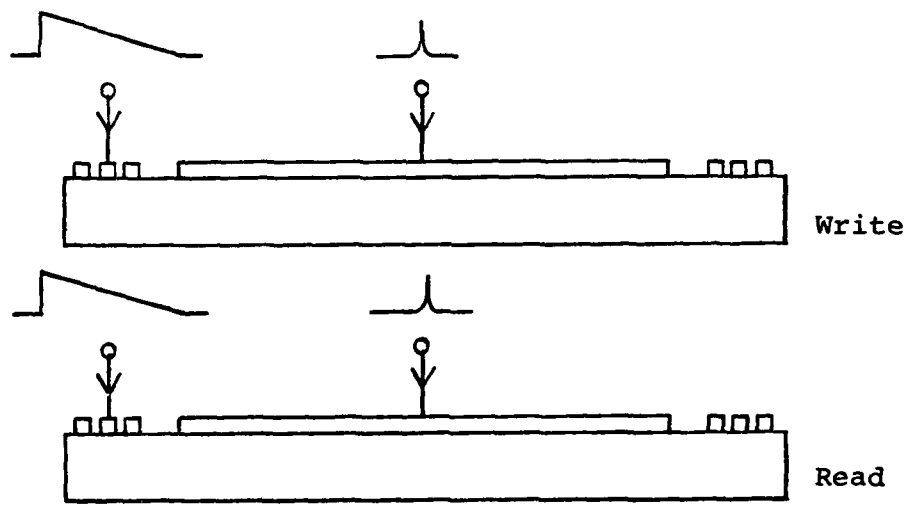


Fig. C-2



(a)



(b)

Fig. C-3

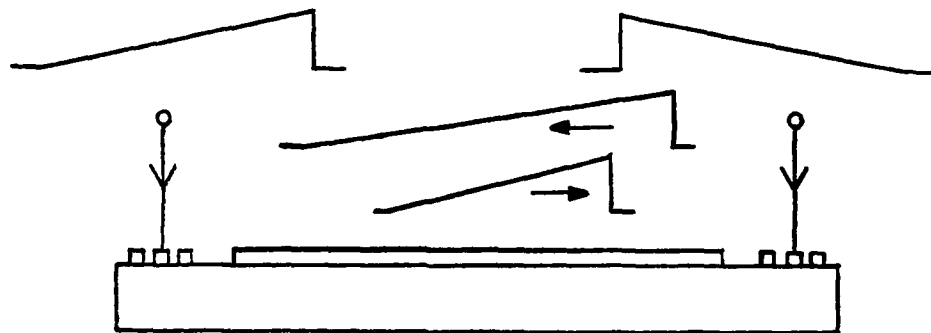


Fig. C-4

Broadband efficient thin-film Sezawa wave interdigital transducers

J. E. Bowers, B. T. Khuri-Yakub, and G. S. Kino
Ginzton Laboratory, Stanford University, Stanford, California 94305

(Received 31 January 1979; accepted for publication 4 March 1980)

The phase velocities and coupling coefficients for Sezawa waves in (001) ZnO on (001) cut, (100) prop. Si and on (111) cut, (112) prop. Si are presented. Experimental results from Sezawa wave delay lines are presented which represent for the first time bandwidths in excess of 30 MHz in a thin-film monolithic device.

PACS numbers: 43.35.Ns, 77.60.+v, 68.60.+q, 43.20.Bi

Acoustic surface wave (ASW) signal processing devices such as convolvers and storage correlators can be monolithic, thin-film devices (typically ZnO on Si)¹ or hybrid arrangements where a piezoelectric substrate (typically LiNbO₃) is pressed against a semiconductor (typically Si).^{2,3} The monolithic approach has the advantages of ruggedness, smaller size, and fewer spurious signals, and the devices are fabricated using standard planar processing and are potentially much cheaper to make. The very important limitation of monolithic ASW devices has been the inherent narrow fractional bandwidth (10–15%) which is a result of the low coupling coefficient ($\Delta v/v < 0.004$) attainable with thin-film Rayleigh wave devices. Larger first-order Rayleigh wave coupling coefficients ($\Delta v/v < 0.015$) are attainable with thicker films ($h \sim 0.5\lambda$ rather than $h \sim 0.07\lambda$).

Armstrong and Crampin⁵ have presented theoretical calculations for the coupling coefficient of second-order Rayleigh waves, commonly called Sezawa waves,⁶ for (001) ZnO on (001) Si. They found a peak coupling coefficient of 0.024 at a velocity of 4921 m/s. Elliot and co-workers^{7,8} have made Sezawa wave signal processing devices with 13% bandwidth.

In this letter, we present theoretical and experimental values for the phase velocity and coupling coefficient for Sezawa waves in (001) ZnO on (001) and (111) Si. Information is also presented on the third-order Rayleigh mode on (001) Si. Finally, results are presented on Sezawa wave delay lines with fractional bandwidths of 19 and 25% at a center frequency of 165 MHz.

The dependence of phase velocity on the normalized film thickness hk of the four lowest-order surface acoustic waves for a film of (001) ZnO on a (001) cut, (100) prop. Si substrate are shown in Fig. 1. The Sezawa mode is cut off at the silicon shear wave velocity, which is 5800 m/s for this

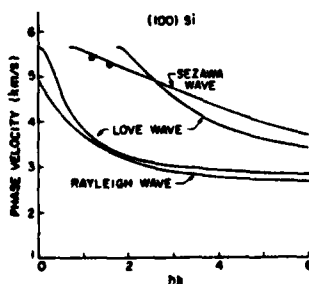


FIG. 1. Phase velocity vs normalized film thickness of (001) ZnO on (001) cut (100) prop. Si.

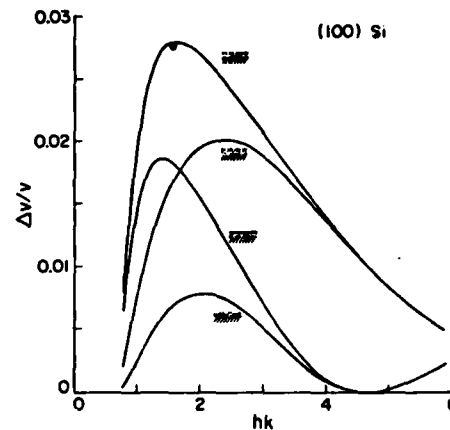


FIG. 2. Sezawa wave coupling coefficient vs normalized film thickness for (001) ZnO on (111) cut, (112) prop. Si.

orientation and propagation direction. This mode is progressively more lossy as k is decreased below the cutoff value ($hk_c = 0.73$). The cutoff value varies by as much as 15%, depending on the electrical conditions at the surface and the film-substrate interface.

The coupling coefficients of the Sezawa mode are shown in Fig. 2 for the four possible transducer configurations. Note that we predict coupling coefficients as large as 0.028, which is six times larger than the first Rayleigh wave peak for this orientation.⁴

The coupling coefficient $\Delta v/v$ must be calculated at a constant value of ω , not k as in Armstrong and Crampin,⁵ since the theories^{4,9} for transducer impedance all use $\Delta v/v$ at constant ω . Our calculations for $\Delta v/v$ at constant k agree with the results of Armstrong and Crampin⁵ and yield a value for the peak coupling coefficient which is 17% lower

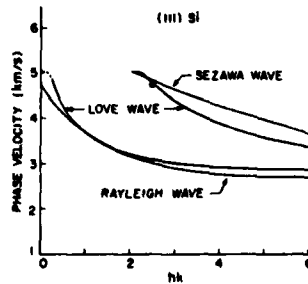


FIG. 3. Phase velocity vs normalized film thickness for (001) ZnO on (111) cut (112) prop. Si.

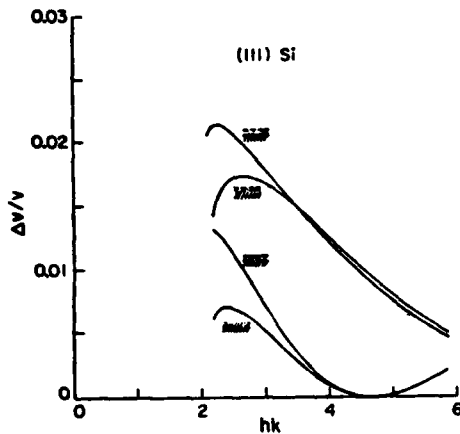


FIG. 4. Sezawa wave coupling coefficient vs normalized film thickness for (001) ZnO on (111) cut, (112) prop. Si.

than the correct value. Armstrong and Crampin report a phase velocity of 4921 m/s, which is significantly lower than our theoretical and experimental results and the experimental results of Elliot *et al.*⁷

The first-order Rayleigh wave coupling coefficient is 0.0002 at the optimum film thickness for Sezawa wave coupling ($hk = 1.65$) for transducers at the free surface and a metal shorting plane at the interface. Thus the spurious Rayleigh wave generation is 50 dB smaller. The coupling coefficient for Love waves to these transducers is zero, so these waves are not excited.

The maximum coupling coefficient for third-order Rayleigh waves was found to be 0.0072 at $hk = 5.8$. This mode is cut off at $hk = 3.2$ and is not desirable for these applications because of the low coupling coefficient.

The Sezawa wave phase velocity and coupling coefficient for (111) cut (112) prop. Si are shown in Figs. 3 and 4, respectively. The silicon shear wave velocity is lower (5000 m/s) for this orientation and propagation, and, consequently, the cutoff occurs at a higher value of $hk_c = 2.15$.

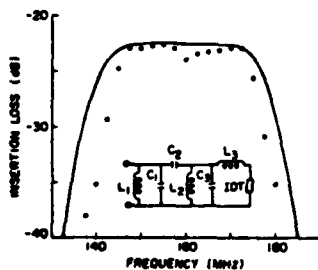


FIG. 5. Insertion loss vs frequency of a Sezawa wave delay line on (001) cut (100) prop. Si.

TABLE I. Delay-line parameters.

Substrate orientation: (001)	$L_1 = 0.048 \mu\text{m}$
Number of finger pairs: 4	$L_2 = 0.048 \mu\text{m}$
Wavelength: $32 \mu\text{m}$	$L_3 = 0.9 \mu\text{m}$
Film thickness: $8 \mu\text{m}$	$C_1 = 36 \text{ pF}$
Beam width: 1 mm	$C_2 = 40 \text{ pF}$
Pad capacitance: 0.2 pF	$C_3 = 9.6 \text{ pF}$

We have built Sezawa wave delay lines on both the (001) and (111) orientations. The experimental agreement with theoretical values for phase velocity (Figs. 1 and 3) and coupling coefficient (Fig. 2) is good.

Using the coupled-resonator tuning network shown in Fig. 5, a 3-dB bandwidth of 31 MHz with 22.8 dB insertion loss was achieved (Fig. 5). The device parameters are given in Table I. The theoretical plot of insertion loss was obtained using the theoretical values for phase velocity and $\Delta v/v$ and the measured values given in Table I for the device and network parameters. The equations for transducer impedance and capacitance derived by Kino and Wagers⁴ for balanced excitation were modified to apply to the case of unbalanced excitation. Using a two-stage π network,¹⁰ bandwidths as large as 42 MHz were attained, although the insertion loss was higher (35 dB).

In conclusion, theoretical and experimental values for the phase velocities and coupling coefficients are presented here. Bandwidths in excess of 30 MHz were achieved for the first time in a monolithic ZnO-on-Si device.

The authors wish to thank R. Wagers and M. Drake for their help and guidance with the computer calculations. The computer calculations were made using a program developed at Stanford¹¹ and used the crystal constants compiled by Auld.¹² This work was supported by the Defense Advanced Research Program Agency and monitored by the Office of Naval Research under Contract No. N00014-76-C-0129.

¹H.C. Tuan and G.S. Kino, *Appl. Phys. Lett.* **31**, 641 (1977).

²K.A. Ingebritsen, R.A. Cohn, and R.W. Mountain, *Appl. Phys. Lett.* **26**, 596 (1975).

³C. Maerfeld and Ph. Defranould, *IEEE Ultrasonics Symposium Proceedings—1975* (IEEE, New York, 1975), p. 208.

⁴G.S. Kino and R. Wagers, *J. Appl.* **44**, 1480 (1973).

⁵G.A. Armstrong and S. Crampin, *Electron. Lett.* **9**, 322 (1973).

⁶K. Sezawa, *Bull. Earthquake Res. Inst.* **3**, 1 (1927).

⁷J.K. Elliott, R.L. Gunshor, R.F. Pierret, and A.R. Day, *Appl. Phys. Lett.* **32**, 515 (1978).

⁸F.C. Lo, R.L. Gunshor, and R.F. Pierret, *Appl. Phys. Lett.* **34**, 725 (1979).

⁹W.R. Smith, H.M. Gerard, J.H. Collins, T.M. Reeder, and H.J. Shaw, *IEEE Trans. Microwave Theory Tech.* **17**, 865 (1969).

¹⁰T.M. Reeder, W.R. Shreve, and P.L. Adams, *IEEE Trans. Sonics Ultrasonics* **19**, 466 (1972).

¹¹R. Wagers, Ph.D. thesis, Stanford University, 1972 (unpublished).

¹²B.A. Auld, *Acoustic Fields and Waves in Solids* (Wiley-Interscience, New York, 1973), Vol. 1, p. 357.

APPENDIX E

ADAPTIVE DECONVOLUTION USING AN ASW STORAGE CORRELATOR

J. E. Bowers, G. S. Kino, D. Behar, and H. Olaisen

Ginzton Laboratory
Stanford University
Stanford, California

Abstract

A new analog adaptive filter for deconvolving distorted signals is described in this paper. The filter uses a storage correlator which implements a clipped version of the LMS algorithm and uses a special iterative technique to achieve a fast convergence. The new filter has a potential bandwidth of 100 MHz and would eventually handle pulsed signals of 5 μ sec width. For signals with time-bandwidth product of less than 100, the adaptation time is less than 1 msec which allows operation in real time for most applications including resolution of radar signals in a cluttered environment, removal of echoes from television signals, deconvolution of distorted signals in nondestructive evaluation, and also in telephony. The filter is particularly suited for radar and communications as it processes signals directly in the VHF range.

Two experiments related to ghost suppression of a pulse and to the field of NDE are described in this paper. The results are in good agreement with computer simulations and show a ghost suppression of 15 dB for the first example and a sidelobe suppression of 8 dB for a transducer signal. The adaptation time is less than 450 μ sec.

I. INTRODUCTION

Adaptive filtering¹ is useful in removing distortion from signals, particularly when the distortion varies in time. Adaptive filters have been used to perform deconvolution of a distorted echo pulse in an acoustic imaging system², to equalize the distortion in a telephone channel³, and to suppress an interfering signal⁴.

Most adaptive filters have been implemented using digital techniques. The limitation of the digital approach is the limited bandwidth (typically 5 MHz) and the practical limit on the number of taps dictated by the complexity and power consumption⁵.

An analog-digital hybrid approach has been implemented using MOS LSI technology⁶. This has the advantage of lowering the power consumption and allowing 32 taps to be used without undue external complexity. Large dynamic range was obtained with this technique (60 dB), but the bandwidth was limited to less than 1 MHz.

Most analog implementations of an adaptive filter have been made using CCDs with analog tap weights held in sample and hold circuits⁷. The limitations here are the narrow bandwidth and variation across the chip in gain and threshold levels. The alternative approach used at Hughes for implementing a wideband adapting filter is to employ tapped ASW filters with complex computer-controlled systems for adjusting the tap weights⁸.

We shall describe here a relatively simple all-analog approach to adaptive filtering which uses the least mean squares (LMS) algorithm to find the optimal set of tap weights. An ASW monolithic ZnO/Si storage correlator with 8 MHz bandwidth and the equivalent of 24 taps was used⁹. The advantages of this approach are:

- (1) fast iteration rate (100 kHz) which means a short learning time ($\sim 100 \mu\text{s}$) and good ability to track time varying signals;
- (2) simple external connections;
- (3) large potential bandwidth (100 MHz);
- (4) large potential number of taps (1000);
- (5) low power consumption (.1 W);
- (6) it is suited for radar and communications systems because it can operate directly at the IF frequency.

A disadvantage is that, at the present time, the dynamic range is less than for digital systems.

A brief introduction to the LMS algorithm is provided, followed by a new derivation of the LMS algorithm. As the class of applications discussed here utilizes continuous, quasistatic filters, a derivation in the frequency domain rather than the time domain allows more physical insight into the processing capability of the LMS algorithm and into its advantages and limitations for these kinds of applications.

Two adaptive deconvolution experiments which used the storage correlator are described. In the first experiment, an undesirable time-delayed ghost pulse is removed. In the second experiment, the ringing in the pulse response of an acoustic transducer is removed by adaptive filtering. The results of these experiments are compared to computer simulations with the LMS algorithm. Conclusions are drawn regarding which properties and nonlinearities of the storage correlator are limiting the performance of the adaptive filter.

II. EXPERIMENTAL PROCEDURE

A. The LMS Algorithm

Consider an adaptive filter with an input $x(t)$ and output $y(t) = x * w$. The tap weights w are adjusted after each iteration such that the output $y(t)$ converges to a desired signal $d(t)$. The time it takes for convergence to occur is commonly called the learning or training time. After the optimum set of weights w is determined, the filter can be used to remove the distortions in signals. For example, in a TV system with a ghost, the filter can be trained on the sync signal (which occurs at the end of each line) to remove the echo sync signal, and then the entire TV line can be passed through the filter, and the "ghosts" will be removed.

The error $\epsilon(t)$ between the desired signal $d(t)$ and the output of the filter $y(t)$ is

$$\epsilon(t) = d(t) - y(t) \quad (1)$$

where

$$y = x * w \quad (2)$$

and $*$ indicates convolution. Then the LMS algorithm specifies that to minimize the error, w must be changed by Δw such that

$$\Delta w = \mu x \star \epsilon \quad (3)$$

where \star indicates correlation and μ is a constant which determines the rate of convergence of the system.

Thus it follows from Eqs. (1), (2), and (3) that

$$\Delta w = \mu x \star (d - x \star w) \quad (4)$$

A proof is given in the following section that if these adjustments Δw are made, then the weights exponentially approach the Wiener filter solution; this is a filter which minimizes the average mean square error, over the frequency band of interest, between its output signal and a desired signal $D(\omega)$.

It can be seen from the expression for the tap weight adjustment (Eq. (4)) that for each iteration, a convolution with x , and a correlation with x must be performed. In addition, an analog storage register is needed for w , and it must be possible to adjust each of the tap weights.

The ASW storage correlator is ideally suited for this purpose, as it can perform all of these operations (convolution, correlation, addition, and storage). A big advantage of this approach is its simplicity. All of the necessary operations are performed inside a two (or three) port device in real time.

B. The Storage Correlator

The ASW storage correlator is a device which utilizes the interaction between a propagating acoustic surface wave and a charge distribution stored in an array of diodes to store, correlate, or convolve two broad bandwidth signals in real time. A series of signals may be added together by successively storing them in the diode array. A brief description of the storage correlator follows. Complete descriptions of the device^{10,11} and its operation¹² as well as a theory of the device¹³ are given in the literature.

A schematic drawing of a storage correlator is shown in Fig. 1. If a modulated carrier x is applied to the acoustic port (#2) and a signal ϵ to port #3, then the charge distribution¹³

$$\Delta w = x \star \epsilon \quad (5)$$

is added to the charge distribution w stored in the diode array. If a signal x is then applied to port #3, then the convolution

$$y = x \star w \quad (6)$$

is the output at port #2. The LMS algorithm can be realized by repeating the process many times. Eventually, the tap weights w converge to an approximation to the Wiener solution, and the programming is complete. The filter may then be used to deconvolve other signals which have been distorted in the same manner.

The external connections used to operate the storage correlator are indicated in Fig. 2a. A much simpler method is indicated in Fig. 2b when two acoustic ports of the correlator are used, and the external delay line and the switches are not needed. A difference amplifier is not needed to subtract $d(t)$ and $y(t)$; rather the carrier frequency is adjusted so that there was a phase difference of π between the delayed signal $y(t)$ and the desired signal $d(t)$. This is explained more fully in the next section.

The storage correlator is not an exact implementation of the Widrow type LMS adaptive filter for two reasons. First, the LMS algorithm requires that each tap be changed individually and the error signal for

the next tap be calculated after the previous tap is changed¹⁴. However, in our implementation, the entire error signal is calculated, and the entire set of taps is changed at once. This difference is not significant except for the case of very high gain and very fast convergence. The second difference is that the effect of the plate signal (port #3) on the tap weights is not linear (Fig. 3). If the error signal is less than a threshold determined by the characteristics of the devices (4V), the tap weights are unaffected. The error signal is clipped around 9V, so only ~6 dB of dynamic range is available at port #3. If the error signal is fed into an acoustic port (as in Fig. 4b), then at least 35 dB dynamic range should be available.

The weight signal $w(z)$ is stored in 2000 diodes; however, the number of equivalent taps is much less since the bandwidth is 8 MHz and the maximum signal duration is 3 μ s. Consequently, the time bandwidth product is 24. The device was represented in the computer simulation by a 24 tap transversal filter. The necessary correlations and convolutions were calculated in the computer, and the error signal was modified according to the transfer characteristic shown in Fig. 3. It can be seen that this transfer characteristic closely approximates the experimentally observed characteristic.

III. THEORY

A. Introduction

The LMS algorithm has been analyzed in detail by Widrow^{14,15}. The first task in his analysis is to transform from the coordinate system consisting of N samples from the waveform to a set of normal coordinates where the correlation matrix is diagonal; the eigenvectors of the correlation matrix are mutually orthogonal, and, most importantly,

the decay modes are uncoupled. Once this transformation is accomplished, expressions for the decay constants τ_p , misadjustment, etc. may be derived.

In the analysis presented here, the transformation is very easily accomplished by taking the Fourier transform of all quantities. Correlations are then simple products, and the convergence of a quantity at a given frequency is independent of other frequencies, i.e., the modes are uncoupled.

B. Convergence

Consider the situation in Fig. 2, where all signals are rf modulated, and the carrier frequency is ω_0 . The desired signal $d_n(t)$ and the distorted signal $x_n(t)$ are repetitive, and as the number of iterations n increases, the only change in these signals is a phase change

$$d_n(t) = d(t) e^{j\omega_0 nT} \quad (7)$$

where T is the iteration time. In the frequency domain

$$D_n(\omega) = D(\omega) e^{j\omega_0 nT} \quad (8)$$

Similar expressions hold for the distorted signal $X(\omega)$.

The filter output is

$$Y_n(\omega) = X(\omega)W_n(\omega) e^{j\omega_0(nT + T_0)} \quad (9)$$

and the error signal is

$$\begin{aligned}
E_n(\omega) &= D_n(\omega) + Y_n(\omega) e^{-j\omega_0 T_D} \\
&= D(\omega) e^{j\omega_0 nT} + X(\omega) W_n(\omega) e^{j\omega_0 (nT + T_0 - T_D)}
\end{aligned}
\tag{10}$$

where T_D is the length of the external delay line, and T_0 is the time between the appearance of $x(t)$ at the acoustic and plate ports.

The weight adjustment is

$$w(t) = 2\mu_a X(t) \star \varepsilon_n(t) \tag{11}$$

Equivalently, we can write

$$\begin{aligned}
W_{n+1}(\omega) &= W_n(\omega) + 2\mu E_n(\omega) X_n^*(\omega) \\
W_{n+1}(\omega) &= AW_n(\omega) + B
\end{aligned}
\tag{12}$$

where

$$\begin{aligned}
A &= 1 + 2\mu X(\omega) X^*(\omega) e^{j\omega_0 (T_0 - T_D)} \\
B &= 2\mu D(\omega) X^*(\omega)
\end{aligned}
\tag{13}$$

Equation (12) has the solution

$$W_n(\omega) = (W_i - W_w) A^n + W_w \tag{14}$$

where W_i is the initial weight distribution and

$$W_w = \frac{D(\omega)}{X(\omega)} e^{j\omega_0(T_0 - T_D)} \quad (15)$$

Equation (14) converges only if $|A| < 1$. The fastest convergence is obtained for the carrier frequencies where the error signal is the subtraction of D and Y , i.e. when

$$\omega_0 = \frac{\pi}{|T_D - T_0|} (2p + 1) \quad (16)$$

where p is a large integer. If the feedback gain μ is sufficiently small

$$\mu < \frac{1}{XX^*} \quad (17)$$

then the convergence requirement $|A| < 1$ is satisfied for carrier frequencies in bands of width $\Delta\omega$ around the frequencies given by Equation (16), where

$$\Delta\omega = \frac{2}{|T_D - T_0|} \arccos(\mu XX^*) \quad (18)$$

It can be seen from Equation (17) that when μ is near its upper limit, the carrier frequency must be close to one of the values given by Equation (16).

If the feedback gain is significantly less than its maximum value, it follows that

$$A = 1 + 2\mu XX^* e^{j\omega_0(T_0 - T_D)} \approx e^{-1/\tau} \quad (19)$$

where

$$1/\tau = 2\mu XX^* e^{j[\omega_0(T_0 - T_D) + \pi]} \quad (20)$$

The convergence of the weight vector (Eq. (14)) is approximately exponential. So we can write

$$W_n \approx (W_1 - W_w) e^{-n/\tau} + W_w \quad (21)$$

The error is

$$E_n = D - X^* W_n$$

$$E_n \approx X^*(W_1 - W_w) e^{-n/\tau} \quad (22)$$

The error decays exponentially to zero. In practice, the bandwidth of the system is limited by the bandwidth B of the acoustic transducers. Consequently, the error outside this frequency range is not affected by the adaptation process. It will also be noted that phase distortion in the system is cancelled out by the application of the convolution and correlation process in turn. So, although this is basically a feedback system, there is no problem with instability provided the convergence criteria are satisfied.

We have implicitly assumed that the signals $x(t)$ and $d(t)$ are sufficiently short compared to the time length of the diode array that all of the signal $\Delta\omega(t)$ is stored in the diode array. If this is not

the case, then different frequencies do not decay independently, and the analysis is more difficult. An important result of this more difficult case is that the error does not decay to zero in the passband.

If noise on the input signal X is included in this analysis, and if the noise on the plate and acoustic ports are correlated, as they would be if a delay line were used to generate the second X signal which is needed during each iteration, then the expression for the convergence of the weight signal is again given by Equation (22) where

$$W_w = \frac{DX^*}{XX^* + \langle NN^* \rangle} \quad (23)$$

$$\tau = \frac{1}{2\mu(XX^* + \langle NN^* \rangle)} \quad (24)$$

Equation (23) is, of course, the Wiener filter solution.

IV. RESULTS AND DISCUSSION

A. Echo Suppression

In this experiment, a square pulse $0.4 \mu s$ long is followed by an echo pulse. The desired signal is a single pulse $0.4 \mu s$ long. For an echo which is 6 dB less in amplitude than the main pulse (Fig. 4a), the sidelobe suppression after 10 iterations ($200 \mu s$) is 15 dB, as shown in Fig. 4b. The dependence of sidelobe suppression on echo height is shown in Fig. 5. The results of computer simulations of the LMS algorithm with 22 taps and using clipping and a threshold 6 dB below the clipping level are also shown in Fig. 5. The computer simulation agrees very well with experimental results except that the maximum sidelobe suppression is 23.5 dB which is 4.5 dB higher than was experimentally

obtained. The reason is that the spurious signals generated in the device during read out limits the dynamic range of the signal input.

An important result obtained in this experiment is that spurious acoustic signals generated by the plate readout signal can be suppressed by up to 13 dB as a result of the adapting process. The filter does not distinguish between echoes and distortions generated externally or by the device itself. This result is demonstrated in Fig. 6. The upper trace is the adaptive filter result after removing an echo from a 0.4 μ s long pulse. If all signals except the plate readout signal are removed, the filter output (lower trace) is the spurious signal generated by the plate signal. A large spurious signal can be seen when previously there had been a null.

The advantage of computer simulation of this adaptive filter is that the threshold and clipping levels may be easily changed to see what effect they have on the performance of the adaptive filter. These results are summarized in Table I. The computer simulated linear LMS result is given in the first row. If a threshold level is included, then the computer simulation converges much faster, but to worse results. The values obtained are in agreement with experimental results. If the feedback gain is increased so that the error signal is now clipped, then much better sidelobe suppression is obtained in both the experimental and computer simulation cases. We note that clipping of the signal increases the rate of convergence radically, as has been noted by others. The algorithm employed is therefore known as the clipped LMS algorithm.

Regardless of the shape of the desired signal (d) and input signal (x), it was always experimentally observed that the feedback gain must be large enough to strongly clip the error signal during the first few iterations for the optimum filtering. After many iterations, the error signal is only slightly clipped.

The threshold and clipping levels can be changed by modifying the design of the storage correlator. For this reason, a series of computer simulations was made to determine the effect of having other threshold to clipping ratios (σ) than the value $\sigma = .5$ which exists in the present devices. Only the ratio σ is important here. The minimum r.m.s. error does not change if the threshold, clipping, and gain values are all multiplied by the same value. The asymptotic value of the r.m.s. error is shown as a function of σ in Fig. 7 for the case of a 6 dB echo. The optimum value for the gain is used at each point. The end point $\sigma = 1.0$ corresponds to the situation of hard clipping where the threshold level equals the clipping level, and the feedback error is either 1 or 0. The r.m.s. error increases linearly with σ . This is intuitively expected since any error values less than the threshold do not affect the tap weights and are not adapted to zero. The r.m.s. error would then linearly increase with threshold level. Consequently, the design of the storage correlator should minimize the threshold value.

B. Reduction of Bulk Transducer Ringing

The object of this experiment was to improve the impulse response of an acoustic bulk wave 1.25 MHz transducer used for acoustic nondestructive evaluation. The impulse response is shown in Fig. 8a. The desired signal is a unipolar pulse with a width of $.3 \mu s$. If the impulse response is correlated with itself (Fig. 8b), the highest sidelobe is 1.7 dB smaller than the peak. However, if the correlator is used as an adaptive filter, then the sidelobe level can be reduced to 7 dB below the peak after 10 iterations (Fig. 8c) and 10 dB below the peak after 35 iterations.

The growth of the peak as the number of iterations increases is shown in Fig. 9. The computer simulation is also shown and can be seen to be in good agreement with the experimental result. The computer

simulation is in good agreement with the experimental result except that the maximum predicted suppression is 2.6 dB better than was experimentally observed.

Linear LMS theory predicts¹ that the time averaged mean square error (MSE) should decay exponentially to a constant value. The ratio of this constant value to the Wiener solution is called the misadjustment M . The misadjustment is approximately related to the decay constant τ by the relation¹

$$M = N/4\tau \quad (25)$$

where N is the number of tap weights. In our case, N is the time bandwidth product of the storage correlator. Thus, the faster the convergence, the larger the misadjustment.

The experimentally observed decay of the MSE for the bulk transducer case is shown in Fig. 9. The decay is exponential except for the first few iterations when the error signal is strongly clipped and the mean square error decays faster than an exponential. The experimental decay constant is 7.5, and the misadjustment calculated from Equation (25) is equal to .8. We interpret this to mean that the final result is close to the Wiener solution.

C. Limitations

The bandwidth of this device (8 MHz) is larger than the bandwidth of other methods of implementing the LMS algorithm; however, larger bandwidths are often desirable. Our technique can work well as an adaptive filter for a 1.25 MHz transducer, but it works poorly for a 2.5 MHz transducer. The diode array length (3 μ s) is also a limitation since we cannot

adapt signals which are longer than this. Also, since the correlation signal is truncated, the filter output is distorted. These two limitations are manifestations of the fact that if the correlator had a larger time bandwidth product than 24, then it would equivalently have more taps and could adapt a broader class of signals. Time bandwidth products of 500 or more are possible with the use of present technology. Note, however, that Equation (25) predicts that if the number of taps is increased, then the convergence time also increases (for a given level of misadjustment). Thus, a larger number of taps is not desirable for applications in which the distortion is changing rapidly. For example, if the timing or amplitude of the echo significantly changes over a time period of 200 μ s (10 iterations), then a larger number of taps would not be desirable.

V. CONCLUSIONS

It was demonstrated that a -6 dB echo could be suppressed to -15 dB in 200 μ s (10 iterations). The sidelobe of the impulse response of a 1.25 MHz acoustic bulk transducer can be reduced from -2 dB to -10 dB with adaptive filtering.

The experimental results are on the whole in excellent agreement with the computer simulations. Thus it appears that the storage correlator is being operated in the optimum manner and that the only major distortion introduced by the storage correlator is the presence of the threshold and clipping levels.

There are many advantages of using a storage correlator to implement the clipped LMS algorithm for adaptive filtering. Only two connections are needed for a device which can correlate, convolve, store, and add

broadband rf signals in real time. The device is small (1 cm^2) and has the potential of much broader bandwidths (100 MHz) than is obtainable with digital techniques. The device is far faster in operation than any competitive inverse filter with its bandwidth.

ACKNOWLEDGMENT

The authors wish to thank C. Williams, B. T. Khuri-Yakub, and H. Tuan for valuable discussions and suggestions. This work was supported by the Defense Advance Research Projects Agency and monitored by the Office of Naval Research under Contract N00014-76-C-0129.

REFERENCES

1. J. M. McCool and B. Widrow, "Principles and Applications of Adaptive Filters," IEE Conf. Publ., 144, pp. 84-95, 1976.
2. D. Corl, "A C.T.D. Adaptive Inverse Filter," Electr. Lett., 14, pp. 60-62, 1978.
3. R. W. Lucky, "Automatic Equalization for Digital Communications," Bell Sys. Tech. J., 66, pp. 547-588, 1965.
4. P. M. Grant and G. S. Kino, "Adaptive Filter Based on SAW Monolithic Storage Correlators," Electr. Lett., 14, pp. 562-564, 1978.
5. D. Behar, et al., "The Use of a Programmable Filter for Inverse Filtering," submitted for publication, Electr. Lett., October 1979.
6. B. K. Ahuja, et al., "A Sampled Analog MOS LSI Adaptive Filter," IEEE J. Solid-State Cir., SC-14, pp. 148-154, 1979.
7. D. F. Barbe, et al., "Signal Processing with Charge Coupled Devices," IEEE J. Solid-State Cir., SC-13, pp. 34-51, 1978.
8. W. K. Masenten, "Adaptive Processing for Spread Spectrum Communications Systems," Report TP 77-14-22, Hughes Aircraft Co., September 1977.
9. D. Behar, et al., "The Storage Correlator as an Adaptive Inverse Filter," submitted for publication, Appl. Phys. Lett., December 1979.
10. K. A. Ingebritsen, et al., "A Scottky-Diode Acoustic Memory and Correlator," Appl. Phys. Lett., 26, pp. 596-598, 1975.
11. C. Maerfeld and Ph. Defranould, "A Surface Wave Memory Device Using pn Diodes," IEEE Ultrasonics Symp. Proc., pp. 209-211, 1975.
12. H. C. Tuan, et al., "A New Zinc Oxide-on-Silicon Monolithic Storage Correlator," IEEE Ultrasonics Symp. Proc., 496-499, 1977.

13. P. G. Borden and G. S. Kino, "An Analytic Theory for the Storage Correlator," IEEE Ultrasonic Symp. Proc., pp. 485-491, 1977.
14. B. Widrow, et al., "Stationary and Nonstationary Learning Characteristics of the LMS Adaptive Filter," Proc. IEEE, 64, pp. 1151-1162, 1976.
15. B. Widrow and J. M. McCool, "A Comparison of Adaptive Algorithms Based on the Methods of Steepest Descent and Random Search," IEEE Trans. Ant. and Prop., AP-24, pp. 615-637, 1976.

TABLE I

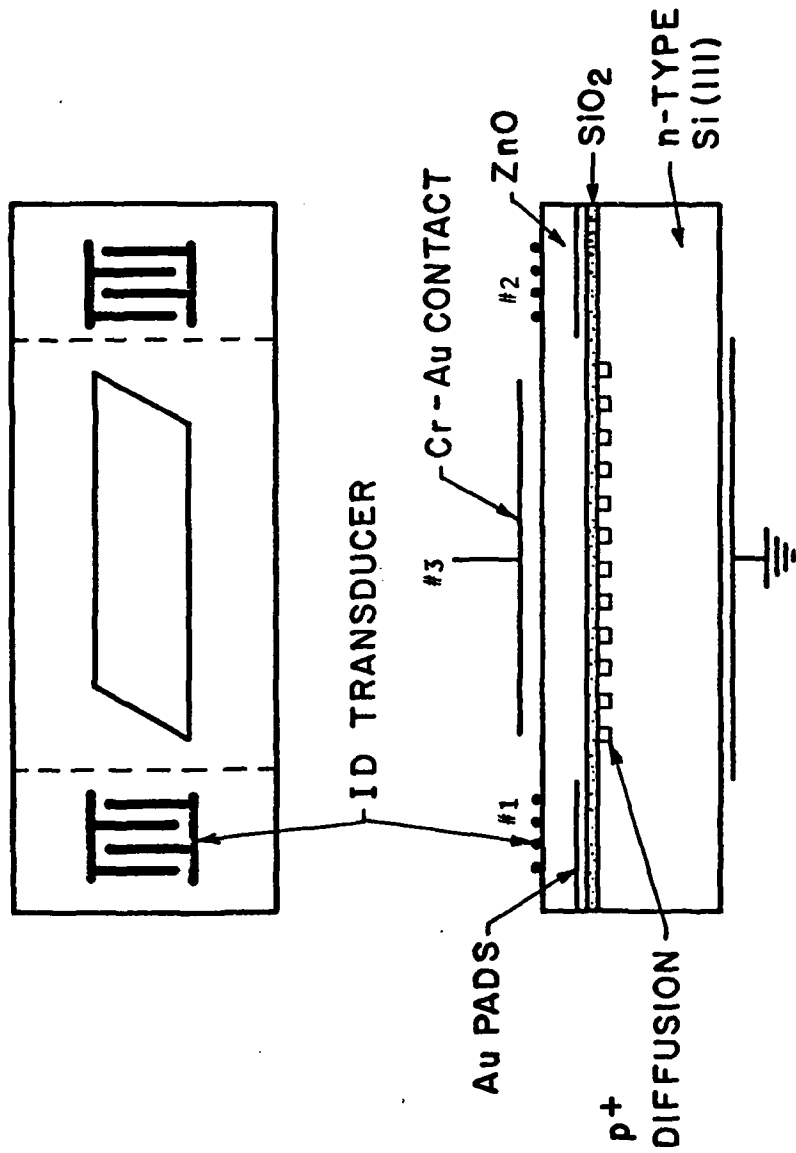
Experimental Results and Computer Simulations for a Filter Input of a $.4 \mu\text{s}$ Wide Pulse with a -6 dB Echo. The Computer Simulation Uses 24 Taps.

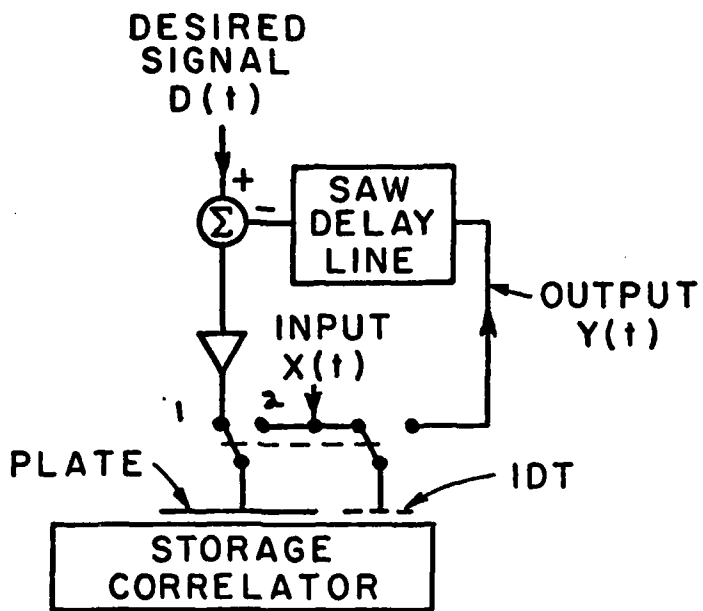
	<u>STORAGE CORRELATOR RESULTS</u>		<u>COMPUTER SIMULATION</u>	
	Sidelobe Suppression (dB)	Number of Iterations for Convergence	Sidelobe Suppression (dB)	Number of Iterations for Convergence
Linear	---	---	14.0	25
Threshold*	10.0	5	10.7	4
Threshold and Clipped	14.8	10	14.2	6

*The maximum feedback signal (ϵ) was not more than 6 dB above the threshold level.

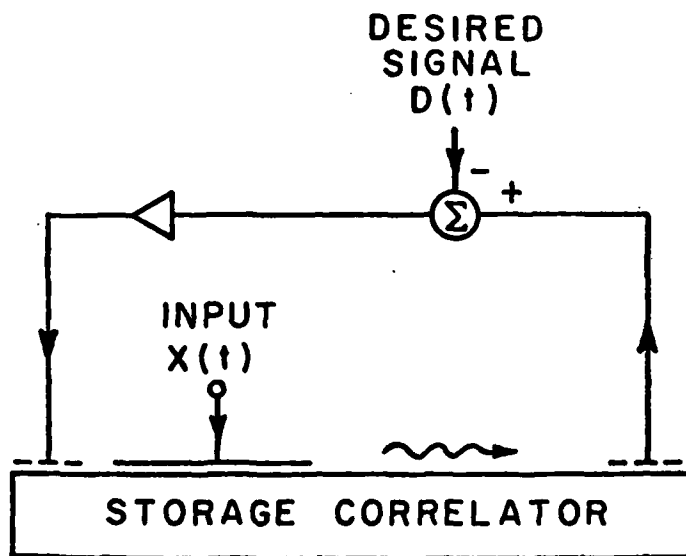
FIGURE LEGENDS

1. Schematic drawing of storage correlator.
2. (a) Actual and (b) proposed implementation of SAW adaptive filter.
3. Correlator output as a function of plate (readout) pulse height.
4. (a) Input signal and (b) output signal after 22 iterations.
5. Experimental and computer simulation results for echo suppression experiment.
6. Echo reduction after 10 iterations (upper trace). Spurious signals generated by plate read-out signal (lower trace).
7. Minimum r.m.s. error as a function of threshold level.
8. (a) Impulse response of 1.25 MHz bulk acoustic transducer; (b) auto-correlation of impulse response; and (c) filter output after 10 iterations of adapting.
9. Output pulse level during adapting process.
10. Mean Square Error during adapting process.

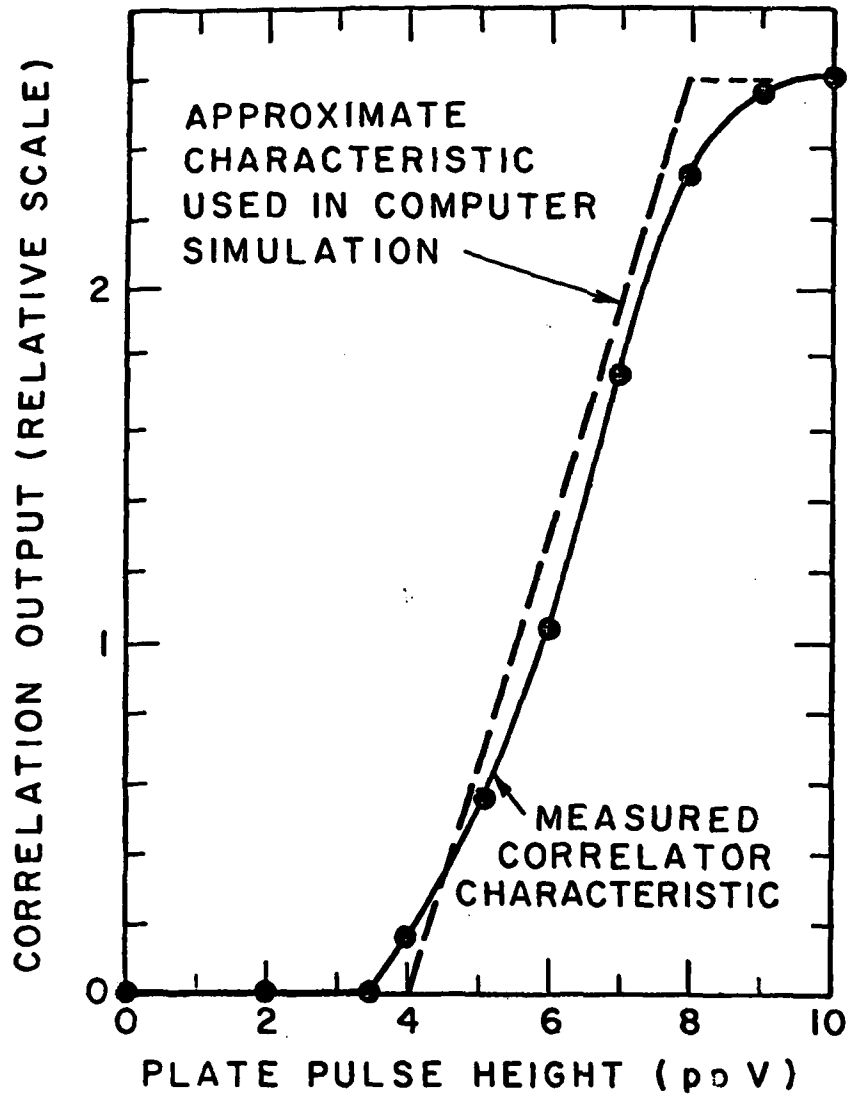


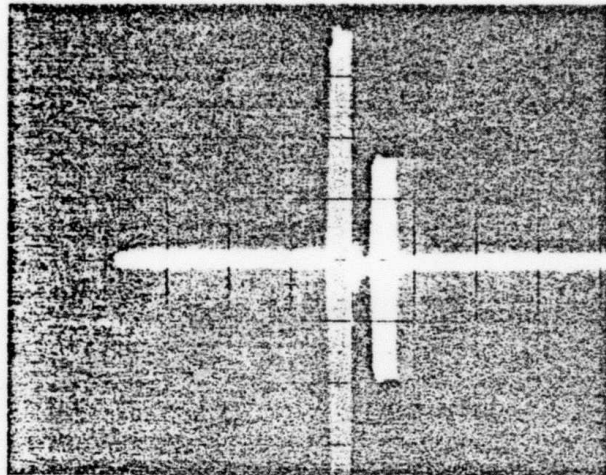


(a)



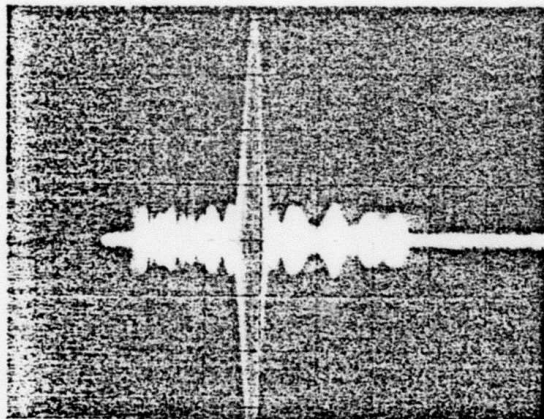
(b)





(a)

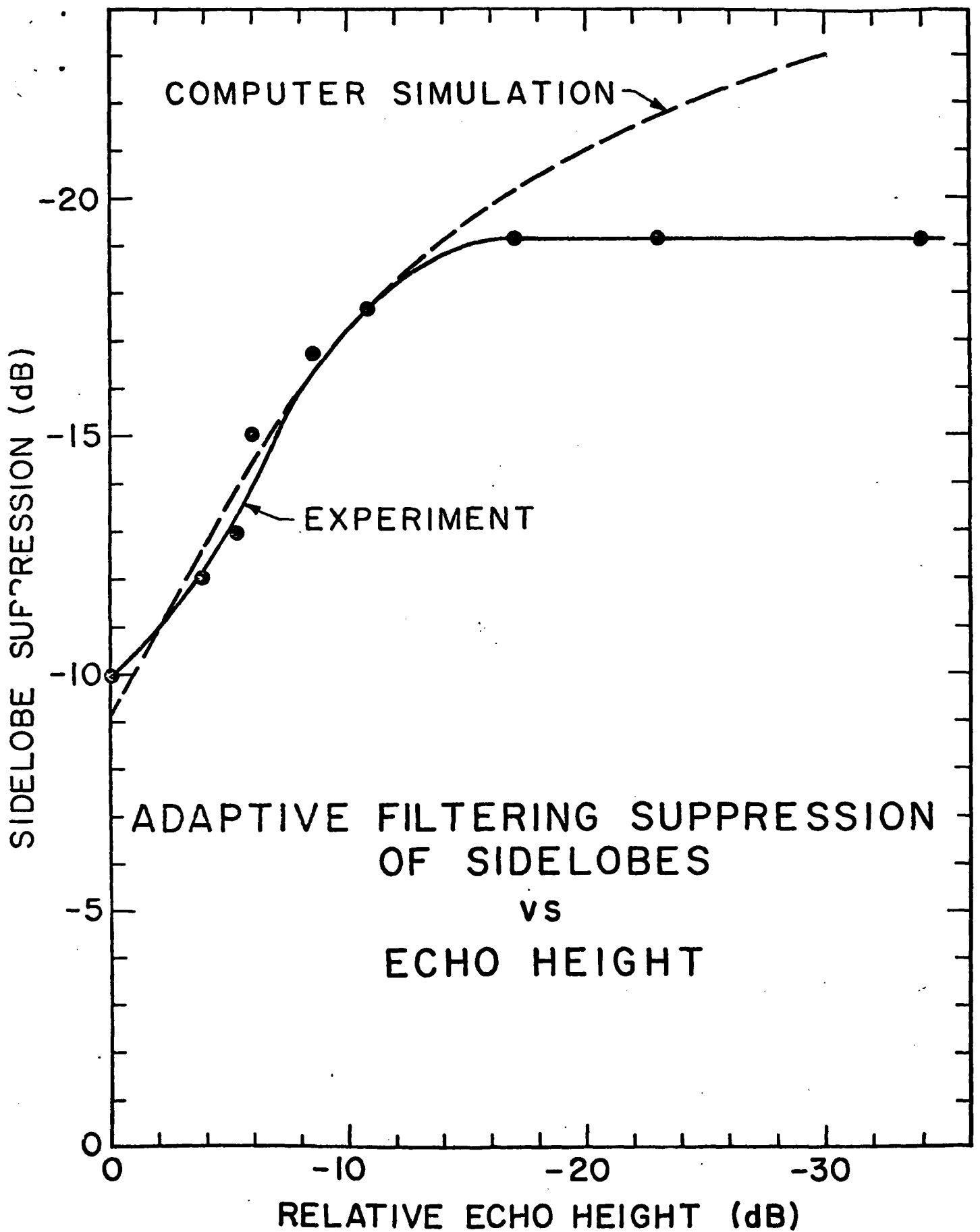
→ | ← 1 μ sec



(b)

→ | ← 1 μ sec

Fig. 4.



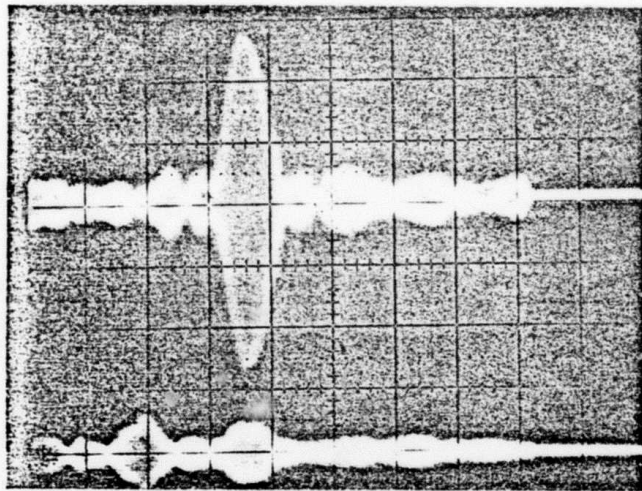
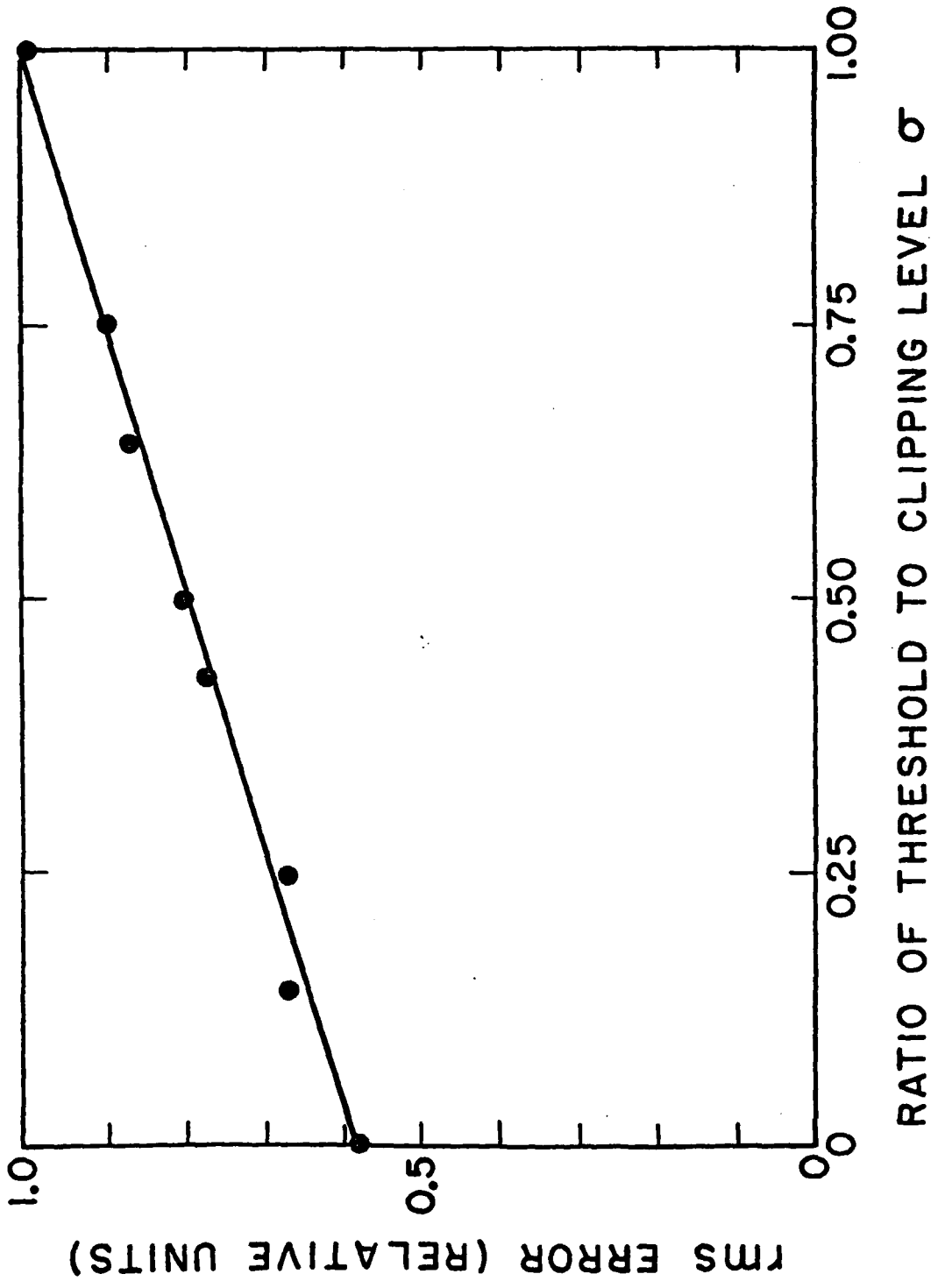
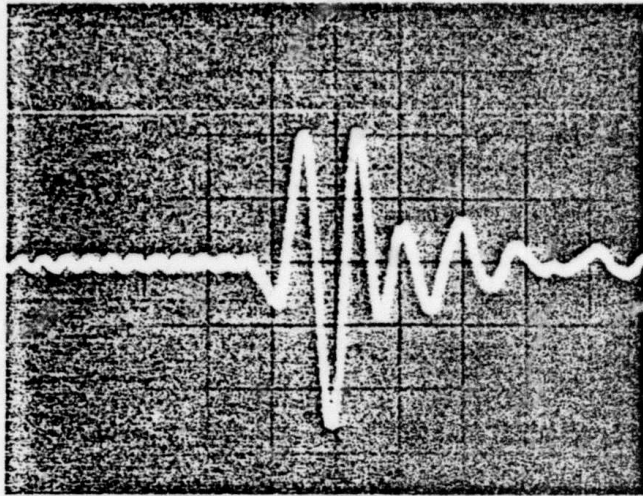


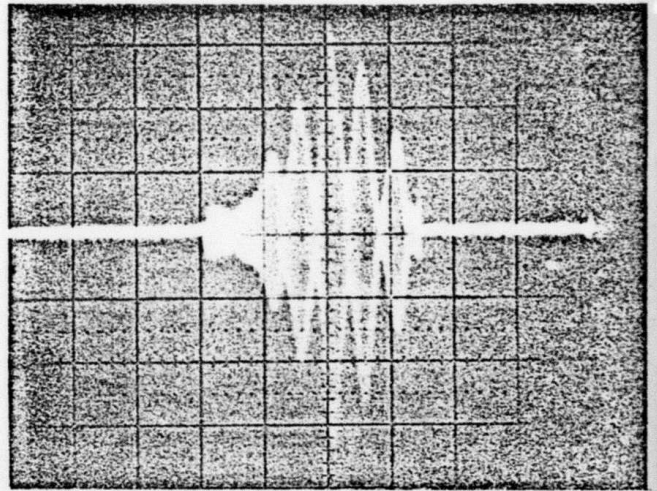
Fig. 6.





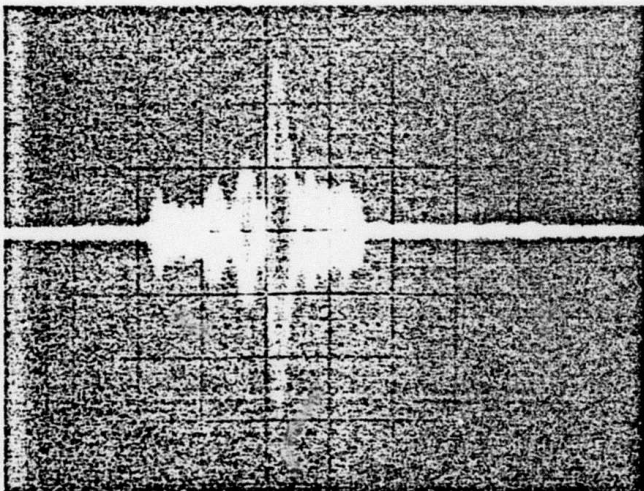
(a)

→ | |←1 μsec



(b)

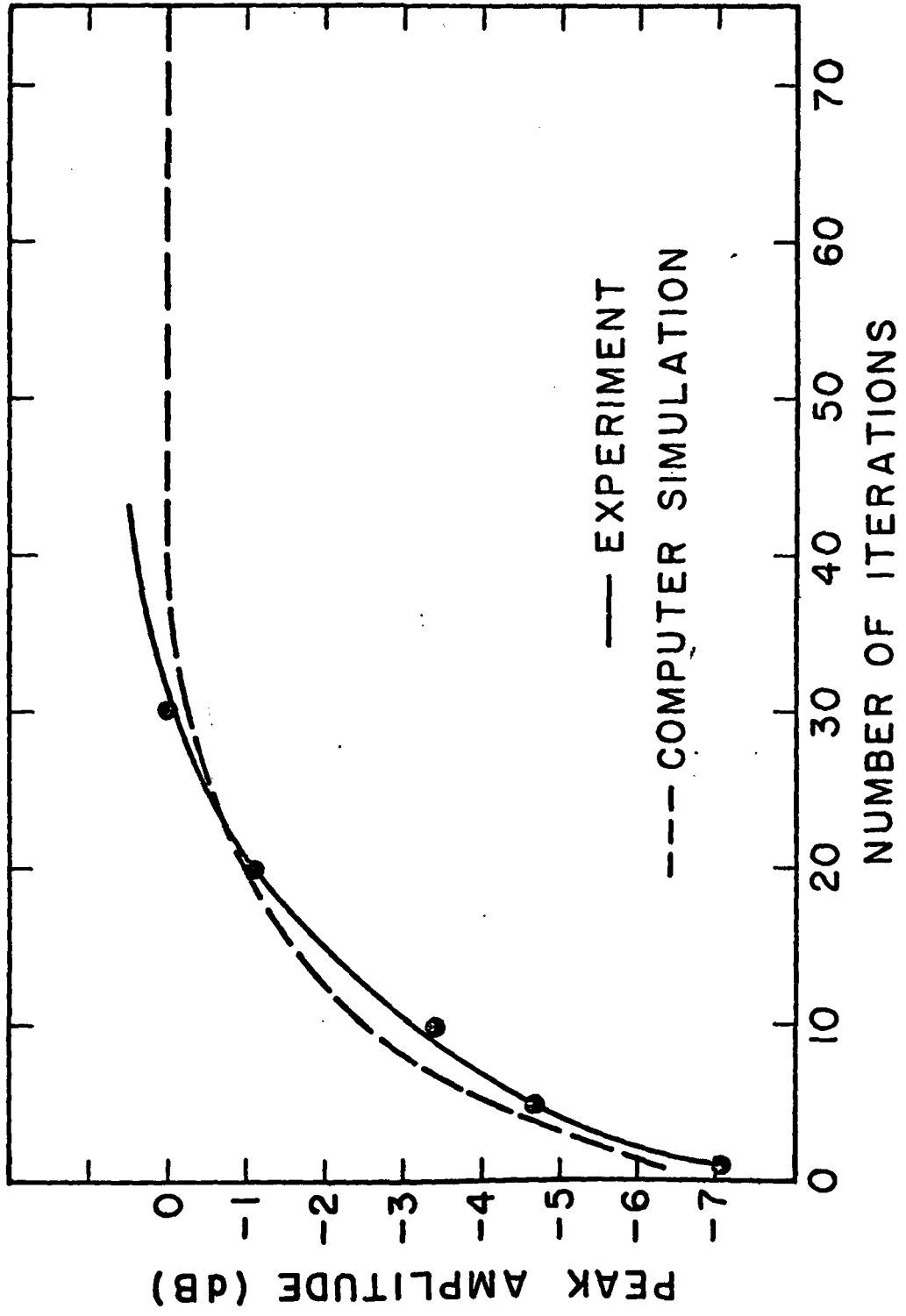
→ | |←1 μsec

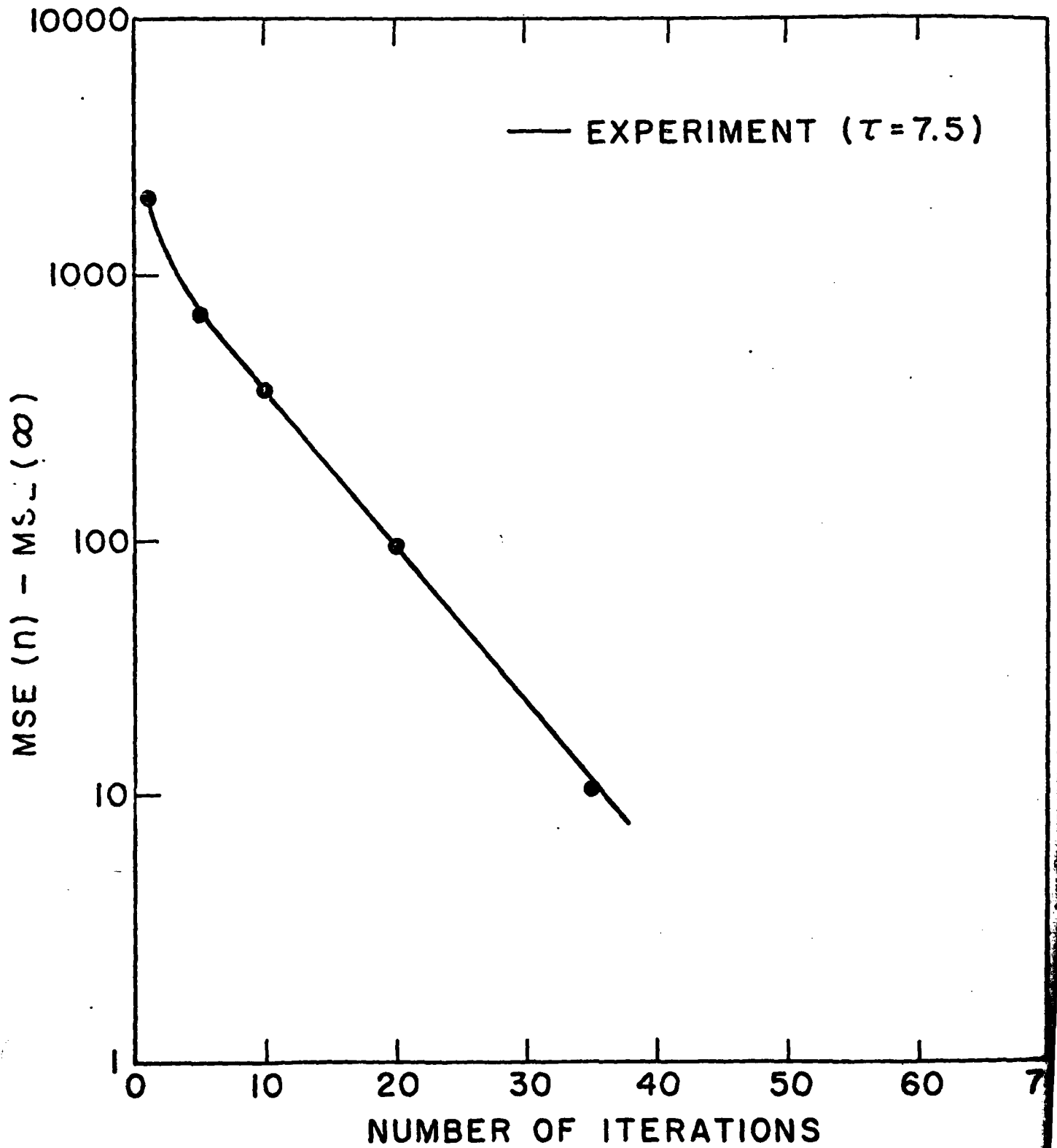


(c)

→ | |←1 μsec

Fig. 8.





DISTRIBUTION LIST

<u>Addresses</u>	<u>Number of Copies</u>
Director Advanced Research Projects Agency 1400 Wilson Boulevard Arlington, VA 22209 Attention: Program Management	1
Scientific Officer	3
Administrative Contracting Officer	1
Director Naval Research Laboratory Attention: Code 2627 Washington, D.C. 20375	6
Defense Documentation Center Building 5, Cameron Station Alexandria, VA 22314	12
Office of Naval Research (Western Regional Office) 1030 East Green Street Pasadena, California 91101	1
Naval Research Laboratory Code 6850 Washington, D.C. 20375	1
RADC (ETEM) Attn: Dr. P. Carr Hanscom AFB, MA 01731	1
AGED ODDR&E 9th floor 201 Varick Street New York, NY 10014	1
Dr. R. Damon Director, Applied Physics Laboratory Sperry Research Center Sudbury, MA 01776	1

Enclosure (1)